NEW ADVANCES IN SHALE GAS RESERVOIR ANALYSIS USING WATER FLOWBACK DATA

A Dissertation

by

AHMAD B A O F ALKOUH

Submitted to the Office of Graduate and Professional Studies of
Texas A&M University
in partial fulfillment of the requirements for the degree of

DOCTOR OF PHILOSOPHY

Chair of Committee,	Robert A. Wattenbarger
Committee Members,	David S. Schechter
	J. Bryan Maggard
	Yuefeng Sun
Head of Department,	A. Daniel Hill

May 2014

Major Subject: Petroleum Engineering

ABSTRACT

Shale gas reservoirs with multistage hydraulic fractures are commonly characterized by analyzing long-term gas production data, but water flowback data is usually not included in the analysis. However, this work shows there can be benefits to including post-frac water flowback and long-term water production data in well analysis. In addition, field data indicate that only 10-40% of the frac water is recovered after the flowback. This work addresses two main question: Where is the rest of the injected frac fluid that is not recovered and what is the mechanism that is trapping it? And how can the water flowback data be used in estimating effective fracture volume using production data analysis tools?

A number of simulation cases were run for single and two phase (gas/water) for modeling flowback and long-term production periods. Various physical assumptions were investigated for the saturations and properties that exist in the fracture/matrix system after hydraulic fracturing. The results of these simulations were compared with analytical solutions and data from actual wells using diagnostic and specialized plots. The results of these comparisons led to certain conclusions and procedures describing possible reservoir conditions after hydraulic fracturing and during production.

Past publications have suggested that the lost frac water is trapped in the natural fracture or imbibed into the rock matrix near the fracture face. Natural fracture spacing could be a possible explanation of the lost frac water. These concepts are tested and the challenge of simulating a natural fracture with trapped water without imbibition is solved

using a new hybrid relative permeability jail. This concept was tested for the period of flowback, shut-in and production.

This work presents the benefits of a new method for combining water flowback and long-term water production data in shale gas analysis. Water production analysis can provide effective fracture volume which was confirmed by the cumulative produced water. This will help when evaluating fracture-stimulation jobs. It also shows the benefits of combining flowback and long-term water production data in the analysis of shale gas wells. In some cases, the time shift on diagnostic plots changes the apparent flow regime identification of early gas production data. This leads to different models of the fracture/matrix system. The presented work shows the importance of collecting and including water flowback data in long-term production data.

DEDICATION

With sincerity and devotion, my work is dedicated to Almighty Allah for His mercies and blessings.

With love and affection, my work is dedicated to my family.

ACKNOWLEDGEMENTS

All praises and thanks to Allah almighty, for His infinite mercies and abundant blessings and allowing me to successfully conclude this phase of my life.

I would like to thank my committee chair, Dr. Robert Wattenbarger for being a father, mentor, supervisor and friend to me. I am honored to have worked with him.

I would like to thank my committee members Dr. David Schechter, Dr. Bryan Maggard and Dr. Yuefeng Sun for being my advisory committee and their suggestions and contributions.

I would like to thank my friends in my faculty group for their support and friendship; Basel Al-Otaibi, Ammar Agnia, Mohammed Kanfar, Hussain Aldaif, Mohit Dholi and Pahala Sinurat, Orkhan Samandaril, Tan Tran, Haider Abdulal, Wahaj Khan, Vartit Tivayanonda.

Finally, thanks to Public Authority of Applied Education and Training (College of Technological Studies) for giving me a chance to pursue my advanced degree and sponsoring my study at Texas A&M University.

NOMENCLATURE

A_{cm}	total matrix surface area draining into fracture system, ft^2
BDF	boundary dominated flow
B_{oi}	oil formation volume factor at initial pressure, res bbl/STB
B_{wi}	water formation volume factor at initial pressure, res bbl/STB
B_{gi}	gas formation volume factor at initial reservoir pressure, rcf/scf
C_{hf}	hydraulic fracture conductivity, md-ft
C_{nf}	natural fracture conductivity, md-ft
c_{ti}	total compressibility at initial reservoir pressure, psi^{-1}
c_g	gas compressibility, psi^{-1}
c_w	water compressibility, psi^{-1}
c_f	formation compressibility, psi^{-1}
D_D	dimensionless drawdown factore
f_{CP}	slope correction factor, dimensionless
FC	fracture conductivity, md-ft
h	reservoir thickness, ft
J	productivity index, STB/D-psi
$k_{f,eff}$	natural fracture effective permeability, md
$k_{f,in}$	intrinsic natural fracture permeability, md
k_{eff}	effective permeability, md
k_m	matrix permeability, md

k	permeability, md
k_r	relative permeability
k_{rw}	water relative permeability
k_{rg}	gas relative permeability
L_f	natural fracture spacing, ft
L_F	hydraulic fracture spacing, ft
L	distance to boundary, ft
ME	microemulsion
$\tilde{m}_4$	slope of the fourth root of time plot
m_{PSS}	slope of the Cartesian plot in the period of unit slope line
$m(p)$	pseudopressure (gas), psi^2/cp
$m(p_i)$	pseudopressure at initial condition (gas), psi^2/cp
$m(p_{wf})$	pseudopressure at flowing bottomhole condition (gas), psi^2/cp
n_F	number of hydraulic fracture
$OGIP$	original gas in place
$OOIP$	original oil in place
p_i	initial reservoir pressure, psi
p_D	dimensionless pressure
$\bar{p}$	average reservoir pressure, psi
p_{wf}	wellbore flowing pressure, psi
p_c	capillary pressure, psi
PNR	pressure normalized rate, $Mcf/D/psi^{-2}/cp$

q_g	gas rate, Mscf/day
q_D	dimensionless rate
q_w	water rate, STB/day
R_{ex}	extent ratio, fraction
R_k	permeability ratio, fraction
R_{sp}	spacing ratio, fraction
RNP_w	water rate normalized pressure, psi/STB/D
RNP_w'	derivative of water rate normalized pressure
S_{gi}	initial gas saturation, fraction
S_w	water saturation, fraction
SRV	stimulated reservoir volume
S_{wirr}	irreducible water saturation, fraction
S_{girr}	irreducible gas saturation, fraction
SG	specific gravity, fraction
STB	stock tank barrel
T	absolute temperature, ^oR
t	time, days
t_{Dye}	dimensionless time
t_{esr}	time to end of straight line on the square root of time plot or end of half-slope line on log-log plot, days
TOC	total organic content
t_{MBw}	water material balance time, day

t_{MBg}	gas material balance time, day
t_{pss}	time when the pseudo steady state starts
V_w	water volume, STB
V_{inj}	injected water volume, STB
V_{bm}	total matrix bulk volume, ft^3
v_p	pore volume
w_F	hydraulic fracture width, ft
w_f	natural fracture width, ft
w_{PF}	hydraulic fracture pseudo width, ft
WIP	water volume in place, STB
$WIBF$	water volume in both fractures (hydraulic and natural), STB
w	width of fracture, ft
x_e	effective well length (Effective perforated interval), ft
x_f	hydraulic fracture half-length, ft
y_e	reservoir half-length, ft

Greek symbols

λ_t	total mobility
ϕ	porosity, fraction
μ	viscosity, cp

Subscripts

esr	end of straight line of the square root of time plot or end of half-slope line of log-log plot
m	matrix (formation)
F	macro-fracture (hydraulic fracture)
f	micro-fracture (natural fracture)
g	gas
i	initial condition
o	oil
t	total system
HF	hydraulic fracture
NF	natural fracture
W	water

TABLE OF CONTENTS

Page

LIST OF FIGURES

Page

LIST OF TABLES

Page

CHAPTER I

INTRODUCTION

1.1 Introduction

Shale gas reservoirs have become an important source of energy in the United States due to the updated production techniques. Well stimulation treatment using frac water (slick water) in horizontal wells is the best practice in very low permeability shale gas reservoirs. Producing shale reservoirs through multi-transverse hydraulic fractures in horizontal wells is a standard production strategy in those reservoirs. However, the understanding of shale gas and frac water characteristics and behaviors are still inadequate and need for further investigation.

There have been many attempts to characterize multi-transverse hydraulic fracture horizontal shale wells including numerical, analytical, and empirical methods. The empirical method is the easiest for analysis; however, this method does not explain the characteristics of the reservoir and will not be used in this work. Numerical and analytical methods are usually applied separately and there is no comparison between the results from both methods.

The analytical method is used to analyze production data with tools like diagnostic and specialized plots. This method is easy and fast in obtaining values like permeability (fracture or matrix), fracture half-length and OGIP. The main disadvantage is it is based on single phase and the chosen model has to apply to the well at all times of production. This is not the case in shale reservoirs which are hydraulically fractured by frac water.

Also, reservoir mechanisms like capillary pressure, relative permeability and gravity segregation are not included in the model.

While the numerical method is considered the most accurate method for analysis, it is time consuming to analyze a number of wells. Nonetheless, it is a powerful tool if the correct model is selected. Two phase (gas and water) analysis provided more understanding of the current issues with water production. Reservoir mechanisms can be included to study their effect on the production data. A better understanding of both gas and water production data is possible using numerical methods.

Most shale wells are fraced then go through a flowback period which is followed by a shut-in period due to delay in bringing the well to sales as shown in **Fig. 1**. After shut-in period, the well is put on sale and this period is called the production period. In both numerical and analytical analysis, the focus is on gas production data and the post-frac water flowback and long-term water production data are often ignored. Flowback data (gas and water) is often ignored and sometimes is not reported. Even from production period, it is common to characterize the well by analyzing long-term gas production data only and water production is usually not included in the analysis.

In this study, it is believed that analyzing the fluid flowback data can complement analyzing the hydrocarbon production data. Therefore, water production data (flowback and production period) is a valuable tool that is used for analysis. We will bridge the gap between analytical and numerical methods by using analytical models in numerical analysis and removing the constraining assumptions.

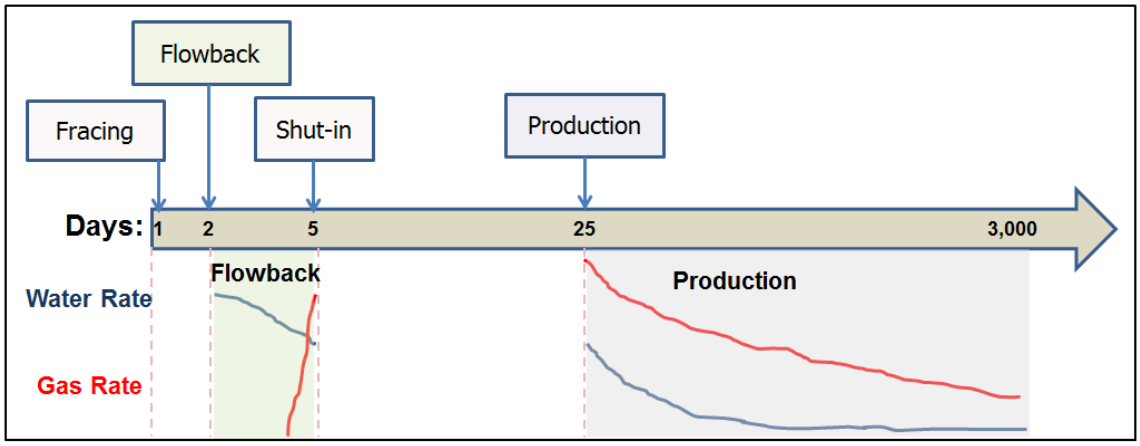

Fig. 1. The flow sequence of a usual shale gas well starts with a frac job. Then a flowback period has high water rates and gas would start after 2 to 5 days; some wells are shut-in due to a connection delay. Then production starts.

1.2 Problem Description

Hydraulic fracturing is a stimulation that involves pumping thousands of barrels of water with proppant and additives into the rock at high pressure. This fracturing fluid leaks off into the formation or is trapped in natural fractures due to high capillary pressure. Some of the remaining fluid imbibes into the formation creating an invasion zone.

Chekani et al. (2010) and many operators indicated that the percent of injected fluid recovered (load recovery) in shale gas wells ranges from 10 – 40%. At least 60 – 90% of the injected fluid is left in the reservoir. This study answered two questions: Where is the rest of the injected fluid that is not recovered, and whether it's trapped or imbibed? And how can flowback data be used in production data analysis to estimate fracture and reservoir properties?

1.3 Motivation

Motivation for this work initially derived from the lack of explanation for the low frac water recovery phenomena. This phenomena is seen in most shale gas wells and partially explained in the literature with widely contradicting assumptions and mechanisms. Also, water data is available for analysis but often ignored. The water data in the production period should be the true representation of the fracture system since it created those fractures.

As the research progressed, we noticed a lack of agreement across the different analysis methods and data and even sometimes contradictions. This motivated us to make our models and assumptions consistence with most methods and data as in Fig. 2.

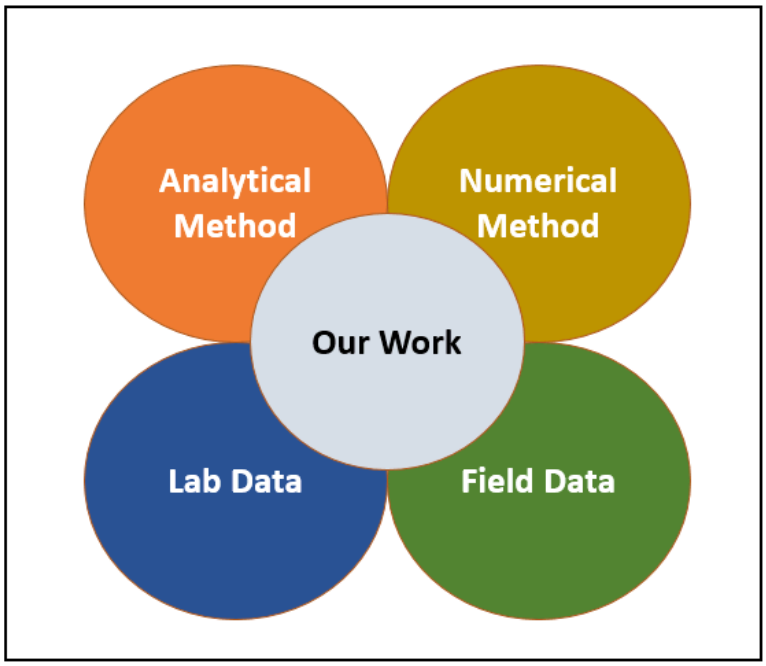

Fig. 2. Different fields of scientific methods and data are sometimes not in agreement unlike our research.

1.4 Research Objective

The objective of this research are as follows:

- Investigate various physical assumptions for water distribution scenarios in the fracture/matrix system to investigate trapping mechanism
- Estimate fracture properties using combined water flowback and long-term production data
- Present pitfalls of ignoring flowback period in production data analysis.

1.5 Organization of This Thesis

The study is divided into eight chapters. The outline and the organization of the dissertation is as follows:

Chapter I is an introduction of the dissertation which consists of problem description, motivation, and objectives.

Chapter II presents a literature review of shale characteristics, main flow regimes in shale gas wells, simulation of shale gas wells and water data analysis.

Chapter III consist of single phase (gas) simulation and a comparison between simulation and analytical solutions used in production data analysis with emphasis on linear and bilinear flow.

Chapter IV presents a two phase (gas/water) simulation to investigate water distribution in shale gas wells.

Chapter V describes a new method that is developed to estimate effective fracture volume using water data in shale gas well.

Chapter VI shows applications of the proposed methodology using single well data.

Chapter VII applies the proposed methodology using multi well data.

Chapter VIII presents conclusions and recommendations.

CHAPTER II

LITRETURE REVIEW

2.1 Introduction

In this chapter, the different flow regimes that are present in gas production data are reviewed with an emphases on rate transient analysis. Also, a review of the main papers that use simulation as means of analysis for shale gas and water data. A comprehensive review of the main characteristics that effect water and gas distribution in shale reservoirs and newly applied concepts like permeability jail. At the end, a review of papers that analyze water data in shale wells.

2.2 Flow Regime Analysis

Shale gas wells have a very low permeability making it hard to use conventional pressure transient for analysis, which shifted attention to production data analysis as a means to calculate permeability, area of flow and OGIP (Original Gas in Place). Pressure transient testing uses constant rate solutions and production data analysis uses constant pressure solutions.

In production data analysis, the log-log plot is used to identify different flow regimes and other specialized plots like square root of time. The flow regime either can be transient (linear, bilinear) or BDF (Boundary Dominated Flow). Each flow regime as a distinct signature on different plots and Fig. 3 shows the three different flow regimes.

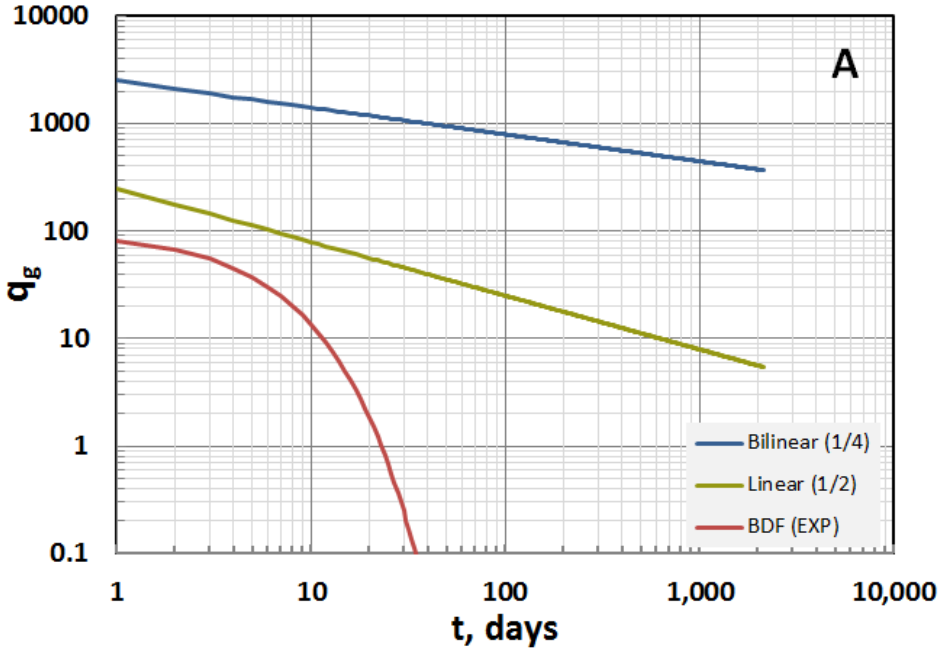

Fig. 3. Signature of different flow regimes in the transient (linear, bilinear) and BDF in synthetic gas well data.

Each flow regime can be explained in relation to reservoir characteristic like matrix, natural fracture and hydraulic fractures. In the next section, the three main flow regimes will be reviewed with the application of rate transient analysis.

2.2.1 Linear Flow

Linear flow solutions of constant pressure case in rectangle area were first adapted into multi-transverse hydraulic fractured gas wells to analyze production data by El-Banbi and Wattenbarger (1998). It is indicated that the transient linear flow type curve for constant pressure and constant rate cases are different. End of linear flow or end of half-

slope line is specified as $t_{Dye} = 0.5$ for constant rate case and $t_{Dye} = 0.25$ for constant pressure case. Using both slope of square root of time plot and end of the half-slope line in log-log plot of constant pressure case to interpret production data are introduced and utilized to analyze gas in-place without assuming thickness, matrix permeability and porosity.

Arevalo-Villagran et al. (2001) showed the production analysis of long term linear flow in tight gas wells. This production data for tight gas well shows transient linear flow for long time because this linear is represented by the flow from matrix to high permeability of fractures.

Ibrahim and Wattenbarger (2005) showed the effect of drawdown on transient linear flow of gas and proposed the correction factor according to the level of drawdown in constant pressure condition. Correspondingly, both the slope in square root of time plot equation and time end of transient linear flow period are used with the correction factor.

In horizontal multi-fraced shale wells, transient linear flow is dominant in the early part of the production profile. Transient linear flow would be shown as a half slope on the log-log plot and a straight line on the square root of time plot. Transient linear flow can occur in the hydraulic fracture, but is not likely since the hydraulic fracture has a high permeability and the linear flow will end quickly. Matrix linear flow in a homogenous reservoir can last longer which is more likely to be the case.

2.2.2 Bilinear Flow

Dual porosity model of a naturally fractured reservoirs was first introduced by Warren and Root (1963). Warren and Root showed the analytical solution of a naturally fractured, radial, infinite-acting reservoir in Laplace space and approximation in real domain. The model assumed as an idealized sugar cube with pseudo-steady state flow in matrix system. The solution was applied for pressure transient testing of two composing mediums which has naturally fractures or vugular reservoir. In the naturally fractured system, the primary porosity is the matrix porosity which has high storativity and low flow capacity and the secondary porosity is the fracture system which has low storativity and high flow capacity.

Kazemi (1969) proposed a dual porosity model with matrix transient flow using s numerical solution. The model is represented by slab matrix and horizontal fracture model of radial closed reservoir which has a logarithmic grid size for matrix layers and a thin layer of fracture. The new transient dual porosity and pseudo-steady state dual porosity models give similar results except the transition period in the semi-log plot for both drawdown and buildup test.

De Swaan O. (1976) developed an analytical solution for the radial infinite acting naturally fractured reservoir for the early and late time regions. The model assumes transient flow from the matrix system to fracture system. The results shows two parallel straight lines. There is no analytical description of the transition period between two straight lines.

Serra et al. (1983) developed an analytical solution for dual porosity system in Laplace space and approximation in real domain. The model assumes the radial infinite slab reservoir with equally spacing horizontal fractures same as De Swaan O. (1976) and transient flow in matrix model. Three flow regimes were introduced. Regime 1 and 3 are the classical two straight lines in semi-log plot as discussed earlier. Regime 2 was introduced to represent the transition between two straight lines.

Previously, dual porosity model was intentionally used in naturally fractured reservoirs. Later, this model has been adapted to use for a multi-transverse hydraulically fractured horizontal well which has two different storage and flow capacity systems. In this case, the secondary porosity is characterized by hydraulic fractures.

Bello and Wattenbarger (2010) presented a mathematical model for analyzing multi-transverse hydraulic fractures in horizontal shale gas well. This model is based on linear dual porosity model presented by El-Banbi and Wattenbarger (1998). Five flow regions and their asymptotic equations are presented by solving analytical solution in Laplace space for both constant rate and constant pressure and bilinear flow is one of those flow regions.

Bilinear flow is one of those flow regions that represent two linear flows existing at the same time and perpendicular to each other. Transient bilinear flow or a quarter-slope line in the log-log plot is also found in production data. The assumption is that it is linear flow in matrix and hydraulic fracture or in matrix and natural fracture or in natural and hydraulic fracture and more can be found in (Tivayanonda et al. (2012)).

2.2.3 Rate Transient Analysis

Production data analysis started gaining acceptance as an equivalent methodology in the theory and procedure to the pressure transient analysis. The constant pressure type curves were the counterpart of the well test constant rate curves. Although both constant rate and constant pressure type curves are valuable tools for the analysis of production data and well test data, neither of their assumptions is the case of the typical gas well. The production conditions through the life of a gas well has variable rate and pressure.

Cooper and Jacob (1946) developed a method for analyzing pressure data of aquifers pumped at variable discharge rate. Everdingen and Hurst (1949) applied the principle of superposition to solve variable pressure and variable rate cases.

Ramey (1965) and then Winestock and Colpitts (1965) introduced the method of normalized drawdown method. The method is applied by graphing the $\Delta p/q$ vs. the logarithm of the production time. The authors noticed that the reciprocal of the productivity index $\Delta p/q$ is often a linear function of the logarithm of producing time. The method theoretically exhibits a straight line whenever the radial flow regime dominates and it provides useful results if the pressure data of the producing well are to be analyzed.

Jargon and Van Poollen (1965) proposed a superposition based method in order to analyze variable rate and variable pressure well tests. The approach converted varying flow rate data to constant rate pressure response and called the unit response function.

2.2.4 Boundary Dominated Flow

Palacio and Blasingame (1993) developed a type curve that gives the performance of constant rate and constant pressure gas flow solution. They presented the material balance time function and algorithm that can lead to harmonic decline and used to analyze gas production data of either gas or oil using type curves analysis. When the well reaches boundary dominated flow regime, gas in place from variable rate or variable pressure production data can be calculated.

El-Banbi and Wattenbarger (1998) presented an analytical method of analysis for gas fractured wells in which the linear flow is dominant with late boundary effect. The authors developed equations for transient linear flow for both constant pressure and constant rate cases. Once the boundary dominated flow started then the OGIP, drainage area and the value of ($\sqrt{k}\, x_f$) can be calculated.

2.3 Simulation of Shale Reservoirs

In most shale simulation papers, two options are used to simulate shale reservoirs. Dual porosity and permeability using shape factor which is very easy to use since fracture spacing does not affect the gridding and it is only a number in shape factor calculation. But this method is not accurate in shale wells since the flow between matrix and fracture is governed by pseudo steady state flow equation ignoring the transient period which might be a year or more in most shale wells. Rubin (2010) used the CMG simulator to show that the standard Dual Porosity and Permeability (DPP) is unable to properly capture very low permeability shale reservoir. This option will not be used in this work.

The second option is single porosity and altering porosity and permeability to account for fracture properties. This work is time consuming but will accurately simulate early and late parts of shale gas wells production according to Rubin (2010). Most papers published in simulation analysis lack the field application and are not crossed checked with analytical solutions due to assumptions in the latter. In most presented work, the transient period is ignored in the analysis.

Cheng (2010) simulated a two phase, single porosity model with reservoir mechanisms like relative permeability, capillary, gravity segregation and invasion zone. Cheng concluded that shut-in does not affect long-term gas production which is not like what others reported. Cheng attributed imbibition of water into the matrix as the main factor for the lost water. Also, shut-in will reduce cumulative water production due to capillary forces. Although, naturally fractured cases were simulated, they were not discussed in detail. Moreover, water saturation in the system after the production was not studied to construct a sound theory of the location of the lost water. In addition, analytical solution was not used as comparison tool with the production results from the simulation.

Gdanski and Walters (2010) simulated the different factors that affected water load recovery like dimensionless fracture conductivity, matrix relative permeability quality and shut-in times. The author did not investigate water distribution in the fracture and gravity segregation. The author concluded that the quality of relative permeability affected good or poor the water load recovery performance. Pressure drawdown of the well had a minor effect if compared to fracture conductivity. Shut-in had no significant impact on gas production.

Clarkson (2012) presented an excellent paper that analyzed and simulated water flowback at early times (hourly data). The author presented a method for calculating fracture permeability and half length using pseudo steady state assumptions in the fracture using early water flowback data. The model did not assume any natural fractures. Although water data was available from the production period, the author only analyzed gas production data and compared the results of early water data with gas production data.

Sharma and Agrawal (2013) studied the effect of liquid loading on well productivity in the hydraulic fracture. One of the main conclusions is that more water can be recovered in a short height fracture compared to long height due to less contact area for water to imbibe (in short height case). Although the authors used large fracture width of 0.1 ft, fracture width variation was not part of the investigation. The authors stated that peak gas production might be harmed by shutting in the well for a long period due to the imbibition effect which will give a low water and gas cumulative.

Shaoul et al. (2011) demonstrated the effect of varying relative permeability curves on production. In the weak relative permeability case where water and gas curves cross at k_r = 0.001, initial gas production rate is reduced removing the transient period and slow recovery process. The authors reported that in the strong permeability jail where water and gas curves do not cross, no water or gas flow.

2.4 Characterization of Shale Reservoir

In this section, a summary of most parameters that play an important role in characterizing shale formation. Shale is different in most aspects from the conventional formation which

will affect water injection and flowback. This summary will help in understanding the challenges facing the simulation of shale wells and will confirm some ideas that will be used later in the research.

2.4.1 Capillary Pressure

In low permeability reservoirs like shale, capillary pressure can be as high as 2000 psi due to small pore size Penny et al. (2006). Since hydraulic fractures have large permeability and width (hence, fracture conductivity), capillary pressure is very small and can be ignored. But, it will play an important role in natural fractures and matrix because capillary pressure will be the force needed to imbibe water into the matrix and then to hold water in the natural fractures.

Arogundade and Sohrabi (2012) concluded that conventional methods of capillary pressure analysis are impractical in shale reservoirs because of the very low connate water saturation and higher capillary pressure. It is usually recommended to combine more than one method in order to reliably estimate capillary pressure curve over a range of water saturation when analyzing shale gas reservoirs.

2.4.2 Relative Permeability Curve

Most literature considers conventional relative permeability as the correct representation for shale formation due to the lack of lab studies. A few papers present relative permeability as lower than the conventional curves. The problem with

conventional curves is that it considers any increase in the formation's water saturation as a lower gas relative permeability. This contradicts with current practices when water is exposed to the shale matrix and it not only does not reduce gas relative permeability but even sometimes enhance gas flow if the well is shut-in.

2.4.3 Permeability Jail Concept

In an effort to explain observed data in the field, a relative permeability curve called permeability jail concept is adapted and derived from low permeability sandstone literature. Blasingame (2008) stated that the reality of poor well performance is explained by the concept of permeability jail. Due to the over burden stress and partial water saturation, relative permeability of a low permeability reservoir can change. As in Fig. 4, permeability jail describes the saturation region across which there is negligible effective permeability to either water or gas (Shanley et al. 2004).

In conventional formations, critical water saturation and irreducible water saturation occur at similar values, but in low permeability formation, they occur at very different water saturation values. In conventional formation, the lack of water production implies the formation is at or near irreducible water saturation. However in a low permeability formation, the lack of water flowback that is due to water saturation is less than the critical water saturation, and not due to the fact that the water saturation is equal to the irreducible water saturation. The potential of using the permeability jail concept will be investigated in this study.

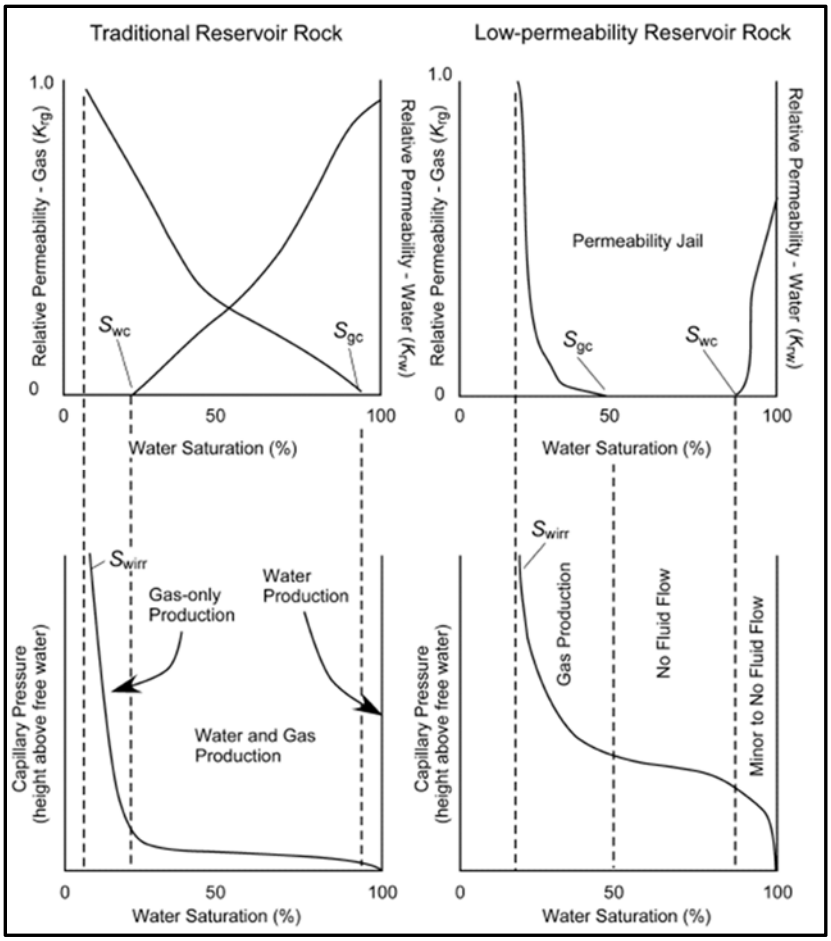

Fig. 4. The relative permeability and capillary pressure in conventional gas formation with irreducible water saturation and critical water saturation are at different values; low permeability gas formation with irreducible water saturation are very small compared to critical water saturation (Shanley et al. 2004).

2.4.4 Water Imbibition

Several studies are presented on water imbibition in shale but only studies with shale samples are presented since some of the papers used low permeability sandstone as an analogy to shale samples.

Odusina et al. (2011) is one of the few studies that did an experiment on 1inch by 1 inch core but reported natural fractures present in the sample, which might show the imbibition effect is from the fractures and not the matrix as shown in Fig. 5. The author concluded that Eagle Ford and Barnett showed preference to water imbibition. Wang et al. (2010) conducted an imbibition study on thin core (1 to 5 mm) that is from a shale outcrop. The author reported mineral dissolution (fracture) and cracking due to clay swelling during imbibition process. This shows that the test is greatly affected by the micro-fractures not the matrix.

Some studies attribute the lost frac water to water imbibition, although a thin section is used where induced fractures are created and no overburden stress which will reduce the pore throat size and will reduce imbibition. Upscaling lab results from those thin sections, to a large field scale carries a large risk.

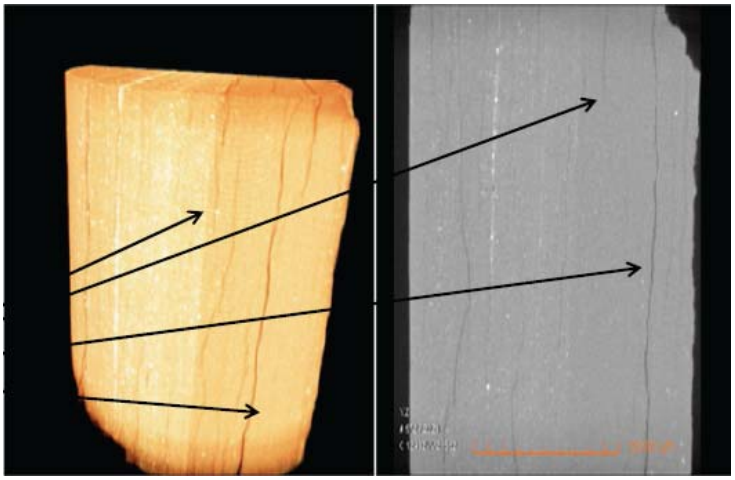

Fig. 5. Image of Barnet shale samples showing the micro fractures with a width around 0.00001 ft which were created after the imbibition process showing that imbibition is mainly due to induced natural fractures, Odusina et al. (2011).

2.4.5 Core Data Analysis

Most shale formation core analysis reported in literature are performed on a very small core with the presence of natural fractures which makes the experiment results show the characteristics of natural fractures instead of the matrix. A common method for analyzing shale samples is to make a "disaggregated sample" where the rock sample is ground and the material is sieved to the desired size range, Pagels et al. (2012). This method will alter the matrix's original properties and cannot be a real representative of the formation matrix.

Also, an imbibition experiment by Roychaudhuri et al. (2011) was performed on 1 cm by 1 cm surface of the sample testing for imbibition. The authors reported that the test was on matrix and induced fractures but could not distinguish between the contribution of each system. Wang et al. (2010) used a very thin core with a thickness of 1 to 5 mm and created micro-fractures during the test as in Fig. 6.

Most studies presented either altered from original status or do not mimic the real case due to lab difficulty.

Fig. 6. Cracks (induced fractures) that developed during water imbibition, Wang et al. (2010).

2.4.6 Mineralogy and Wettability

Chalmers et al. (2012) showed a mineralogical ternary diagram of the different mineral for shale formations like Barnet, Haynesville, Woodford and Marcellus as in Fig. 7. Most of these formations consist of mainly clay and quartz. A significant portion of the pore geometry is contained as voids in the organic material. The walls of the organic matters are not water-wet since they were created by the generation of gas and never contained water. Unlike organic material, clays are water-wet.

Roychaudhuri et al. (2011) performed water imbibition on shale sample and concluded that both clay and organic content percentages have an effect on imbibition. If the samples has less clay and more total organic content (TOC), it imbibes less water and vice versa. The reason for this is that clays are usually water-wet which causes more water

to be attracted to the matrix surface. On the other hand, organic matters are not water-wet so they actually repel water, their presence causes more water to be repelled off the matrix surface.

This section is presented to show that although we simplify numerical model to water wet only, reality is more complex in shale due to the presence of organic matters that affect wettability. Also, this supports the concept that shale formation has a complex heterogeneous wettability system.

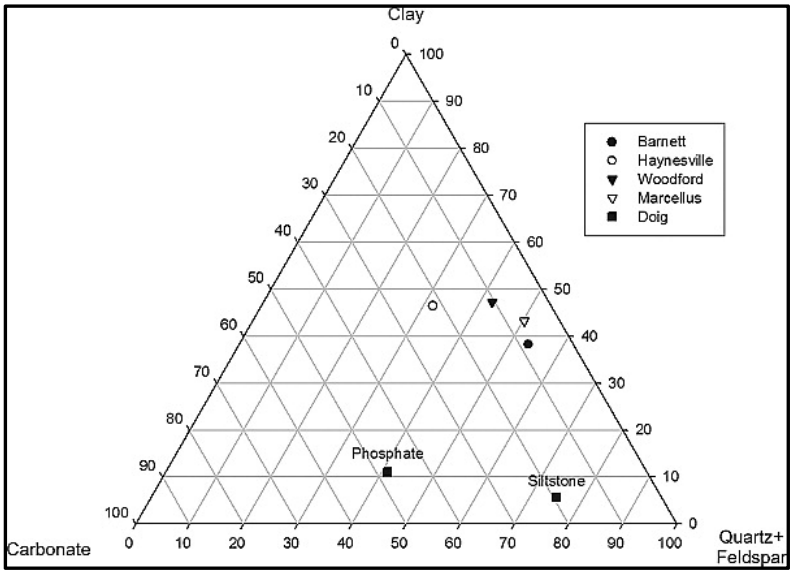

Fig. 7. Mineralogical ternary diagram showing the composition for several shale formation with a high percentage in clay and quartz as in Barnett, Haynesville, Woodford and Marcellus, Chalmers et al. (2012).

2.4.7 Frac Fluid

Frac fluid has several additives; one of the main ones is surfactant which alters water-matrix interaction. Surfactant is a surface agent which will establish a favorable wettability and a lower surface and interfacial tension which can prevent water blockage. Non-ionic surfactants are used in fracturing to enhance water recovery. In a water-wet surface, an additive that makes the surface more not water-wet may be used so water can be easily expelled or not imbibe in the first place.

Also, surfactant can be used in microemulsion (ME) which is a thermodynamically stable combination of surfactant, solvent or oil and water. It is shown that ME can enhance water recovery by altering the wettability of the fracture face or the surface tension between gas and water. King (2010) reported that the addition of microemulsion to the water would lower the capillary pressure to about 300 psi instead of the high 3000 psi in low permeability rock. The addition of these additives increase the heterogeneity in the fracture face wettability and reduce imbibition.

2.5 Water Data Analysis

Water data analysis literature is mainly for very early data of 1 day and reported by hour and some papers analyze water in the production period ignoring early data.

Abbasi et al. (2012) developed a mathematical model based on material balance equation and diffusivity equation for radial flow. The authors divided the flowback period into three regions: water dominated, transition, hydrocarbon dominated. The model is based on water dominated region and gas compressibility is neglected, but the analysis is

using data from all three regions. A radial fracture volume can be calculated if the fracture permeability is known. Fracture permeability is not known unless an early linear flow is presented which is not usual.

Crafton (2008) simulated the flowback period effect without including parameters like capillary and gravity segregation. Through experiments and flowback data, Crafton concluded that the use of the "Load Recovery" metric is a very misleading performance indicator. This analysis focuses on the first four days of production period "Flowback Period" ignoring the long-term production period.

Crafton (2010) observed that in many wells the time from stimulation shut-in until first production has an important impact on early-time and ultimate performance, sometimes adversely, sometimes beneficially. However, shut-in effect on flow regime identification was not shown.

Noe and Crafton (2013) concluded that shut-in or the delay from the end of stimulation until first production is harmful which is contrary to widely executed practices and beliefs. The duration of the shut-in has no obvious correlation to the severity of the damage arising from the shut-in. The authors based his conclusions on changes in fracture half length before and after the shut-in. Thompson et al. (2010) observed that flowing back lower load recovery resulting in a better wells which is contradictory to Crafton's finding.

2.6 Summary

A comprehensive review the main fields of analysis was presented. This review was needed since this project covers different areas of analysis.

CHAPTER III

SINGLE PHASE SIMULATION

3.1 Introduction

In this chapter, single phase gas model is analyzed for linear and bilinear flow and comparing the model with production data analysis using analytical solutions. The main limitation of linear flow model in analytical solution is the assumption of no natural fractures will be investigated using a numerical model. Also, Modifications for gridding fractures are presented.

3.2 Linear Flow Model

El-Banbi and Wattenbarger (1998) developed a model for linear flow and later was modified to fit horizontal multi-fraced shale wells transient linear flow as in Fig. 8.
In horizontal multi-fraced shale wells transient linear flow is dominant in early period of the production profile. Transient linear can occur in hydraulic fracture which is not likely since it has high conductivity. Matrix linear flow in a homogenous reservoir can last longer which is more likely to be the case. The interpretation of homogeneous linear flow solution focuses only for linear flow from matrix block to hydraulic fractures. The flow in hydraulic fractures is not considered because of assuming infinite conductivity of hydraulic fractures.

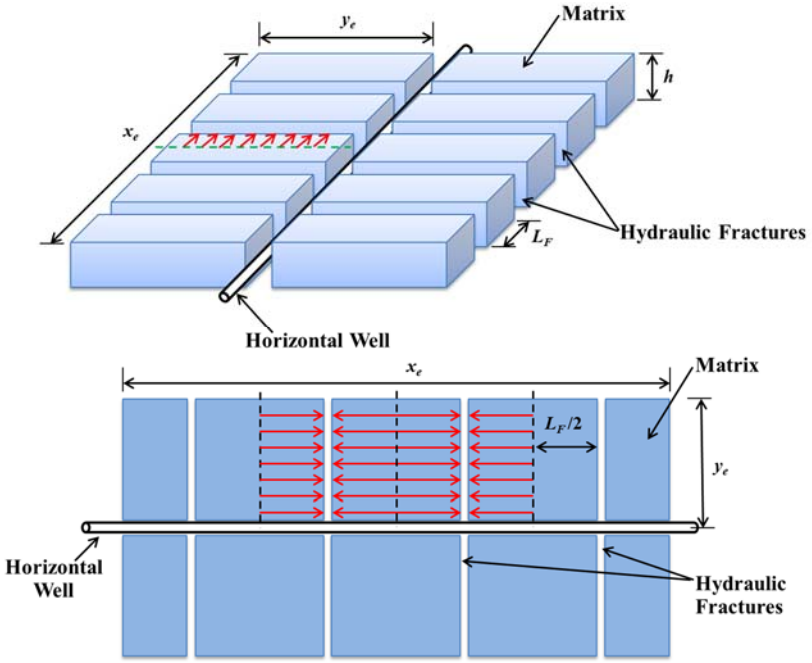

Fig. 8. Matrix linear flow in multi-transverse hydraulic fractures horizontal well.

Fig. 9 shows dimensionless solution for linear flow from El-Banbi and Wattenbarger (1998), both constant rate and constant pressure cases are presented. An important feature of the type curve is the end of the infinite acting (transient) linear flow. Linear flow is the straight line with slope of ½ for both cases which ends at t_{Dye} = 0.25 (constant pressure) and at t_{Dye} = 0.5 (constant rate). These values are taken to be values where the curves visually depart from straight lines, making them useful for identifying the end of linear flow period. Using the definition of dimensionless time and the end of linear flow, a matrix effective permeability is derived as shown below in Eq. 3.1. This equation depends on two parameter only, L_F which is hydraulic fracture spacing and t_{esr}

which is the end of straight line of the square root of time plot. Appendix A shows detailed procedure for analyzing shale gas wells using analytical solution.

$$k_{eff} = \frac{9.87\ \theta\ \mu\ c_t\ L_F^2}{t_{esr}} \qquad \text{..... (3.1)}$$

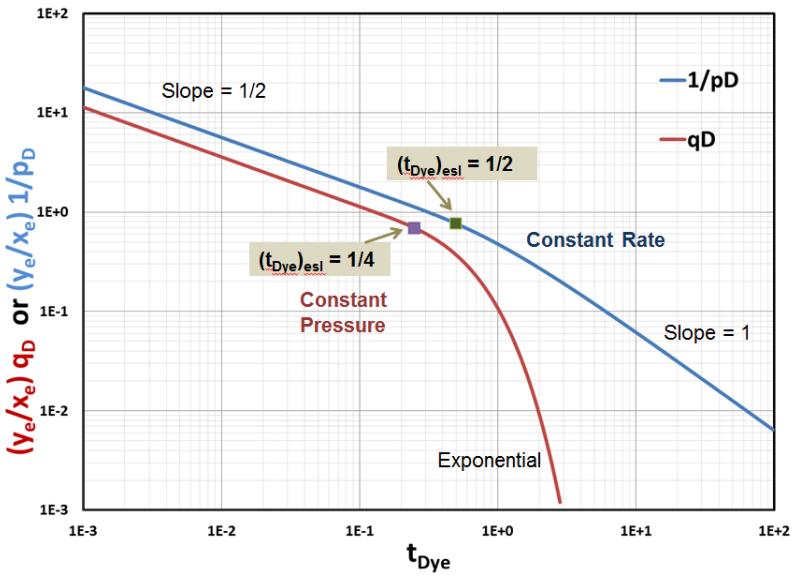

Fig. 9. Dimensionless linear flow type curve for constant rate (*pD*) and constant pressure (*1/qD*) with the end of linear as the visual departure from straight line.

As can be noticed, the model does not consider any natural fractures in the matrix and assume that the matrix is homogeneous. This is not the case in actual shale gas wells which is dominated by natural fractures. Natural fractures are effected mainly by two factors conductivity and spacing and both will be investigated. Numerical models will be used to investigate the presence of natural fracture and its effect on the analytical assumption.

3.3 Linear Flow Simulation

CMG (IMEX) simulator was used to model 2-D areal fractures with only gas flowing. Typical Barnett shale properties are used as in **Table 1**. Since all hydraulic fractures are symmetric, only one fracture is modeled and scaled to the full well size. Fig. 10 shows the simulated segment with hydraulic fracture spacing as L_F.

Table 1 – Shale gas simulation properties

Initial pressure, p_i (psi)	3000	Fracture & matrix porosity, φ (fraction)	0.06
Flowing BH pressure, p_{wf} (psi)	500	Reservoir thickness, h (ft)	300
Specific gravity, SG_g	0.65	Matrix permeability, k_m (md)	1.5×10^{-4}
Water saturation, S_w	0.3	Natural Fracture Conductivity, C_{nf} (md-ft)	0.001
Reservoir temperature, T (°R)	620	Hydraulic Fracture spacing, L_F (ft)	500
Total compressibility, c_t (psi^{-1})	2.199×10^{-4}	Fracture half length, x_f (ft)	550

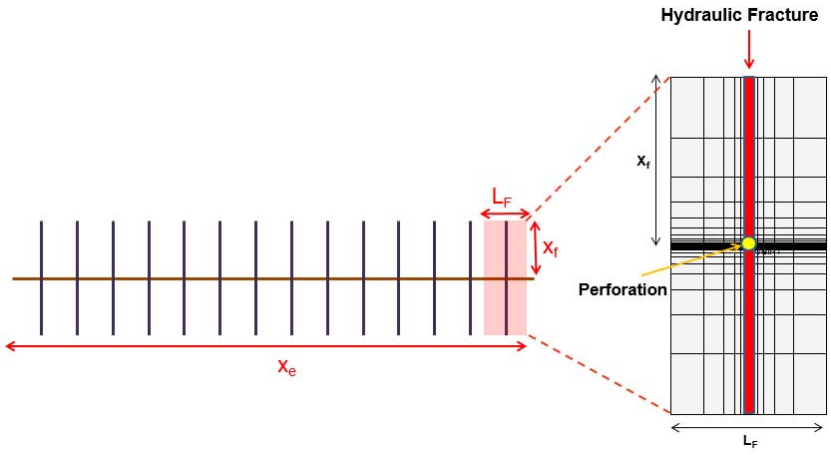

Fig. 10. Simulating only a segment of a hydraulic fracture as shown on right and then scaled to full shale well.

Natural fractures are simulated to investigate the limitation of the analytical solution for excluding natural fractures. Two major system used in this simulation, Hydraulic Fracture and Matrix (*HF-M*) and Hydraulic Fracture, Natural Fractures and Matrix (*HF-NF-M*). The *HF-M* system is exactly the same as the analytical solution which can be compared directly. But, *HF-NF-M* system will have linear flow from (*NF-M*) toward *HF* only if the natural fracture have a low conductivity and large spacing.

Fig. 11 shows the three cases simulator, first case of *HF* which is exactly like the analytical solution. Second case *HF-2NF* has two low conductivity and largely spaced natural fracture and third case has eight natural fractures.

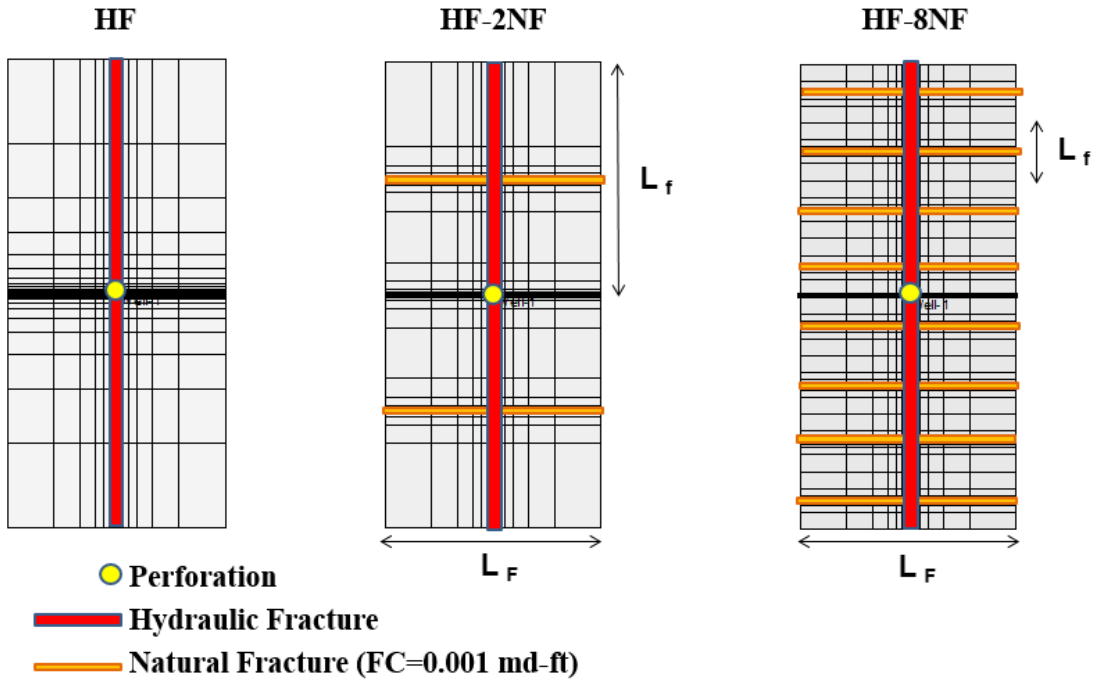

Fig. 11. The different cases for a symmetrical segment of shale well. No natural fractures (*HF*), two natural fractures (*HF-2NF*) and eight natural fractures (*HF-8NF*). These three cases were used for simulation and analysis.

The simulation results of the three cases are shown in Fig. 12. Gas production curves are shown for hydraulic fracture with homogenous matrix, two natural fracture and eight natural fractures. All the curves have the same production profile since *NF* has a low conductivity and the natural fracture spacing is large. Fig. 12 suggests that all the three cases can be evaluated as symmetrical reservoir elements, which is the analytical assumption. Although the *HF-NF-M* case does not correspond to the analytical solution assumption, it can be approximated as a homogeneous *HF-M* as long as *NF* has low conductivity and large natural fracture spacing, L_f.

In Fig. 12, a transient linear flow from matrix to hydraulic fracture can be observed in *HF-M* case (no natural fractures). Also, transient linear flow from both matrix and natural fracture to hydraulic fracture can be observed in both cases *HF-NF-M*. Although natural fractures are contributing to the flow, their effect is not significant to divert from the homogenous case *HF-M*.

At the end of linear flow, the effective permeability which depends on end of linear flow time (t_{esr}) can be calculated using Eq. 3.1. The value of calculated k_{eff} will be equal to k_m = 1.5 x 10^{-4} md for all three cases. This effective permeability can also be defined for natural fracture as shown in Eq. 3.2. If the *NF* has a low conductivity or L_f is large (widely spaced natural fracture) then $k_{f,eff} = k_m$ and the homogenous analytical solution can be applied. This example clearly supports the use of the homogenous analytical solution in shale reservoir which might have low conductive and widely spaced natural fracture.

$$k_{f,eff} = \frac{k_m L_f + k_{f,in} w_f}{L_f} \quad \text{..... (3.2)}$$

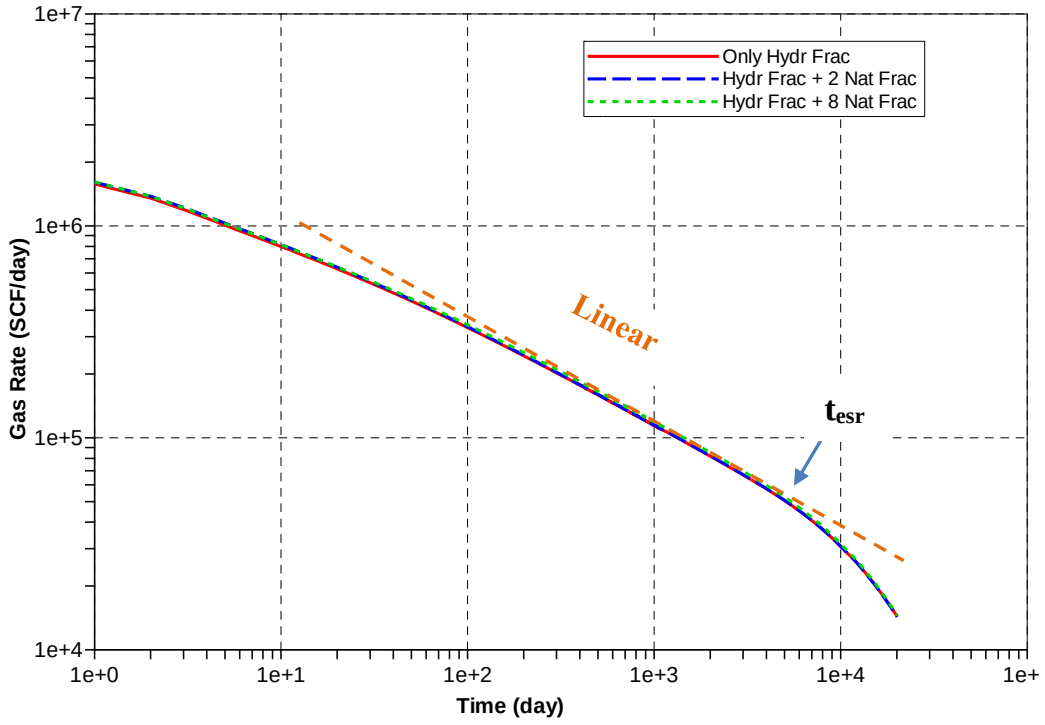

Fig. 12. Simulated curves of the three cases, (*HF*, *HF-2NF*, and *HF-8NF*). The linear flow is transient flow in the matrix toward the *HF*. The *NF*s show no effect on rates because of relatively low *NF* conductivity and large *NF* spacing.

3.3.1 Ignoring Natural Fracture

This analysis is presenting a method for ignoring the effect of natural fractures because they are largely spaced and low conductive. The answer using both analytical solution and simulation will be the same. Two ways to use the analysis: production data or natural fracture data.

In the production data method, the engineer will use Eq. 3.1 with the linear production data (t_{esr}) to calculate k_{eff}. If $k_{eff} = k_m$ which is calculated from core or known from other wells, then natural fracture effect can be ignored.

In the natural fracture data method, the engineer will use image log or an outcrop to measure natural fracture spacing, L_f and other methods to calculated natural fracture conductivity (induced). Using Eq. 3.2 $k_{f,eff}$ can be calculated, if $k_{f.eff} = k_m$, then natural fracture effect can be ignored. This method is not practical and is uncertain. The production data method is recommended.

Based on the presented methods, the engineer can determine if the effective permeability has a value close to matrix permeability. If that is the case, analytical solution and simulation can be used to analyze the linear flow regime and will give the same results. In next sections, the case of high conductivity and small spacing natural fractures will be presented.

3.4 Bilinear Flow Simulation

In some shale gas wells, a transient bilinear flow or a quarter-slope line in the log-log plot of gas rate vs. time is also found. Analyzing the data and comparing it to the analytical solution can cause some errors since the analytical solution has an assumption for the bilinear flow case. The bilinear flow assumption in analytical solution is matrix only flowing to the natural fracture then the natural fracture flows to the hydraulic fracture. Permeability of matrix perpendicular to the hydraulic fracture is equal zero in analytical solution as shown in Fig. 13. This restriction is necessary to create the bilinear signature

that is observed in production data. In practical simulation procedure, matrix flow toward hydraulic fracture cannot be ignored.

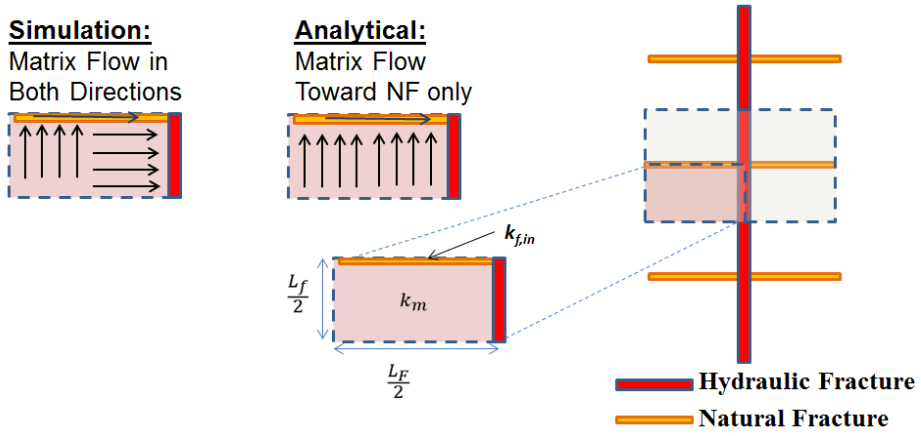

Fig. 13. In bilinear flow, Simulation has no restriction for matrix permeability and analytical has matrix permeability flow toward natural fracture only; a diagram showing the geometry of a quarter natural fracture that was simulated.

As shown in Fig. 13, quarter of natural fracture is simulated with two case; accounting for k_m in both direction and setting $k_m = 0$ in hydraulic fracture direction as assumed in analytical solution. Aspect ratios for spacing and permeability are used to set a cut line as when to use each method as shown below in the equations. If R_{sp} is small, then we have more natural fractures with a small spacing.

$$R_{sp} = \frac{L_f}{L_F}; \text{ and } \quad R_k = \frac{k_m}{k_{f,in}} \qquad \text{..... (3.3)}$$

Appendix A shows a relationship between the different aspect ratios which was derived from analytical solution presented in Tivayanonda et al. (2012). Notice that natural

fracture permeability is defined differently in analytical and simulation. In analytical since the matrix is a source term, the fracture permeability is C_{nf} averaged over L_f but in simulation it is the intrinsic (inside) permeability of the fracture grid $k_{f,in}$.

The different simulated cases are shown in Table 2. In cases (1-A & 2-A), matrix permeability is isotropic and in cases (1-B & 2-B) matrix permeability in the direction of hydraulic fracture is zero as in the analytical solution assumption. Low spacing ratios are used to represent heavily fractured shale with low natural fracture spacing as in case 4. In most cases, R_k is very low due to the low matrix permeability.

Table 2 - Aspect ratio for bilinear flow simulation cases

Case	k_m (*M-NF*), md	k_m (*M-HF*), md	R_k	R_{sp}
1-A	1.5E-08	1.5E-08	1.5E-08	1
1-B	1.5E-08	0	1.5E-08	1
2-A	1.5E-04	1.5E-04	1.5E-08	0.1
2-B	1.5E-04	0	1.5E-08	0.1
3-A	1.5E-08	1.5E-08	1.5E-08	0.05
3-B	1.5E-08	0	1.5E-08	0.05
4-A	1.5E-07	1.5E-07	1.5E-07	0.005
4-B	1.5E-07	0	1.5E-07	0.005

The result of all simulated cases are shown in Fig. 14 to Fig. 17. In Case 1 and 2 as shown in Fig. 14 and Fig. 15, no bilinear flow is observed in (1-A & 2-A) due to the

effect of flow of matrix toward the hydraulic fracture which will mask the bilinear flow even though k_m is low. In cases (1-B & 2-B), bilinear flow is reproduce since $k_m = 0$ in the hydraulic fracture direction as in the analytical solution assumption. These cases clearly show that the analytical solution is not valid for these aspect ratios since it is forcing the solution to have bilinear when it is not the case as in (1-A & 2-A).

In cases 3 and 4 as in Fig. 16 and Fig. 17, bilinear is observed in both A and B which make both simulator and analytical solution applicable. As the values of R_{sp} get low, the bilinear flow become longer and at later time if compared to higher values. In the low values of R_{sp} , the area of hydraulic fracture exposed to matrix flow is low which makes the effect of matrix flow negligible.

Since most shale gas wells has a hydraulic fracture spacing between 100 ft, a value of $R_{sp} = 0.05$ (start of bilinear) would have a minimum natural fracture spacing of 5 ft. To flow the well in bilinear flow, natural fracture spacing has to be small and highly conductive. In shale reservoirs with natural fractures that are high in conductivity and small in spacing, bilinear flow can be established and both simulation and analytical solution can be used.

From previous section, natural fractures with low conductivity and large spacing will produce linear flow and both simulation and analytical solution should give the same answer. In this section, natural fractures with high conductivity and small spacing will flow the well in bilinear flow and both simulation and analytical solution can be used. For any case in between, the analytical solution should not be used and only simulation should be used.

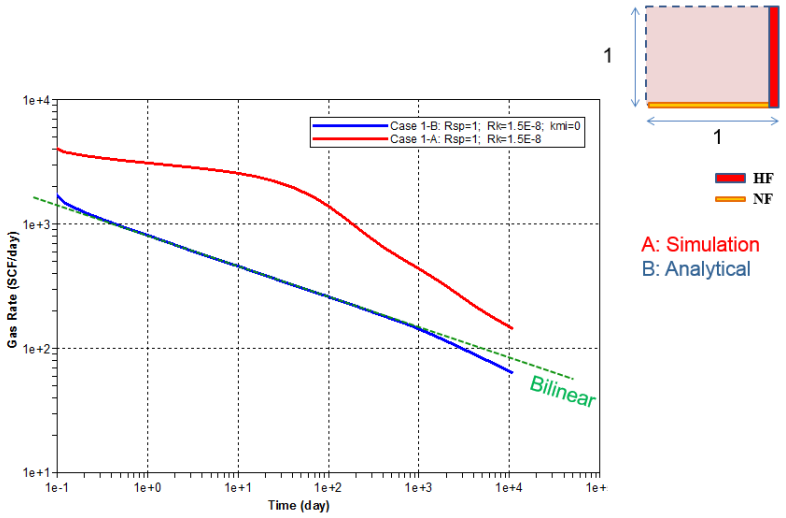

Fig. 14. Production curve for analytical and simulation case for R_{sp} = 1; the simulation case does not show bilinear flow due to flow from matrix to hydraulic fracture that is ignored in analytical solution.

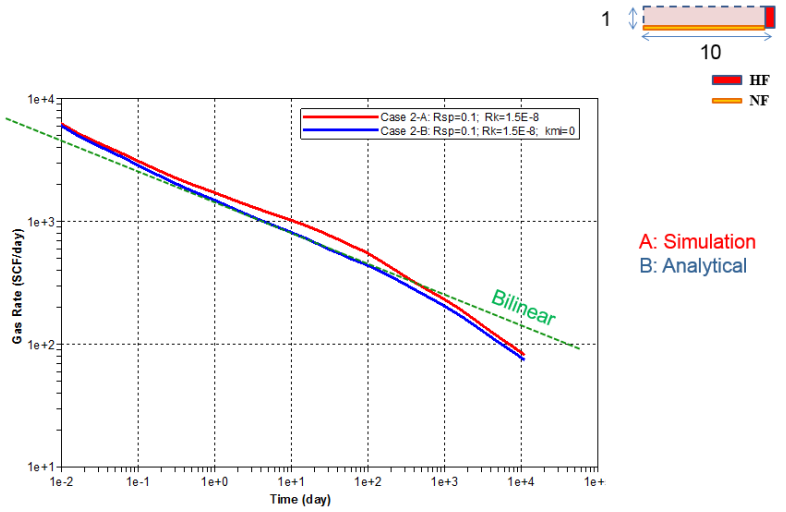

Fig. 15. Production curve for analytical and simulation case for R_{sp} = 0.1; the simulation case does not show bilinear flow due to flow from matrix to hydraulic fracture that is ignored in analytical solution.

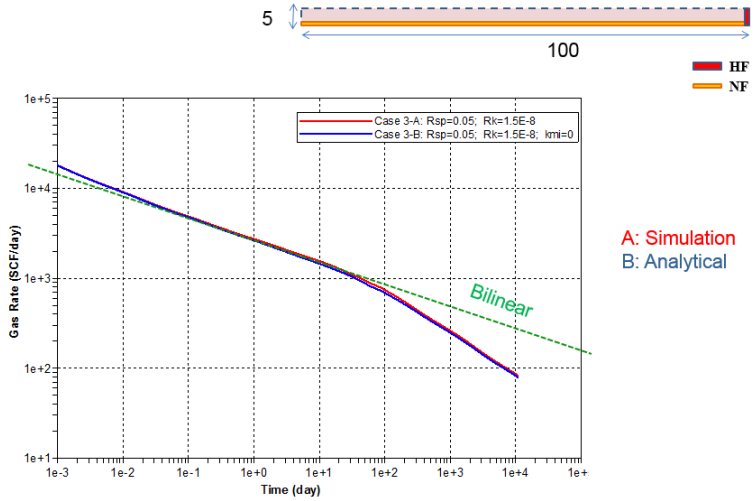

Fig. 16. Production curve for analytical and simulation case for R_{sp} = 0.05; the simulation case shows bilinear flow and is matching analytical solution.

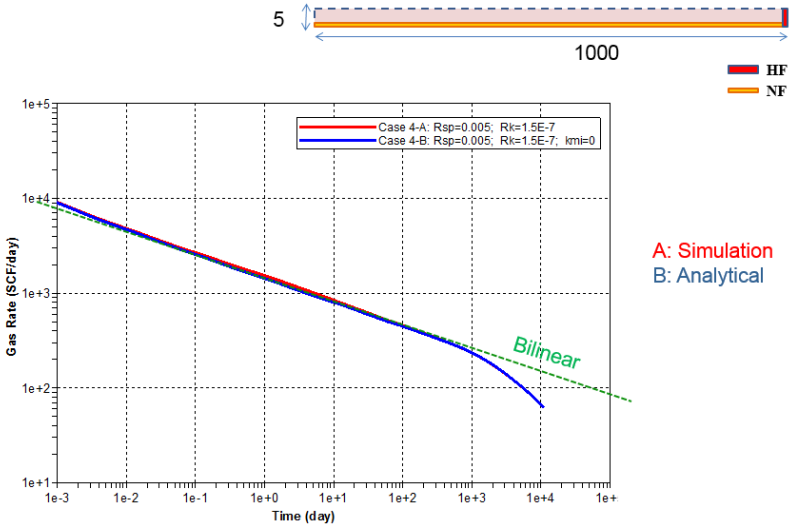

Fig. 17. Production curve for analytical and simulation case for R_{sp} = 0.005; the simulation case shows bilinear flow and is matching analytical solution.

3.5 Grid Modification

In simulation of linear flow, the hydraulic fracture is modified in several ways. The hydraulic fracture is modified in size and volume (porosity) to capture the transient period. Also, a comparison between automated and manual gridding is presented.

3.5.1 Fracture Modification

Hydraulic fractures are simulated as a modified matrix grids to avoid the use of "transfer function" (Pseudo Steady State assumption) which does not capture the transient effect. The fracture is modeled as part of the matrix allowing the flow between matrix and hydraulic fracture directly. For more details on this subject, Rubin (2010) is a good resource.

Also, the fracture is modified by increasing the fracture actual width w_F to a fracture pseudo width w_{PF} as shown in Fig. 18 to reduce run time due to small w_F. In the modification the fracture conductivity is preserved by using a low value of fracture intrinsic permeability $k_{F,in}$. A porosity modification is necessary in the case of w_{PF}. Eq. 3.4 shows the required modification for the porosity to preserve the volume. Also, if the Non-Darcy flow in gas wells is considered, it has to be modified as address by Rubin (2010).

$$\emptyset_{PF} = \emptyset_F \frac{w_F}{w_{PF}} \qquad \text{..... (3.4)}$$

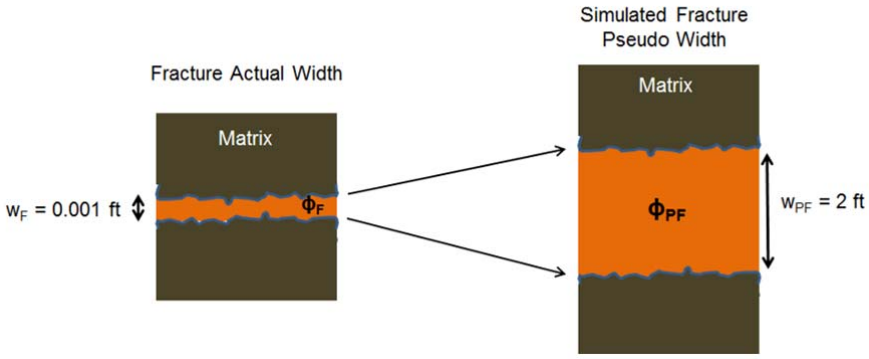

Fig. 18. Modification of fracture width to the larger pseudo width with porosity modifier.

The number of grids in the matrix has a major effect on the linear flow perpendicular to the hydraulic fracture. Grids number depends on many parameters like grid size, time step and the reservoir properties. As a general rule for linear flow, gridding 10 grids in each direction increasing logarithmically is enough to capture the transient linear flow in gas wells.

Parameters like fracture pseudo width, porosity modification and grid number (logarithmic grid refinement) in matrix are investigated as in Fig. 19. Converting w_F to a w_{PF} will not have an effect on linear flow analysis since $k_{f,in}$ was corrected to preserve C_{hf}. Porosity modification will have an effect at early times since it is a property of hydraulic fracture, but the later time of linear flow in matrix will not be affected by porosity modification. Number of grids in the matrix as long it is above 10 grids in each direction (fracture wing) increasing logarithmically, the linear flow will not be effected. Increasing

the grid numbers is unnecessary computational work as can be seen with 51 grids had the same results as 13 grids.

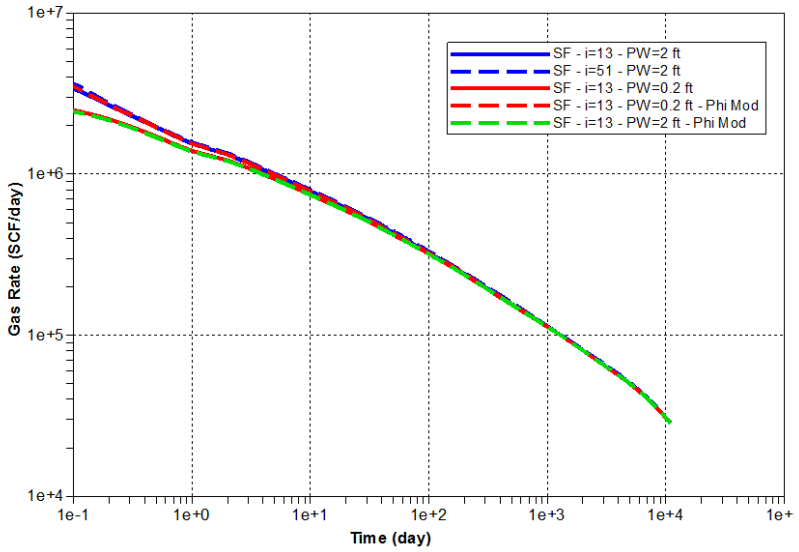

Fig. 19. Gas production for several runs with different grid numbers and modified porosity; porosity modification has an effect at early times only and increasing the number of grids in matrix (i), does not have an effect on linear flow if i>13 grids on both sides of the fracture.

Complex shale formations tend to have intersecting fractures, creating a network of simulated reservoir volume SRV as in Fig. 20. This feature was investigated on the same bases as in single hydraulic fracture. The same conclusions of single fracture apply to SRV of intersecting fracture as can be seen in Fig. 21.

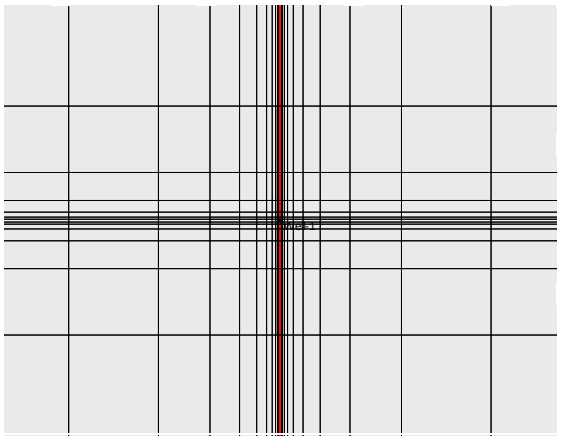

Fig. 20. Gridding and Geometry of intersecting fractures SRV with matrix logarithmically spaced.

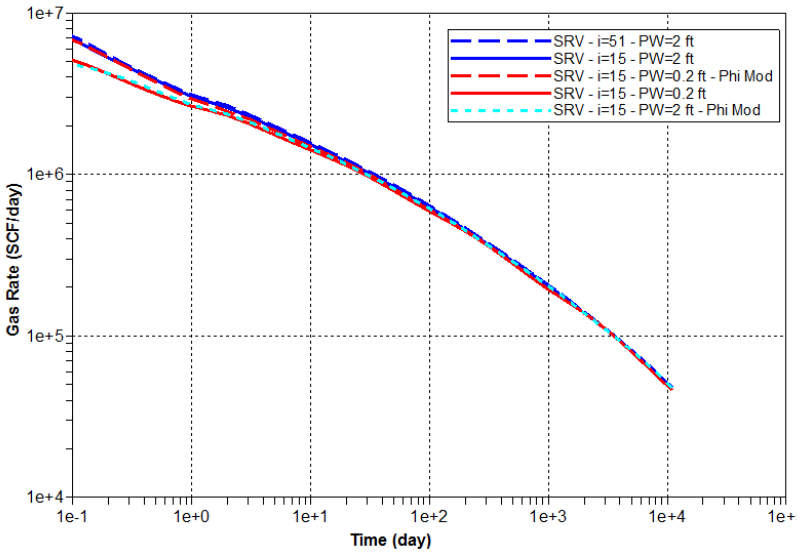

Fig. 21. Investigating different parameters in intersecting fractures; porosity modification has an effect at early times only and increasing grids in matrix (i) does not affect linear flow if i > 15 for both sides of the fracture.

3.5.2 Fracture Tip Refinement

In some simulators, automated grid refinement is a built in function where grids are refined logarithmically in the matrix near the perforation and near the hydraulic fracture as in Fig. 22 (left) to account for high pressure drop near the fracture. But the matrix grids at tip of the fracture are not refined logarithmically in the simulator's automated gridding. In order to capture the pressure drop correctly in two different grids (fracture and matrix), it is recommended to use refined grids as in Fig. 22 (right). Fracture tip refinement effect was studied to see when it is necessary and when it can be ignored.

Different fracture extent ratios R_{ex} which is defined in Eq. 3.5 are used in the analysis. In this equation, x_f is the fracture half-length and y_e is the reservoir distance to the boundary perpendicular to the hydraulic fracture. $R_{ex} = 1$ in a fully penetrating fracture which is the assumption in the analytical solution.

$$R_{ex} = \frac{x_f}{y_e} \qquad \text{..... (3.5)}$$

In the automated full model, both wings of the fracture are modeled but in the manual model only quarter is modeled then scaled up to the full size of the fracture. Four different cases of $R_{ex} = 0.2$, 0.4, 0.8 and 1 are investigated to test for tip refinement effect. The results of all cases are presented in Fig. 23 to Fig. 26. In the case of $R_{ex} = 0.2$ and 0.4 where the fracture is extending 20% and 40% of the reservoir boundary, modeling with tip refinement is more accurate. Also, in those case, linear flow is not established yet.

But in the cases of $R_{ex} = 0.8$ and 1 which is the case in most shale wells, tip refinement will not have any effect since most of the linear flow is from the refined sides

of the hydraulic fracture. In those cases, a clear linear flow trend is well established regardless of tip refinement. In shale wells, fully penetrating hydraulic fracture is a good assumption, so extra refinement at tip is not needed.

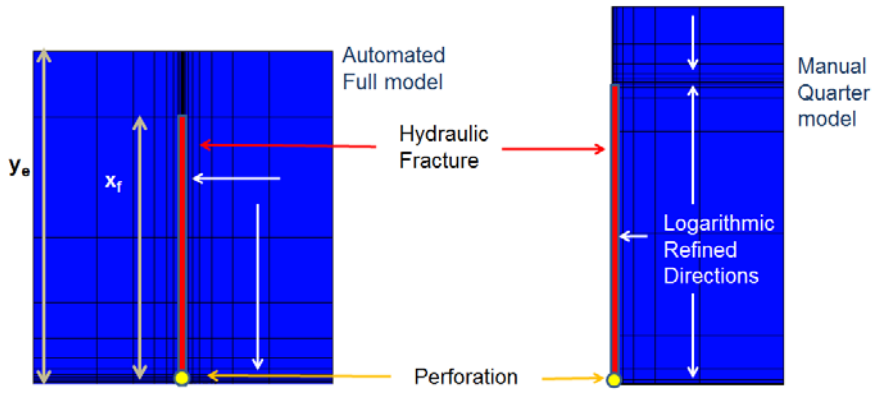

Fig. 22. Automated model showing a partially penetrating hydraulic fracture with refinement in two directions as indicated by white arrows (left), quarter manual model with the same fracture and extra refinement at the tip (right).

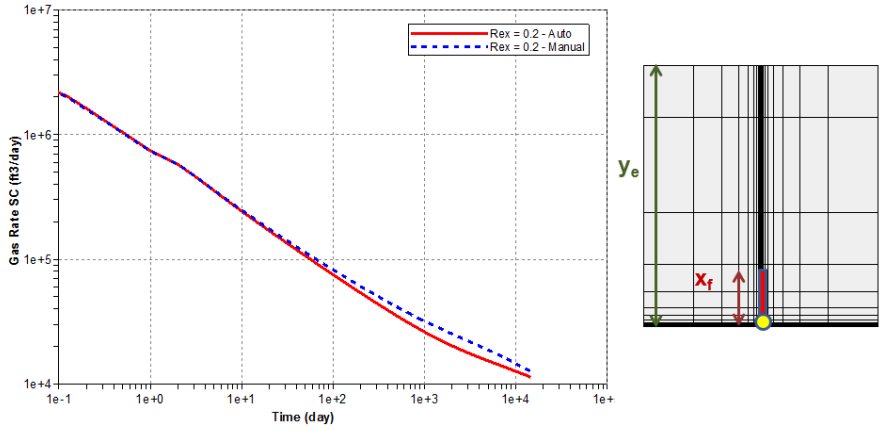

Fig. 23. In short fractures with larger drainage area (R_{ex} = 0.2), tip refinement has the most effect as can be seen the difference between the two production profiles from Auto (no tip refinement) and Manual.

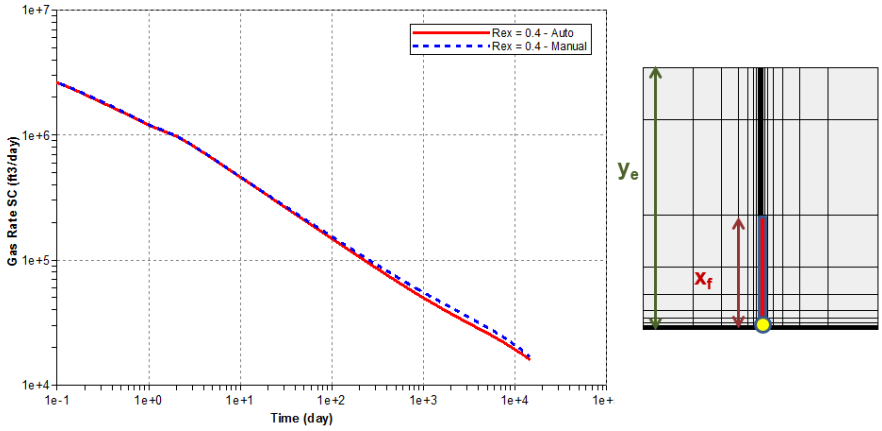

Fig. 24. In a fractures that is half the drainage area (R_{ex} = 0.4), tip refinement has small effect as can be seen the difference between the two production profiles from Auto (no tip refinement) and Manual.

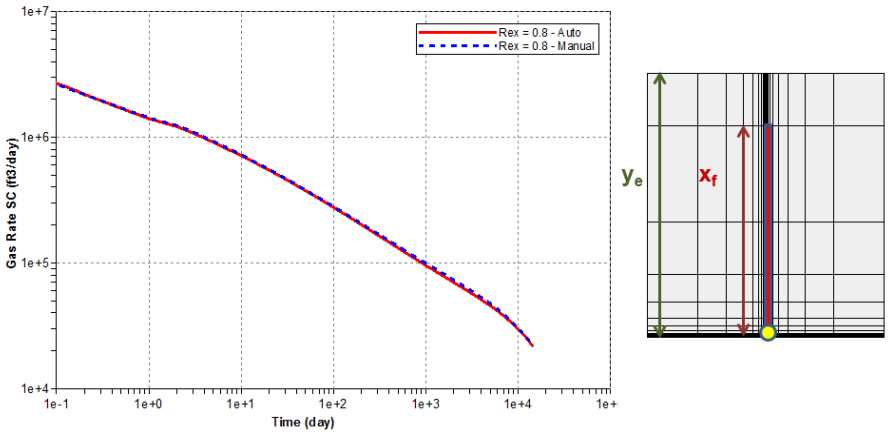

Fig. 25. In a fractures that is almost fully penetrating (R_{ex} = 0.8), tip refinement has no effect as can be seen the difference between the two production profiles from Auto (no tip refinement) and Manual; a clear linear trend is observed.

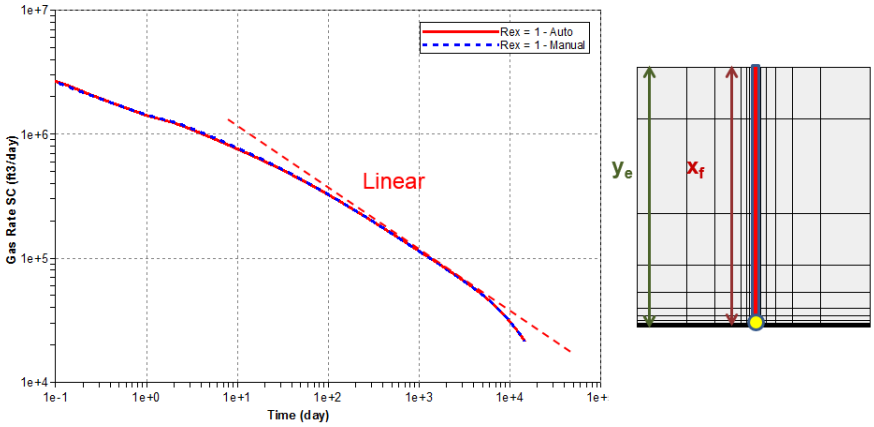

Fig. 26. In a fully penetration fractures as assumed in the analytical solution (R_{ex} = 1), tip refinement has no effect as can be seen the difference between the two production profiles from Auto (no tip refinement) and Manual; a clear linear trend is observed.

3.6 Field Application

Two field examples are presented in this section. First one is a Bakken well which will show the use of effective permeability equation (Eq. 3.1). Second well is from Barnett formation with bilinear flow and it will serve as a confirmation of the aspect ratio values that are presented.

3.6.1 Well 6

Although this research is focused on gas wells, this well is an oil well from Bakken formation that has linear flow. This example will show the benefits of using Eq. 3.1. This well was analyzed by Tran et al. (2011) as shown in Fig. 27 and Table 3. This production data had a clear linear flow for a long period which was ended at $\sqrt{t_{esr}} = 22$ with a slope

$\tilde{m}_4 = 0.775$. To calculate a value for crossectional area, matrix permeability value had to be assumed. The authors first assumed a low value of value of k_m=1x10^{-2} md, and the calculated A_{cm} = 1.87x10^6 ft^2. But if Eq. 3.1 was used with the valid assumption of homogenous reservoir, $k_{eff} = k_m$ = 6.1x10^{-3} md and the corresponding A_{cm} = 2.39x10^6 ft^2 (Procedure in Appendix A).

The authors tried to match the production data using a 2D simulator but could not match until the area was increased from A_{cm} = 1.87x10^6 ft^2 (assumed k_m=1x10^{-2} md) to A_{cm} = 2.4x10^6 ft^2 which was very close the calculated using k_m from Eq. 3.1.

In this example, it is clear that using Eq. 3.1 to find the permeability with the assumption of homogenous model can help the engineer avoid extra simulation work to match the model. Although the calculated OOIP is correct, it will help avoid errors in calculating A_{cm} and give a good estimate for permeability.

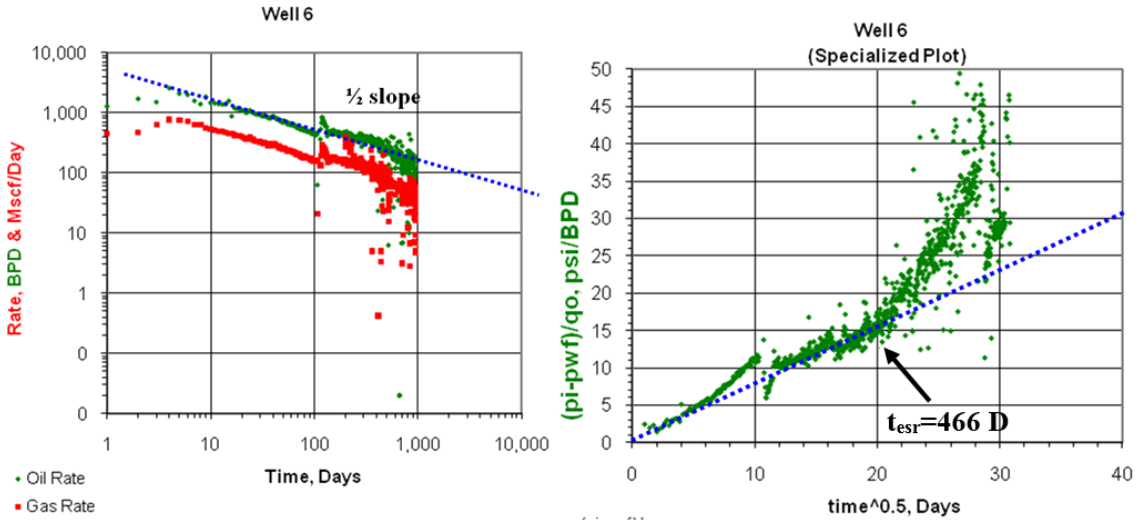

Fig. 27. Oil and Gas production data for Well 6 showing linear flow (left), square root of time plot showing the time for end of linear flow at 462 days (right).

Table 3 - Data for Well 6

Perforation Interval	x_e	2948	Ft
Hydraulic Fracture Spacing	L_F	737	Ft
Number of Hydraulic Fracture	n_F	5	
Porosity	ϕ	0.075	
Water Saturation	S_{wi}	0.23	
Oil Formation Volume Factor	B_{oi}	1.377	rbl/stb
Viscosity	μ_{oi}	0.593	cp
Total Compressibility	c_{ti}	11.8E-06	psi^{-1}

3.6.2 Well B-86

Field production data of the multi-transverse hydraulic fractures horizontal well B-86 in Barnett formation are shown in Fig. 28 and Table 4. The production plot shows a quarter-slope and a half-slope on the log-log plot of rate versus time representing bilinear and linear flows, respectively.

Values of $R_{sp} = 0.026$ and $R_k = 1.1 \times 10^{-6}$ are used to model bilinear flow which were obtained from analytical solution, Tivayanonda et al. (2012). It is noticeable that the value for R_{sp} is lower than the cut line that was established as guideline for using both simulation and analytical solution. A quarter of a natural fracture was used to model the total production of the field after scaling up the production rate. In Fig. 29, a good fit of the simulation to the production data except at early times which is due to water flowback period.

This example clearly shows the use of the aspect ratio which will give the engineer the choice to use either method (simulation and analytical) with confident for the bilinear case.

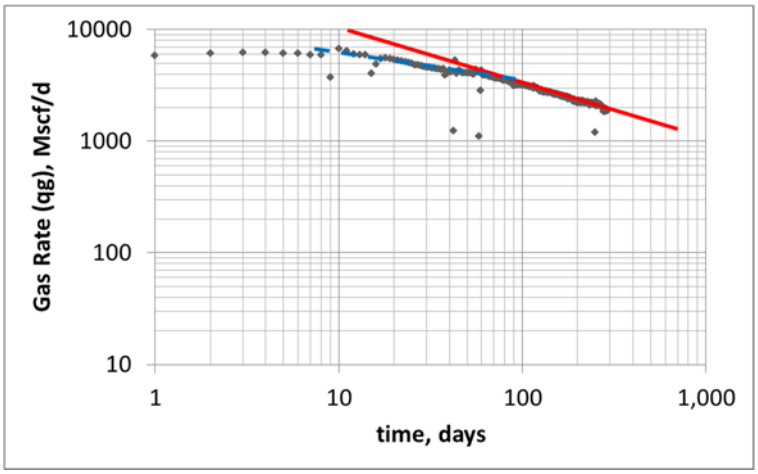

Fig. 28. Production data for Well B-86 with a bilinear flow (quarter slope) then followed by linear flow (half slope).

Table 4 - Data for Well B-86

Thickness	h	300	ft
Perforation Interval	x_e	3550	ft
Hydraulic Fracture Spacing	L_F	142	ft
Number of Hydraulic Fracture	n_F	25	
Porosity	ϕ	0.085	
Water Saturation	S_{wi}	0.3	
Formation Volume Factor	B_{gi}	0.0051	rcf/scf
Viscosity	μ_i	0.0195	cp
Total Compressibility	c_{ti}	2.23E-04	psi^{-1}
Pseudo Initial Pressure	$m(p_i)$	5.96E+08	psi^2/cp
Pseudo Bottomhole Flowing Pressure	$m(p_{wf})$	2.01E+07	psi^2/cp
Temperature	T	610	°R

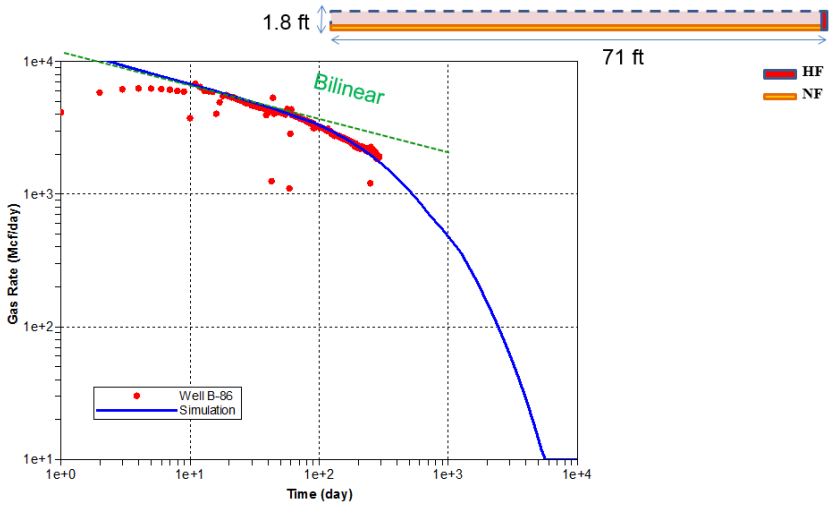

Fig. 29. Simulation of a quarter of a natural fracture with R_{sp} = 0.026 and R_k = 1.1x10^{-6} (obtained from analytical solution) matches production data except at early time which is due to water flowback effect.

CHAPTER IV

TWO PHASE SIMULATION

4.1 Introduction

In this chapter, two phase numerical model will be used to explore different hypothesis on water distribution scenarios in shale wells. Also, the reason for low injected water recovery is investigated.

4.2 Water Distribution Scenarios

One of the main motivation for this research is to know the distribution of the injected water in shale gas wells. In this section, some observations are reported and a discussion of the main hypothesis about injected water distribution in the reservoir.

4.2.1 Field Observations

The amount of frac fluid recovery in gas shale varies with the shale character, the frac design and the type of fluid as the main drivers, as discussed in King (2010). Fan et al. (2010) stated that wells with less flowback water have better early production rates. Crafton (2010) observed that in many wells the time from stimulation shut-in until first production has an important impact on early-time and ultimate performance, sometimes adversely and sometimes beneficially. Through experiments, Crafton (2008) concluded that the use of "load recovery" metric is a very misleading performance indicator.

Water salinity was also used as an indicator for the source of water and whether or not it was in contact with the matrix. Novlesky et al. (2011) reported that the produced water salinity is high but quickly decreases during the production process which denotes that the saline formation fluid remains immobile while the injected water (less saline) is flowing back having higher mobility. The first production period is mainly saline water that was in contact with the matrix as indicated by its high salinity. Then the salinity decreases due to the water that was not in direct contact with the matrix and stored in the fracture.

4.2.2 Hypothesis

Ehlig-Economides and Economides (2011) and Fan et al. (2010) hypothesized possible water distribution scenarios and both were not simulated. Both have in common that there is no water imbibing into the formation since the gas production will drop due to the conventional relative permeability curves. In both papers, there are two possible models depending on stress contrast in the formation as in Fig. 30.

These scenarios basically differ by the presence and the effect of natural fractures with the main hydraulic fractures. As seen in the previous chapter, Scenario 1 might have natural fracture but are ineffective because of the large spacing and low conductivity. Ehlig-Economides and Economides (2011) hypothesize that both models have lost water that is trapped due to capillary pressure. Fan et al. (2010) relates between high water recovery in scenario 1 and low gas flow due to low contact area between the hydraulic

fracture and matrix. In scenario 2, the author relates between low water recovery due to lost trapped water and high gas flow due to the large contact area.

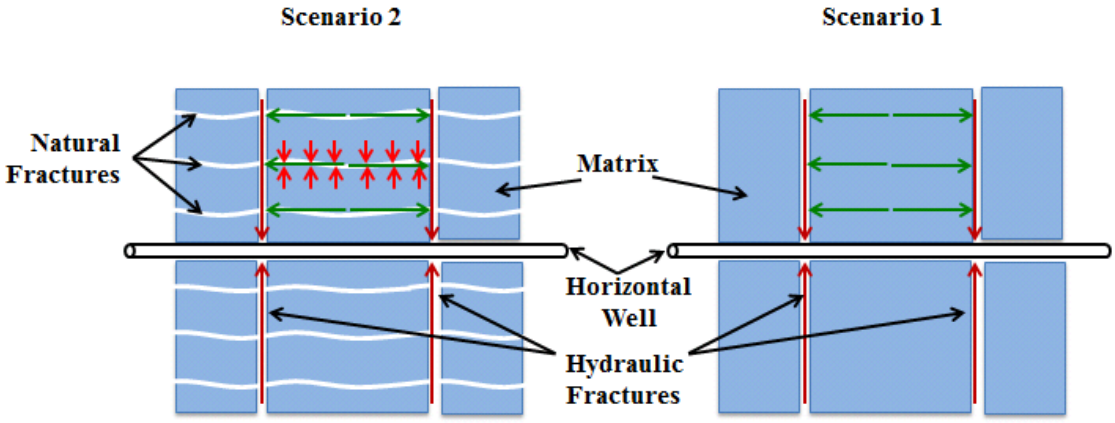

Fig. 30. Scenario 1 represents the hydraulic fracture only without natural fracture (or natural fracture present but ineffective) and scenario 2 with the natural fractures (effective in gas flow).

Pagels et al. (2012) presented three mechanisms that cause water to be lost. The first mechanism occurs when the water filled natural fracture, it losses contact with the main hydraulic fracture. The second mechanism is caused by capillary pressure where the water is trapped in the natural fracture. The third mechanism is imbibition of water into the matrix. All the presented work and hypothesis were not supported and confirmed by simulation. This study simulated the proposed scenarios to investigate these hypotheses.

4.3 Simulation of Water Distribution Scenarios

In the two phase simulation case, some properties have been changed. A horizontal well with 6,000 ft lateral length with 6 fracture stages is simulated using a 3-D gas-water black

oil simulator. In each single stage, 5 transverse hydraulic fractures are created with a spacing of 200 ft and fracture half-length of 150 ft. Added to the hydraulic fracture, 6 natural fractures which are orthogonal to the hydraulic fractures to account for the complex fracture networks generated by the fracture treatment. A quarter of natural fracture is simulated as in Fig. 31 and then the results are scaled back to the full lateral. The base case model is designed to capture the typical characteristics of a shale gas well as shown in Table 5.

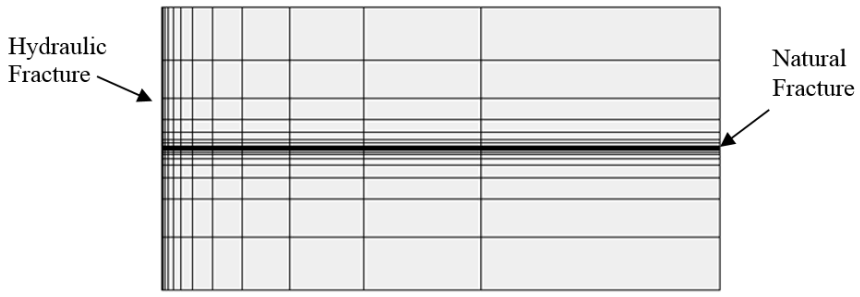

Fig. 31. A quarter model of one natural fracture orthogonal to a hydraulic fracture which is logarithmically spaced toward hydraulic and natural fractures to capture linear flow.

Table 5 - Two phase simulation properties

Initial pressure, p_i (psi)	3000	Reservoir thickness, h (ft)	150
Flowing BH pressure, p_{wf} (psi)	500	Matrix permeability, k_m (md)	1×10^{-4}
Specific gravity, SG_g	0.65	Natural Fracture permeability, k_f (md)	0.1
Matrix Water saturation, S_w	0.25	Natural Fracture width, w_f (ft)	0.0001
Hydraulic Fracture Conductivity, C_{nf} (md-ft)	10	Hydraulic Fracture width, w_F (ft)	0.01
Reservoir temperature, T (°R)	620	Natural Fracture spacing, L_f (ft)	50
matrix porosity, φ (fraction)	0.06	Hydraulic Fracture spacing, L_F (ft)	200
Fracture porosity, φ (fraction)	0.95	Fracture half length, x_f (ft)	150
Irreducible water saturation, S_{wirr}	0.25	Natural and Hydraulic Fracture water saturation, S_w	1
Number of Hydraulic Fractures, n_F	30		

4.3.1 Base Case

A base case is simulated to characterize the distribution of water within the fracture/matrix system. In this case, the conventional capillary pressure and relative permeability are used in the matrix and natural fracture. Set 1 (k_{rw} 1 & k_{rg} 1) as in Fig. 32 is used for relative permeability in the matrix and natural fracture. Fig. 33 shows the relative permeability that was used in the hydraulic fracture which is very close to gravity segregated curves. Also, set 1 (p_c 1) as in Fig. 34 is used for the conventional capillary pressure curve in both the matrix and natural fracture. The capillary pressure in the hydraulic fracture is neglected.

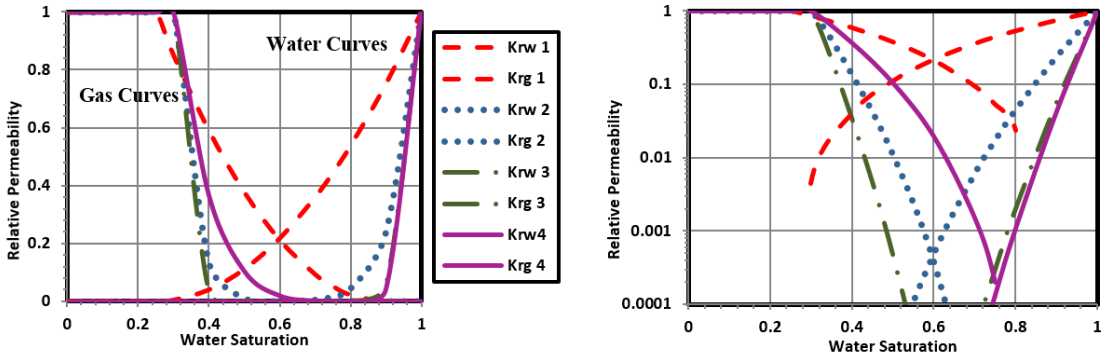

Fig. 32. Four sets of relative permeability curves that are used in the matrix and natural fractures with set 3 showing a permeability jail and set 4 showing the hybrid permeability jail curve.

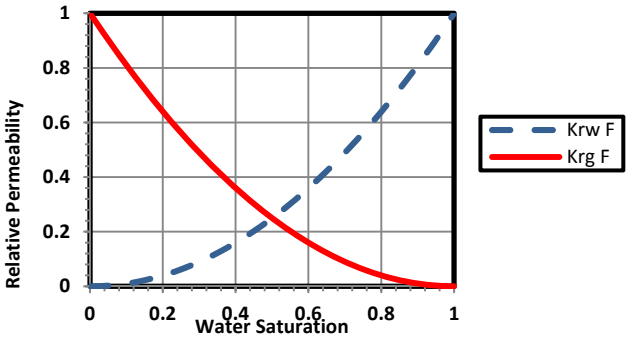

Fig. 33. Relative permeability curves for hydraulic fracture which is almost gravity segregated curve.

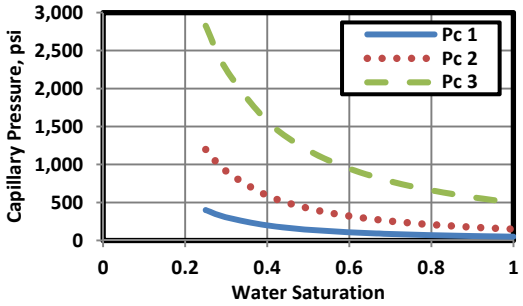

Fig. 34. Capillary pressure curves used in the simulation with p_c 1 representing the conventional curve and p_c 3 representing a low permeability formation.

As in Fig. 35, plot A shows the water saturation profile in the hydraulic fracture (first point) and matrix next to the hydraulic fracture (rest of the points) with the conventional relative permeability and capillary curves at 1 and 1,000 days of production. As mentioned previously, imbibition is evident and factors like capillary pressure and pressure drawdown will determine the length of the invaded zone and water saturation magnitude in the matrix. In plot B at 1,000 days, the natural fracture trapped some water (S_{wirr}) unlike the hydraulic fracture which trapped no water (HC has larger width, high

permeability and no capillary forces). Even the magnitude of the water saturation in the invaded zone and its length is very low compared to the hydraulic fracture. In the next case, the effect of increasing capillary pressure will be investigated.

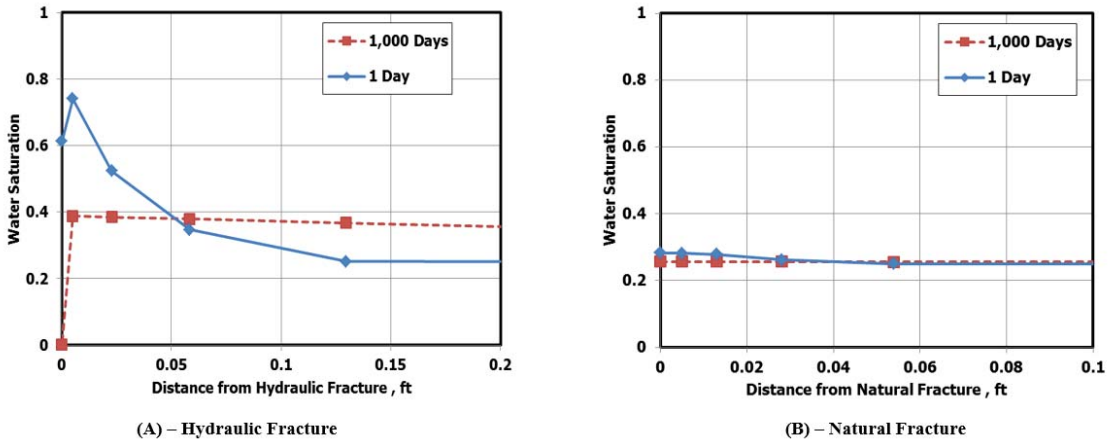

Fig. 35. Water saturation profile of base case: A) hydraulic fracture was affected by imbibition from day 1 (S_w increased from 0.22 to 0.38); B) natural fracture did not imbibe water was at the irreducible water saturation.

4.3.2 Impact of Higher Capillary

In this case, base case was used with only increasing the capillary pressure to set 3 (p_c 3) which represents the usual capillary in low permeability but the relative permeability curve used is still the conventional curve set 1 (k_{rw} 1 & k_{rg} 1). As in Fig. 36, plot A shows the saturation profile at 1,000 days in the hydraulic fracture and it is noticed that magnitude decreased in the invaded zone and the length increased. As in the base case, water saturation in the hydraulic fracture is still zero. Similarly to the base case, water saturation profile did not change since the capillary is used in the natural fracture.

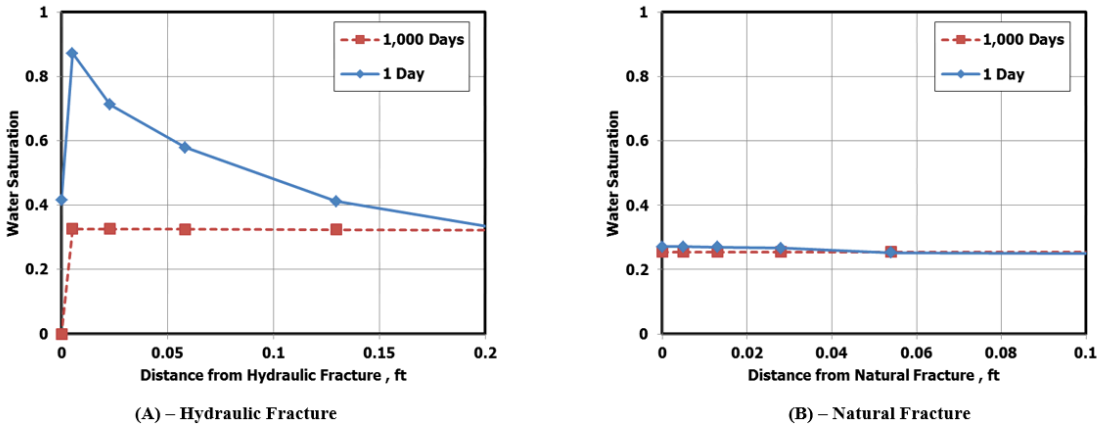

Fig. 36. Water saturation profile of higher capillary pressure case: A) more water is imbibing after 1,000 days; B) did not change compared to the base case.

4.3.3 Impact of Lower Relative Permeability (Unconventional Case)

The unconventional case is similar to the base case in regards to lowering the relative permeability curve to set 2 (k_{rw} 2 & k_{rg} 2). In the plot A of Fig. 37, the hydraulic fracture saturation in day 1 is lower in length and magnitude compared to the base case. After 1,000 days, water saturation is lower in magnitude and invasion depth. It is almost as though only the fracture face is affected by imbibition. The natural fracture in plot B is similar in finding as in the hydraulic fracture. The only difference between them is the inside final saturation. Natural fracture trapped more water at S_w = 0.4 which is expected since water relative permeability in set 2 is extremely low for this saturation. In the next run, the increase in hydraulic and natural fracture width is studied.

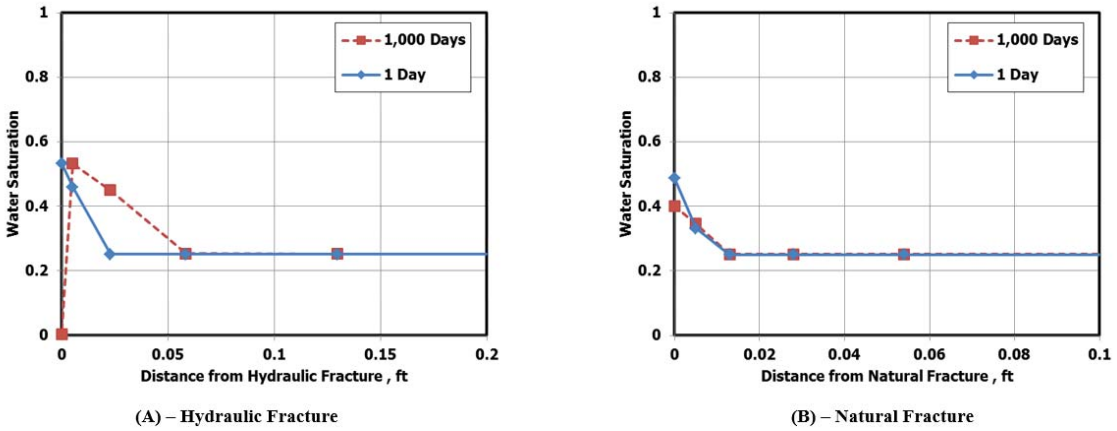

Fig. 37. Water saturation profile of unconventional case: A) less water is imbibing almost fracture surface affected only; B) natural fracture trapped water at 40%.

4.3.4 Impact of Increasing Width of Hydraulic and Natural Fracture in Unconventional Case

The unconventional case is used with only increasing the width of the hydraulic and natural fracture (higher fracture conductivity) to w_F = 0.1 ft and w_f = 0.001 ft respectively. If Fig. 38 is compared to the results of Fig. 37, the width increase increased water presence in both the fracture and the matrix and had a negligible effect on the invasion length. The hydraulic fracture had more water trapped but this is due to liquid loading as the saturation at 1,000 days increased from 0 (unconventional case) to 0.9 (increased width case). It is worth noticing that the saturation reading is at one single point in both the hydraulic and natural fractures. The full saturation profile for the hydraulic fracture is Fig. 39 (unconventional case) and Fig. 40 (increased width case).

In Fig. 39 and Fig. 40, the water saturation profile for the full length in both hydraulic and natural fractures is shown. Fig. 39 shows the change of water saturation in the hydraulic fracture for the unconventional case at different production times. It is clear that liquid loading is not a main concern. But after increasing the width, liquid loading is present as soon as 1,000 days of production as shown in Fig. 40. This corresponds to the work presented by Sharma and Agrawal (2013) where liquid loading is an issue. Decreasing the hydraulic fracture width to more realistic width of 0.01 ft removed the concern of liquid loading. It is worth mentioning that there is no liquid loading in the natural fracture in either case due to small width and low permeability.

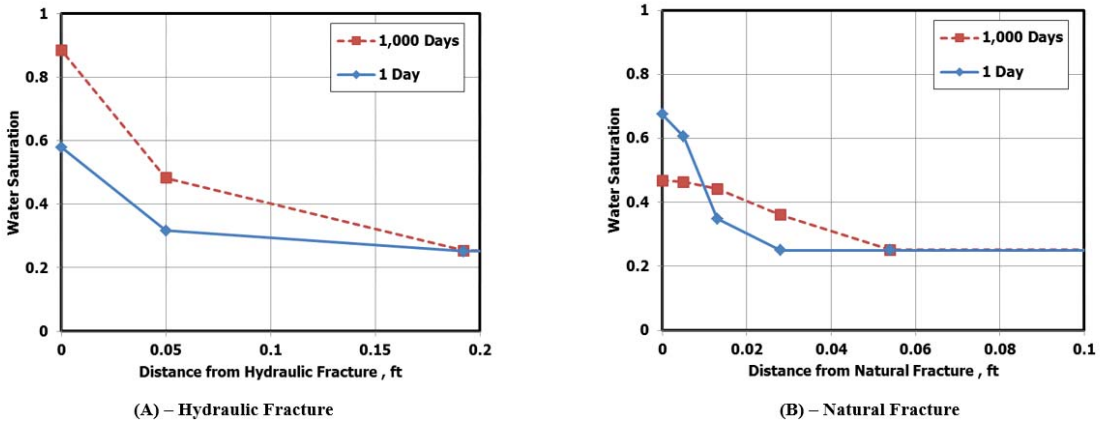

Fig. 38. Water saturation profile of unconventional with increased width case: A) water saturation is high at 1,000 days due to liquid loading; B) similar to the unconventional case.

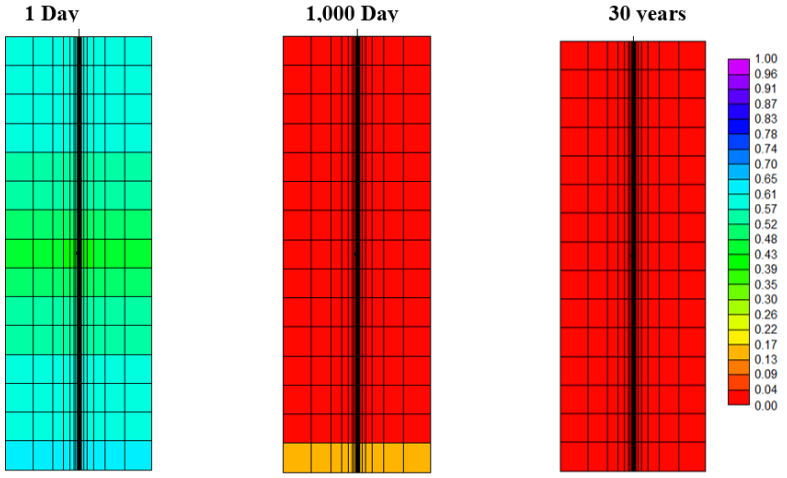

Fig. 39. Water saturation profile in the hydraulic fracture of unconventional case at different times showing no liquid loading effect.

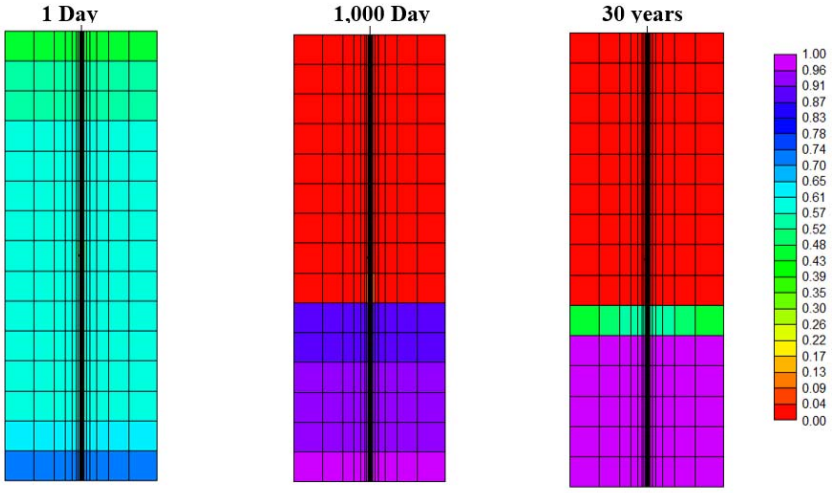

Fig. 40. Water saturation profile in the hydraulic fracture of unconventional case with increased width showing liquid loading effect at day 1 and in 1,000 days third the fracture is filled with water and the same situation after 30 years.

4.3.5 Impact of Permeability Jail

In the previous cases, water saturation in the natural fracture was around 40% at the end of 3 years of production. The water distribution scenario with natural fractures fully holding the water could not be proved by the previous tools. Relative permeability jail as in set 3 (k_{rw} 3 & k_{rg} 3) of Fig. 32 is used in the base case to prove the concept of water held in the natural fracture. If the water saturation results from Fig. 41 were compared to the unconventional case, no change would be noticed in the hydraulic fracture. On the other hand, the natural fracture will hold more water with a saturation of 60% after 1,000 days of production. The permeability jail would have a negative effect on gas production, in order to avoid this effect, a hybrid permeability jail was presented in the next section.

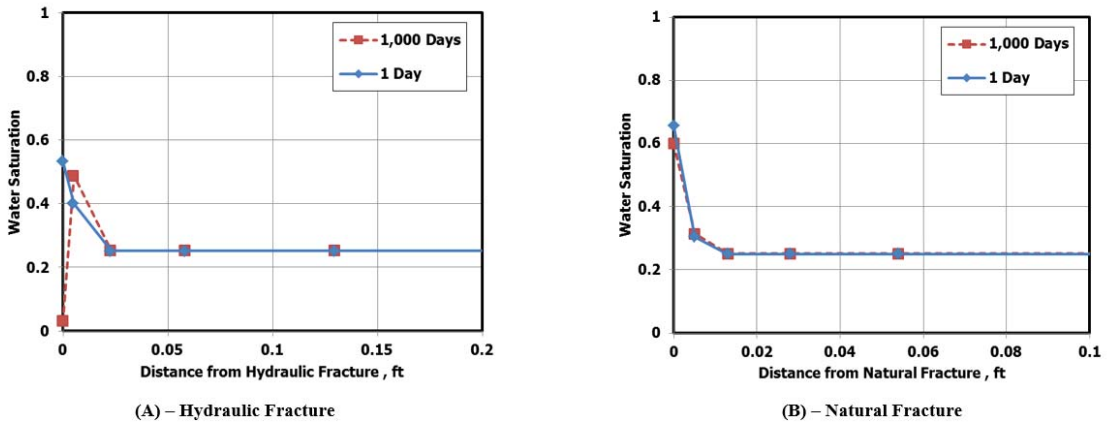

Fig. 41. Water saturation profile of permeability jail case: A) similar results to the unconventional case with no imbibition; B) 60% of the water is trapped at 1,000 days and no imbibition.

4.3.6 Impact of Hybrid Permeability Jail

Hybrid relative permeability jail as in set 4 (k_{rw} 4 & k_{rg} 4) of Fig. 32 is used in the base case to show the effect of shifting the jail area (no phase flow area). This curve was constructed from a gas relative permeability higher than the unconventional case and water from permeability jail case; it was also created to match observed data from both production and the lab. If the water saturation results from Fig. 42 were compared to the permeability jail case, the result is almost the same since water relative permeability is similar. The maximum water that can be held in the natural fracture is 60% after 30 years of production. This hybrid curve was developed to match the effect of shut-in after a flowback period that is observed in the field as can be seen in the next section.

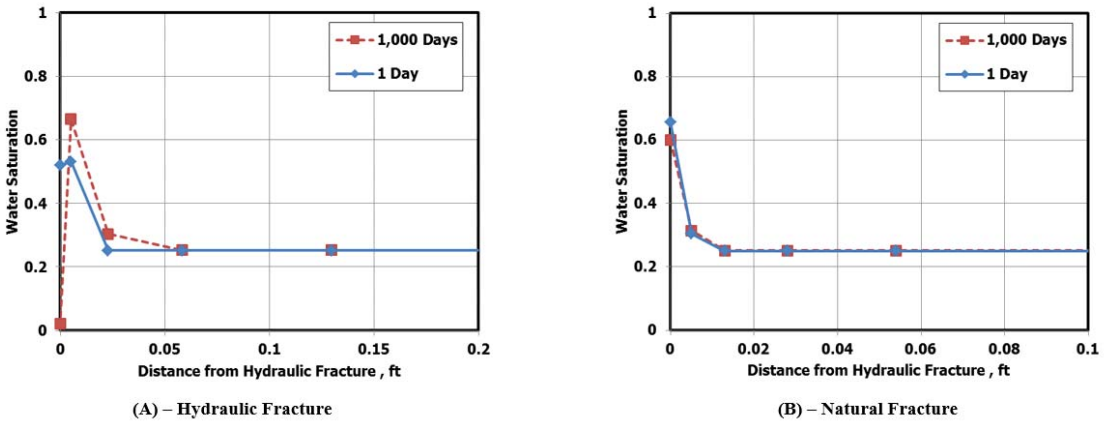

Fig. 42. Water saturation profile of hybrid permeability jail case: A) similar to permeability jail case; B) similar to permeability jail case.

4.3.7 Impact of Shut-in after Flowback

Shut-in after a short period of flowback gives a challenging signature that is hard to simulate. Both the permeability jail and hybrid permeability jail cases are tested for the shut-in of 30 days after a 10 days period of flowback. This procedure is used in some fields due to the delay of connecting the well to the main pipeline.

Fig. 43 shows the gas flow rate for both cases, the permeability jail case has very low gas rates after the shut-in period which reflects that this relative permeability set 3 is not the true representative of filed data. On the other hand, the hybrid permeability jail shows the trend that observed in the field and serves the purpose of trapping 60% of the water in the natural fracture. The water production in Fig. 44 shows the steep increase and decrease of water in the hybrid case. Several extreme permeability jail curves were tested but the results were unreasonable low gas production after the shut-in due to water blockage.

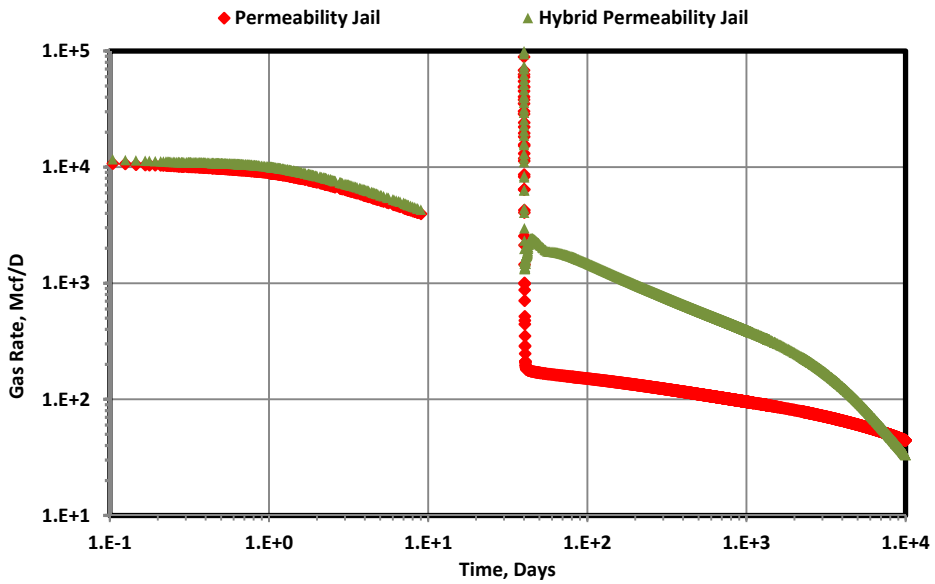

Fig. 43. Gas production with 30 days shut-in after 10 days for flowback showing the hybrid case with a curve coming back to the main flow regime after a spike, but the permeability jail is dropping to low rates due to the very low gas relative permeability curve which was avoided in the hybrid case and does not represent observed field data.

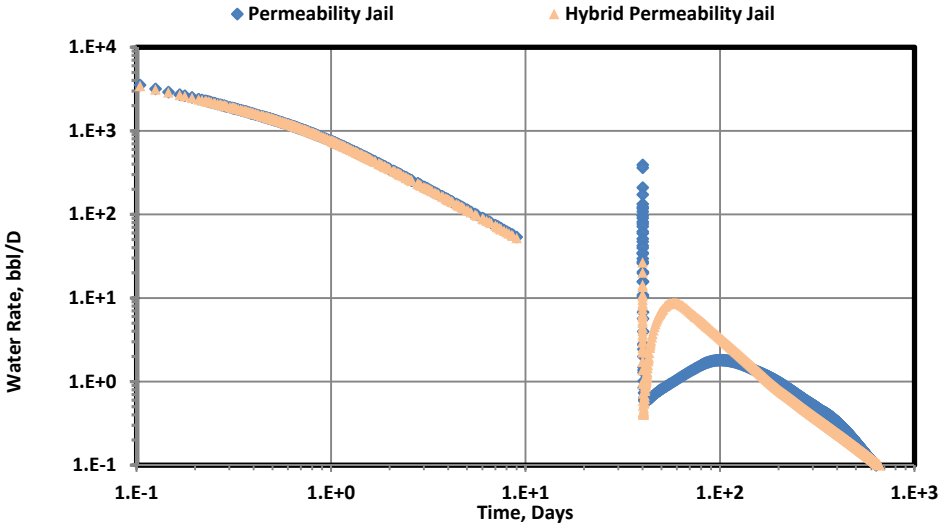

Fig. 44. Water production with 30 days shut-in after 10 days of flowback showing water flow in the permeability jail case start increasing slowly unlike the hybrid case with a steeper increase and decrease in rate representing the observed field data.

4.3.8 Impact of Natural Fracture Spacing

The default value that was used in the previous cases for natural fracture spacing was 50 ft which is considered high. In this case, the original gas in place (*OGIP*) = 2.4 Bcf and water in place (*WIP*) = 729,000 STB and water in both hydraulic and natural fractures (*WIBF*) = 2,375 STB. IF we compared *WIBF* to the usual injected water of 100,000 STB, we notice the need to increase fracture spacing to 1ft.

After increasing natural fracture to 1 ft, *WIP* = 752,000 STB increased from the original value due to more volume occupied by natural fractures. *WIBF* did not increase much and the value was 6,852 STB. In an effort to match field results, natural fracture spacing was decreased to 0.1 ft.

In the natural fracture spacing of 0.1 ft, *WIBF* = 47, 965 STB is higher than the 1 ft spacing case. This represents around 50% of the usual injected volume and the rest of the injected water is lost water that is not connected to the effective flow path of the well. The hydraulic fracture is occupied by 2,284 STB and the natural fracture is occupied by most of the water of 45,681 STB.

In the previous simulation results, the hydraulic fracture will flowback all the water and that at most 60% of the water in the natural fracture is trapped. Around 20,000 STB (HF volume + 40% NF Volume) would flowback which represents 20% flowback as usually observed in the field. The existence of more natural fracture trapping water could be a possible explanation for the low water recovery in some wells.

4.4 Summary

In this section, different relative permeability curves and capillary pressure curves were tested in a two phase model to construct a model that represent the published water distribution scenarios. Also, the model trapped high percentage of water and do not contradict with lab and field observations. Hybrid permeability jail curves satisfied the conditions and presented a production profile similar to the field after shut-in.

CHAPTER V

ESTIMATION OF EFFECTIVE FRACTURE VOLUME

5.1 Introduction

Several authors divided the production profile in shale gas wells into three regions base on the type of fluid flowing. Abbasi et al. (2012) divided into: first water production, second transition of declining water and increasing gas and third is gas dominates. Another way is to divide the well's production profile based on dominating phase in the diffusivity equation of two phase (water and gas).

In this chapter, a new method is developed for analyzing water production data from all periods (flowback and production) based on the phase dominating the diffusivity equation. This method is based on numerical model with modified compressibility calculations.

5.2 Diffusivity Equation

Diffusivity equation of two phase flow (water and gas) take into account both fluids. A water dominating region is where the compressibility of water is dominating and is very short. A gas dominating region is the main region and it starts at early times. In production data analysis, it is assumed that the dominant phase is gas which makes the analyst ignore the previous period since gas dominates the diffusivity equation. Eq. 5.1 shows the diffusivity equation for a two phase system (water and gas).

$$\nabla \cdot \lambda_t \nabla p = \emptyset \, c_t \, \frac{\partial p}{\partial t} \qquad \text{..... (5.1)}$$

Where the total mobility λ_t is defined as

$$\lambda_t = \left(\frac{k}{\mu}\right)_t = k\left(\frac{k_r}{\mu}\right)_t = k\left[\left(\frac{k_r}{\mu}\right)_g + \left(\frac{k_r}{\mu}\right)_w\right] \quad \text{..... (5.2)}$$

Where the total compressibility c_t is defined as

$$c_t = c_f + S_w\, c_w + S_g\, c_g \quad \text{..... (5.3)}$$

When significant gas flows, the two conditions are satisfied.

Condition one: $\lambda_t \approx k\left(\frac{k_r}{\mu}\right)_g$ and Condition two: $c_t \approx S_g\, c_g$

If those conditions are true, then the real gas diffusivity equation can be used to analyze gas production data, using the real gas pseudo-pressure.

$$\nabla^2 m = \frac{\emptyset\, \mu\, c_t}{k}\frac{\partial m}{\partial t} \quad \text{..... (5.4)}$$

Although water rate is high in the flowback period, any gas in the fracture can make gas dominate the system. With this in mind, gas compressibility cannot be ignored in the water analysis. This concept is the main drive for this research. Even though the analyzed fluid is water, gas compressibility should be used which was verified using a numerical model.

5.3 Single Fracture Model Simulation

This simulation run is slightly modified from the model shown in Chapter 4. A single fracture is used with water filling the fracture and gas in the matrix. The simulation properties are shown in Table 6. The relative permeability curve in the fracture is gravity segregated as shown in Fig. 45.

Table 6 – shale gas simulation properties for single fracture model

Initial pressure, p_i (psi)	3000	Matrix porosity, φ_m (fraction)	0.06
Flowing BH pressure, p_{wf} (psi)	500	Reservoir thickness, h (ft)	300
Specific gravity, SG_g	0.65	Matrix permeability, k_m (md)	1.5×10^{-4}
Reservoir temperature, T (°F)	160	Hydraulic Fracture Conductivity, C_{HF} (md-ft)	4
Fracture porosity, φ_F (fraction)	1	Fracture spacing, L_F (ft)	500
Water volume in the fracture, V_w (STB)	6,995	Fracture half length, x_f (ft)	550
Water formation volume factor, B_w (Res bbl/STB)	1.01	Formation Compressibility, C_f (psi^{-1})	1×10^{-6}
Gas Compressibility, C_g (psi^{-1})	3.9×10^{-4}	Water Compressibility, C_w (psi^{-1})	2.9×10^{-6}

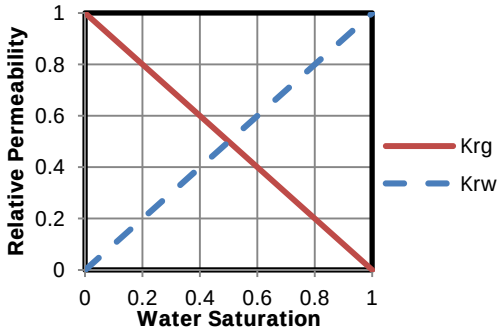

Fig. 45. Gravity segregated relative permeability curve of the single fracture model.

Two cases are simulated to illustrate the effect of gas flow from matrix on water volume calculations in the fracture as in Fig. 46. In both case, no water is flowing from the matrix to the fracture only water is placed in the fracture and flowing to the perforation.

The single phase flow case has water flowing in the fracture only no gas flow from matrix. The two phase flow case has gas flowing from matrix into the fracture which is filled with water. Water volume in both cases in the fracture is constant. The concept behind the cases is to build linear flow of fracture filled with water and compare it with the effect of gas flowing from matrix which provides an extra compressibility to the water flow. In both cases, water flow is analyzed to calculate different parameters.

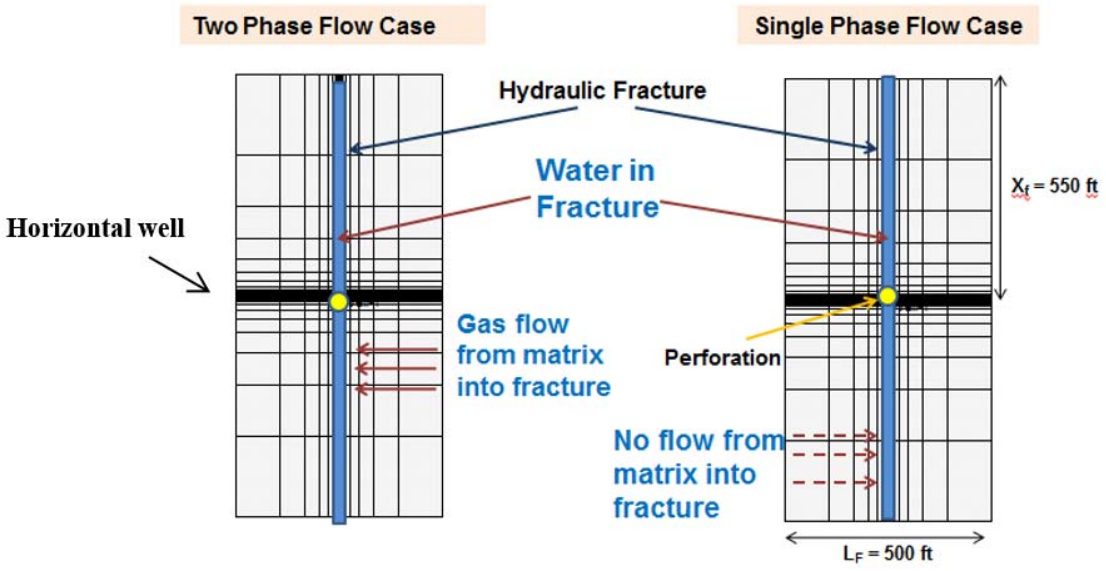

Fig. 46. Two simulated single fracture cases with the single phase case water is filling the fracture and is the only flowing phase (gas from matrix is not flowing); in the two phase case, gas is flowing from matrix into fracture that is filled with water.

The results of the two cases is presented in Fig. 47 with water rates plotted versus time for a single fracture. The single phase case represent linear flow of water in a fracture with the signature of ½ slope and then declines exponentially. This curve can be

reproduced using an analytical solution. When the gas flow from the matrix is included as in the two phase flow, the linear flow departed from the single phase case coming to another linear due to flow of gas from the matrix into the fracture. The second linear flow line is not informative since it depends on several unknown parameters; this type of flow is very early and is not observed in the field water data. In the two phase case, the water rate declines in a different manner if compared to the single phase case.

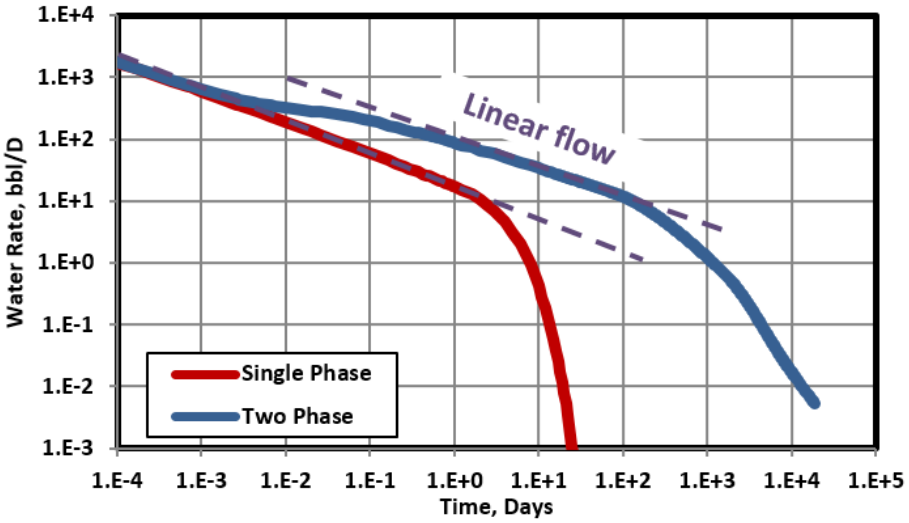

Fig. 47. Water flow rate of a single fracture with/without gas flow from matrix, linear flow (1/2 slope) dominates early time in single phase and then declines exponentially; higher flow rates and longer time in the case with gas flow matrix into water filled fracture increasing total compressibility.

5.4 Fracture Volume Calculation

In this section, fracture volume will be calculated and confirmed with values used in the simulator for both cases. Water material balance time plot is used to calculated water

volume that is occupying the fracture. In Fig. 48, water rate for both cases is plotted using material balance time to observe the boundary dominated flow regime as unit slope line. In both cases, water volume in the fracture is similar but the results indicate that those volumes are different since the unit slope lines are not overlying each other. Under the assumption of similar compressibility values in both cases, the plot is showing that water volume in the two phase case is larger than the single phase case. This assumption is not valid since water volume in both fractures is the same.

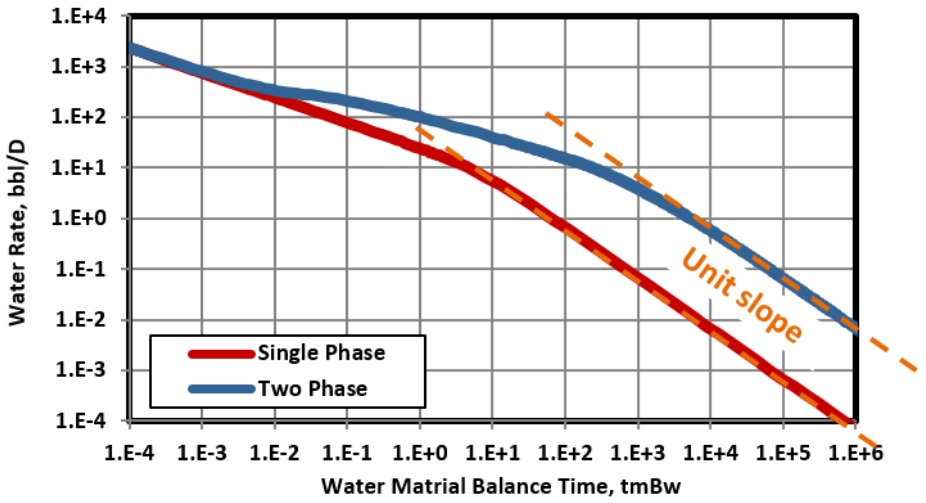

Fig. 48. Water flow rate versus water material balance time showing two different unit slope lines indicating two different volumes when the same volume is used for both cases. This difference is due to gas compressibility.

In the two phase case, gas is flowing into the fracture which will tend to increase the total compressibility which will affect water volume calculations. A new method is implemented to rigorously account for how the gas present effects water volume

calculations. This method is based on the plot of water rate normalized by pressure (RNP_w) plot versus material balance time as in Fig. 49. RNP_w is used to correct for variable bottomhole pressure (p_{wf}) as in the case of an actual well (the simulated cases are constant p_{wf}). This method is based on Eq. 5.5 which calculates water volume based on the slope (m_{pss}) and total compressibility (c_t). The complete derivation of Eq. 5.5 is shown in Appendix D. m_{pss} is the slope of the Cartesian plot in the period of unit slope line as in Fig. 49 where the line or RNP_w is over RNP'_w (derivative) line. m_{pss} can also be calculated using Eq. 5.6 with the data in the unit slope period of Fig. 49.

$$V_w = \frac{B_w}{c_t\, m_{pss}} \qquad \text{..... (5.5)}$$

$$m_{pss} = \frac{RNP_w}{t_{mBw}} \qquad \text{..... (5.6)}$$

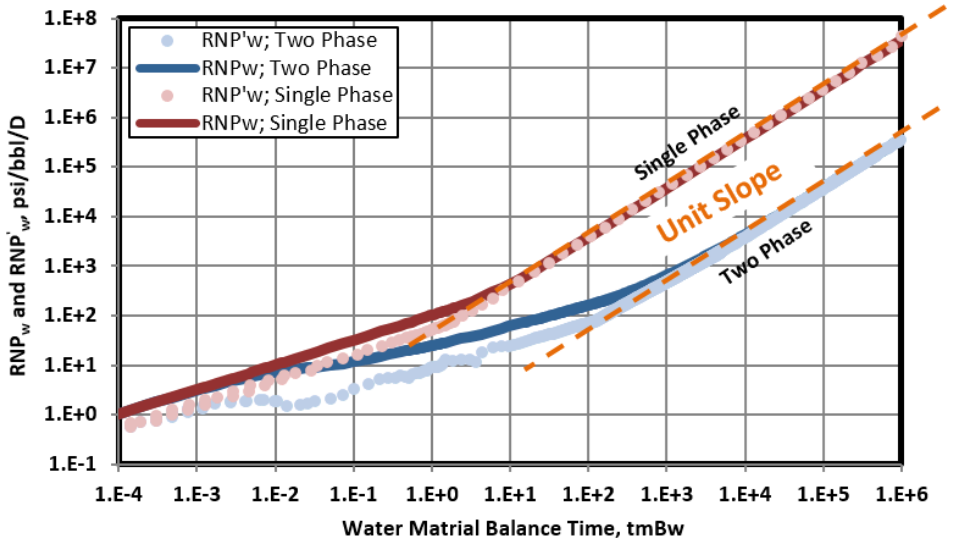

Fig. 49. Water rate normalized pressure and derivative versus water material balance time showing two different unit slope lines indicating two different volumes when the same water volume is used for both cases. This difference is due to gas compressibility.

To back calculate water fracture volume, the total compressibility in the single phase case is water and formation compressibility but it is different in the two phase case. The two phase case compressibility is first dominated by water then gas is dominating due to gas saturation increase in the fracture. To get the correct water volume in the fracture, an approximation is used by equating total compressibility to the gas compressibility.

The results of both cases are presented in Table 7 where the simulated water volume is back calculated. In the single phase case, the total compressibility (water and formation) is used. But gas compressibility (at p_i and S_g = 1) is used to calculate water volume in the fracture. This method will be used with field data for further confirmation.

Table 7 - Calculations results of simulation of single fracture cases

Parameters	Single Phase Case	Two Phase Case
m_{pss}	37	0.37
c_t, psi^{-1}	3.9×10^{-6}	3.9×10^{-4}
Input V_w, STB	6,955	6,955
Calculated V_w, STB	6,999	6,930

5.5 Sensitivity Study

As in Fig. 50, water saturation is changing with time and location in the fracture which will affect the total compressibility. Also, pressure is changing with time and location in the fracture which will affect gas compressibility (hence, total compressibility). In order to confirm the accuracy of the assumption, a sensitivity study is conducted to confirm it.

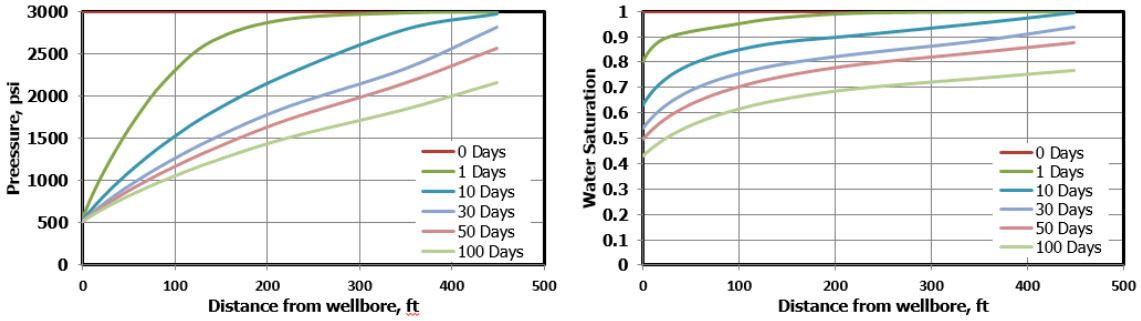

Fig. 50. Pressure and water saturation variation in the fracture starting from the wellbore to the tip of fracture with different times. This variation will affect total compressibility which is due to the gas flow.

In the presented method, total compressibility is calculated as gas volumetric compressibility ($c_g S_g$) at initial pressure and gas saturation = 1. Fig. 51 shows the assumed value for volumetric gas compressibility as the constant dashed line and the variation in volumetric gas compressibility in the fracture. The fracture volume is calculated when the fracture reach boundary dominated flow which is at later time. At later times, the volumetric gas compressibility is high near the wellbore (perforation) and low at the tip of the fracture. The assumed initial pressure value is a rigorous approximation for the volumetric gas compressibility that is used in the calculation.

To confirm the domination of gas phase in the fracture and the assumed method of calculations, plots of total mobility and compressibility in the fracture at different times are compared to gas mobility and compressibility as in Fig. 52 and Fig. 53. The difference is very small at early times (transient period) and at later time. This confirm that the assumption will not cause errors in the calculations.

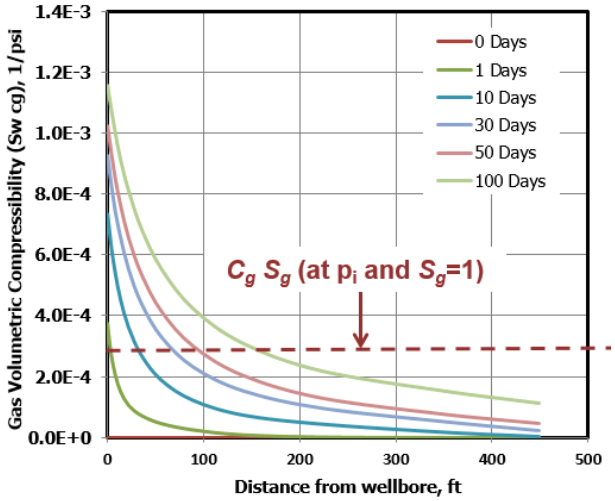

Fig. 51. Volumetric gas compressibility in the fracture at different time is affected by variations in pressure and saturations. The assumption of cg at pi and Sw = 1 shows an average value at all times since it is high near the perforation and low near the tip.

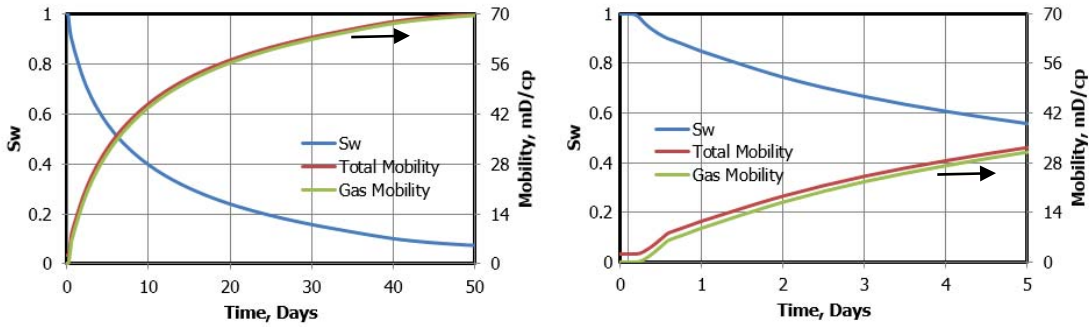

Fig. 52. Total mobility in the fracture is dominated by gas at different times with a small difference at early times which the fracture is still in transient period. As the water saturation decrease in the fracture the mobility difference is smaller.

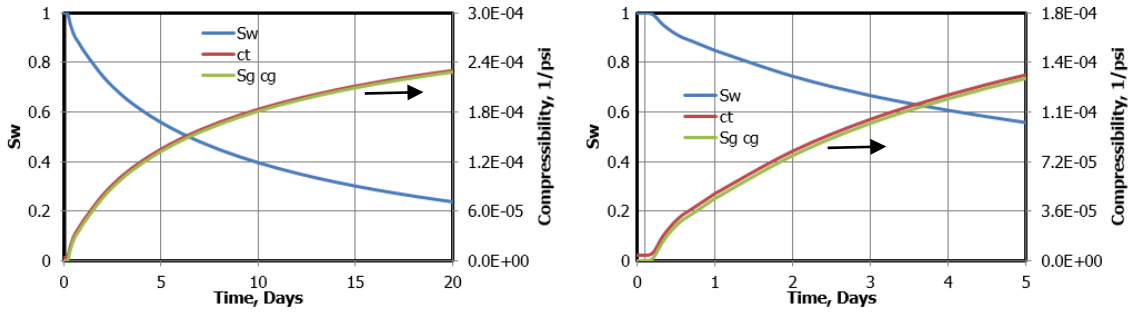

Fig. 53. Total compressibility in the fracture is dominated by gas at different times with a small difference at early times when the fracture is still in transient period. As the water decrease in the fracture, the compressibility difference is smaller.

5.5.1 Diffusivity Conditions

For gas to dominate the diffusivity equation of two phase system, two parameters to be dominated by gas: total mobility and total compressibility. The satisfaction of the mobility conditions depends on the relative permeability of the gas which depends on water saturation. The satisfaction of the compressibility condition depends on water saturation also. To illustrate this concept, Table 8 and Table 9 are constructed based on the values used in the single fracture simulation case.

As in Table 8, gas will dominate the total mobility at saturation value of 80% and any water saturation below (1- S_{girr}) is dominated by gas. For example, if S_{girr} = 0.3 then any location in the fracture with water saturation below 0.7, gas will dominate this location in the system.

As in Table 9, the volumetric gas compressibility is dominating the total compressibility also at high water saturations of 80%. The difference between volumetric

gas compressibility ($S_g\ c_g$) and total compressibility is 3% at $S_w = 0.7$. In general, if the water saturation is below 0.7, then gas is dominating the diffusivity equation (mobility and compressibility). Since the well flows high water rates at early time, gas will dominate the fracture volume at early times too.

Table 8 - Percentage of gas dominating the total mobility in the fracture at different saturation values

S_w	k_{rw}	k_{rg}	$(k_r/u)_w$	$(k_r/u)_g$	$(k_r/u)_t$	% gas Domination
0	0	1	0.0	50	50.0	100
0.1	0.1	0.9	0.2	45	45.2	99
0.2	0.2	0.8	0.5	40	40.5	99
0.3	0.3	0.7	0.7	35	35.7	98
0.4	0.4	0.6	0.9	30	30.9	97
0.5	0.5	0.5	1.2	25	26.2	96
0.6	0.6	0.4	1.4	20	21.4	93
0.7	0.7	0.3	1.6	15	16.6	90
0.8	0.8	0.2	1.9	10	11.9	84
0.9	0.9	0.1	2.1	5	7.1	70
1	1	0	2.3	0	2.3	0

Table 9 - Percentage difference between the volumetric compressibility of gas and total system in the fracture at different saturation values

S_w	S_g	c_t	$S_g\ c_g$	Difference
0	1	3.9E-4	3.9E-4	0.3%
0.1	0.9	3.5E-4	3.5E-4	0.5%
0.2	0.8	3.1E-4	3.1E-4	0.7%
0.3	0.7	2.7E-4	2.7E-4	0.9%
0.4	0.6	2.4E-4	2.3E-4	1.2%
0.5	0.5	2.0E-4	2.0E-4	1.6%
0.6	0.4	1.6E-4	1.6E-4	2.3%
0.7	0.3	1.2E-4	1.2E-4	3.3%
0.8	0.2	8.1E-5	7.8E-5	5.4%
0.9	0.1	4.3E-5	3.9E-5	11.0%
1	0	4.0E-6	0.0E+0	100.0%

5.6 Effective vs. Actual Fracture Volume

In the simulator, actual fracture volume is calculated and correlates with the input value. In field data, an effective fracture volume is calculated using water data since the fracture volume can be larger but not contributing to the gas flow. In most cases, the calculated fracture volume is around 20% of injected water. The rest of the injected water is either a fracture volume that is not connected to the contribution fracture system (lost) or it is produced from a nearby wells as can be seen in some cases.

5.7 Summary

A new method is developed to calculate fracture volume using single fracture model. Two cases of single phase water and two phase water and gas were simulated. Through modifying the total compressibility calculation, fracture volume that is occupied by water was back calculated in both cases. This method will be applied to field data to estimate fracture effective volume using water data.

CHAPTER VI

SINGLE WELL EXAMPLE

6.1 Introduction

In this chapter, single wells from Fayetteville and Barnett formation are analyzed. These wells provide clear examples of the methodology conformation and practical use. Well FF-1 was studied thoroughly and shows the details of calculating effective fracture volume along with the effect of flowback period on flow regime identification. Well B-151 was an example of how to apply the method if the flowback data is not available.

6.2 Well FF-1

This well is in the Fayetteville formation and has the properties shown in Table 10. The well was flowed back for 10 days and shut-in for 30 days and then produced for 4 years. This well was fraced with 72,600 STB of slick water. The cumulative produced water after 4 years of production = 10,160 STB and the rates at this time around 1 bbl/d. This well recovered only 15% of the injected water in 4 years which is similar to the reported values in the literature.

Table 10 - Properties of Well FF-1

Initial pressure, p_i (psi)	1736	Matrix porosity, φ (fraction)	0.04
Specific gravity, SG_g	0.58	Reservoir thickness, h (ft)	293
Reservoir temperature, T (°F)	118	Injector Water, V_{inj} (STB)	72,600
No. of Hydraulic Fractures, n_F	24		

6.2.1 Flow Regime Identification

This well will be explored on log-log plots with either time or material balance time in the x-axis for both water and gas rates for flowback, production and combined periods. Fig. 54 presents the flowback data of the well that has high water rates and low gas rates at the end showing the time the well was shut-in. After the shut-in, production period started as in Fig. 55 and this period is used in the usual PDA. Water production data does not have a clear signature in the time plot.

In the gas production period, a bilinear flow line (1/4 slope) can fit the early data for 100 days, but then followed by a linear flow for the rest of the period. Those two lines would be interpreted as early linear flow in the natural fracture and matrix at the same time creating the bilinear flow for 100 days. Then, the natural fracture reached the boundary and the matrix continues linear flow which shows that natural fractures have a clear contribution in the system. This conclusion can be reached when flowback data is ignored and only production period is analyzed.

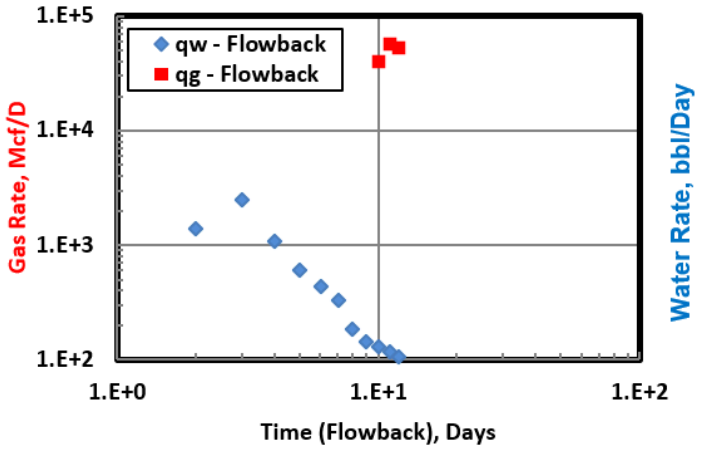

Fig. 54. Flowback period with gas starting to flow before shut-in.

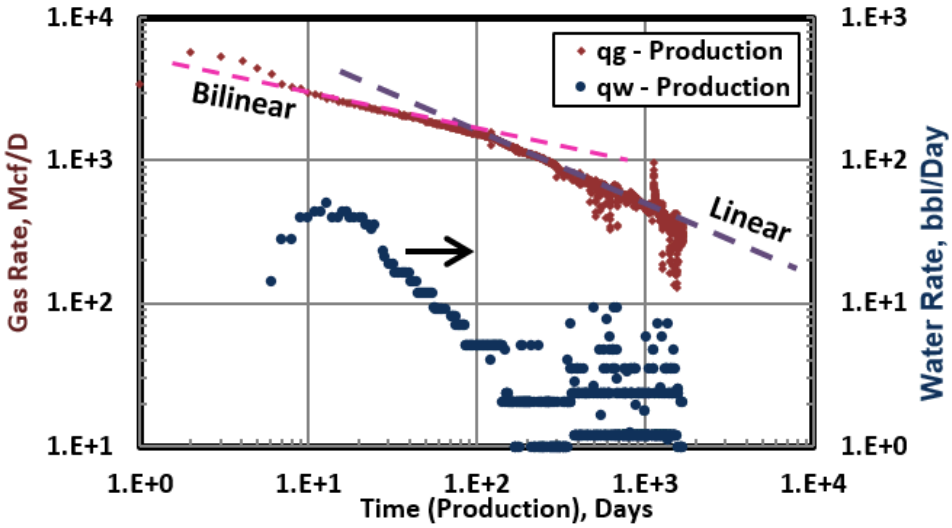

Fig. 55. Production period with gas data showing bilinear flow up to 100 days followed by linear flow. Water data does not have a clear signature.

To confirm the bilinear flow followed by linear flow, plots of pressure normalized rate for gas in the production period versus time is shown in Fig. 56 and versus material

balance time is shown in Fig. 57. The pressure normalized rate is used to remove the effect of non-constant bottomhole pressure. All the presented PDA diagnostic plots conclude that this well has a long period of bilinear flow, but combining flowback and production data will correct this conclusion.

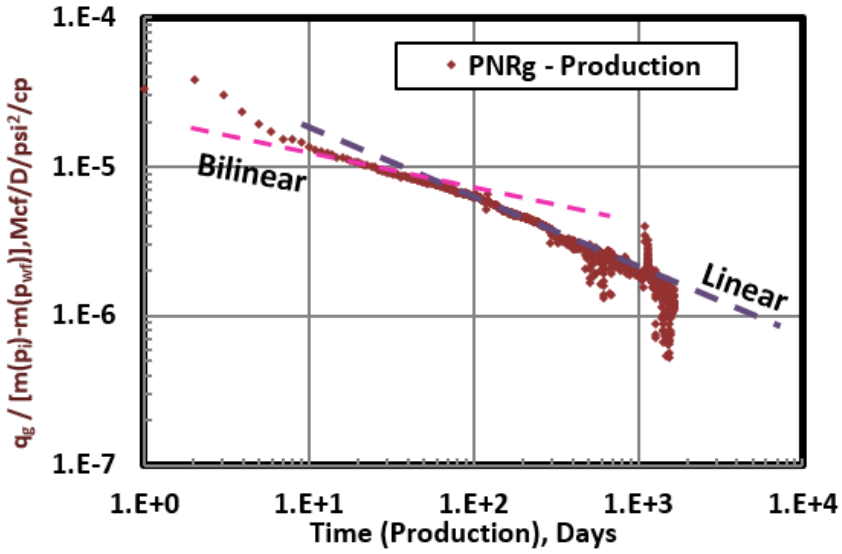

Fig. 56. Rate normalized by pressure versus production time indicates the bilinear flow followed by linear flow just like in the rate plot.

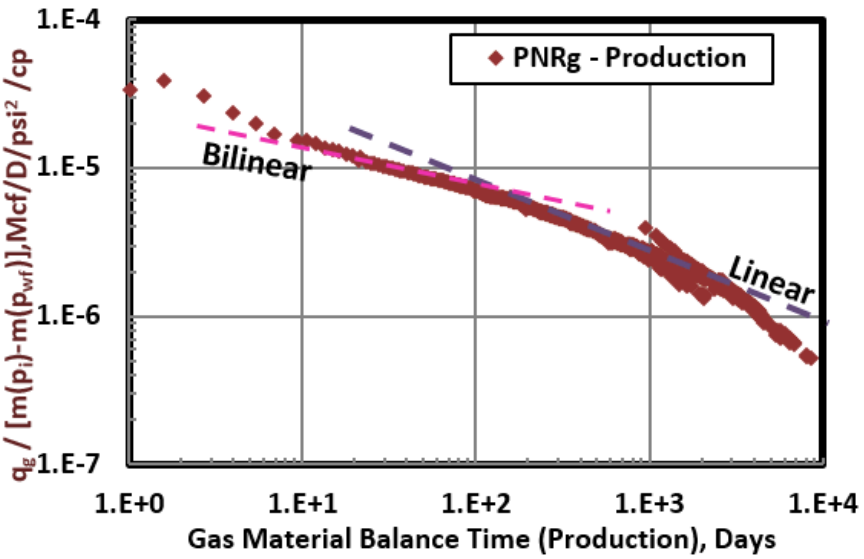

Fig. 57. Rate normalized by pressure versus material balance time showing the bilinear flow.

Although it is the practice in some companies, there is no reason to remove flowback data from production period if they are separated by a shut-in period. In Fig. 58, flowback data was combined with the production data and noticed a big difference in the gas rate signature of the well versus time. The bilinear flow disappeared and was replaced by a longer linear flow with a spike at the beginning which is normal; the gas rate typically starts flowing at higher rates after a month of shut-in. Including the flowback period with the shut-in time shifted the production data in time to give the correct signature of longer linear. Taking the first point of the production data to be at 1 day instead of 45 days (adding flowback and shut-in) would make the early linear flow look bilinear.

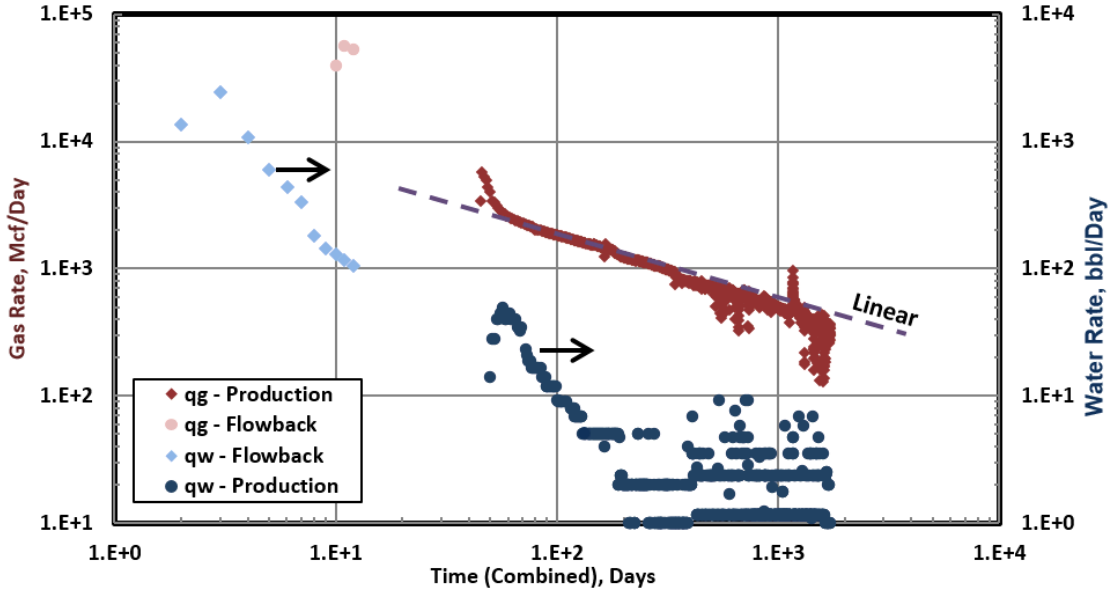

Fig. 58. Combining flowback and production data made the bilinear flow in gas disappear and be replaced by a longer linear flow with a spike at the beginning due to the shut-in period of a month.

To confirm the misleading bilinear flow, gas pressure normalized rate is plotted versus time for production period only and then compared with combined period as in Fig. 59. Adding 3 points of gas rates to the PDA can shift the data which causes it to give the correct flow regime. This shows the benefit of including flowback data in flow regime identification. In the next section, water data is analyzed and effective fracture volume was calculated.

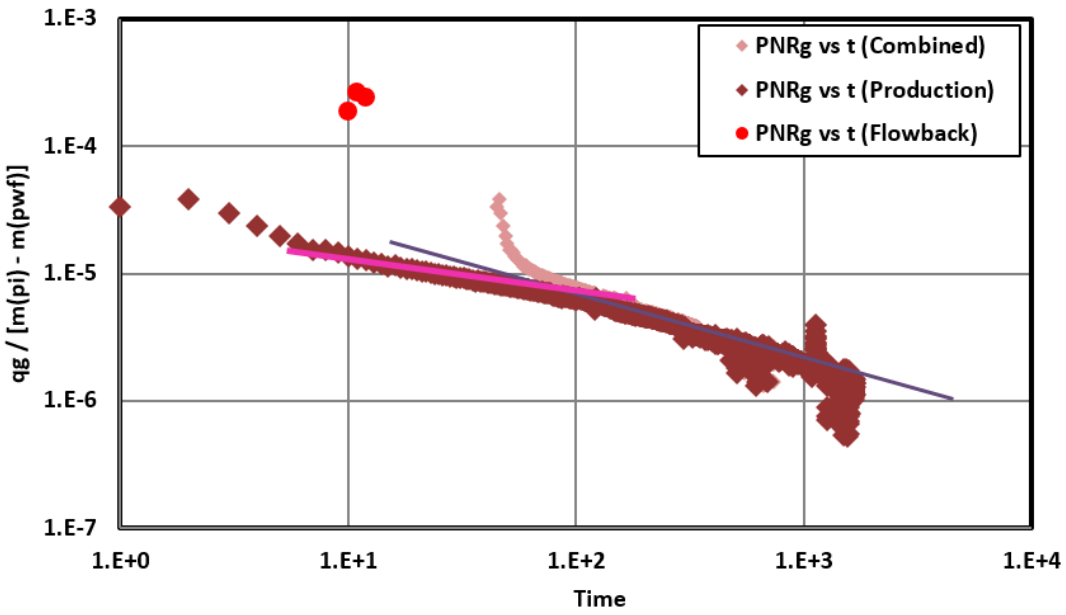

Fig. 59. Gas rate in production time only showing bilinear flow and the same data under combined time (flowback + shut-in + production) showing only linear flow.

6.2.2 Effective Fracture Volume Calculation

Combining flowback and production data affected the material balance time plot of water normalized rate. In Fig. 60, the pressure normalized rate is plotted for the production period (dark blue square) and a unit slope line (1) is indicated at the end of the data. This data is missing around 10 days of high rates from the flowback period which will shift production data since the material balance time value will be higher due to higher cumulative. In the same plot, the flowback period (light circle) is plotted with the production period (dark circle). It is noticed that the production period falls on the same unit slope line (2) that started in the flowback period. The unit slope line (1) from this production period would give smaller effective water volume compared to the combined

data unit slope line (2). Ignoring the water flowback period might indicate a smaller effective water volume if the flowback period is long with high rates.

Fig. 61 is showing combined data with the derivative to find the slope m_{pss} which is the slope of the Cartesian plot in the period of unit slope line where the line or RNP_w is over RNP'_w (derivative) line. The solutions are shown in Table 11 with the calculated effective water volume as 14% of the injected water volume. Around 96% of the calculated effective water volume is produced which is in agreement with the low water rates of 2 STB/D. Also, water data were analyzed using empirical equation and the water EUR for 30 years is 10,500 STB which is close to the calculated effective fracture volume.

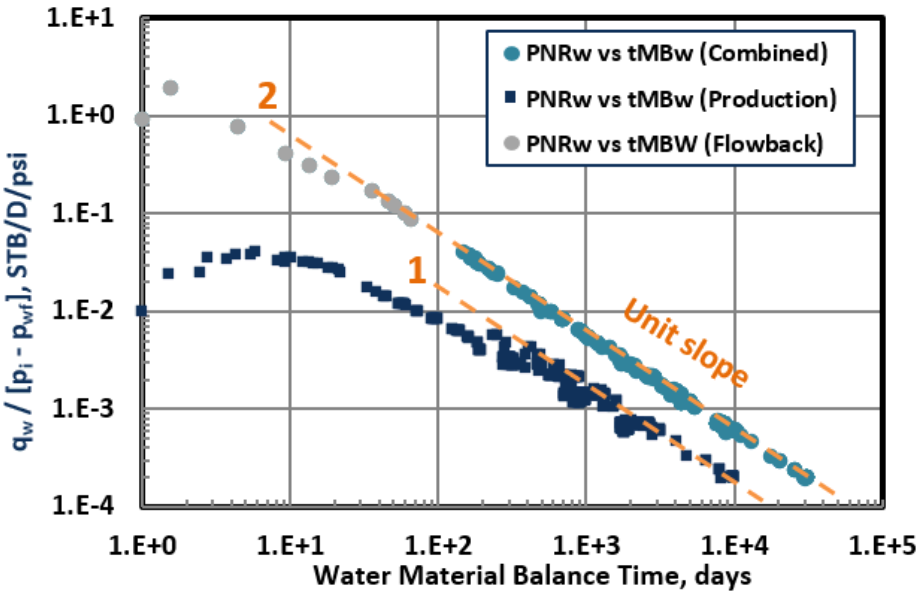

Fig. 60. The lower points (dark) are for the production rates and times. The upper curve (light) is created by adding flowback rates and times. The time shift results in a larger effective water volume.

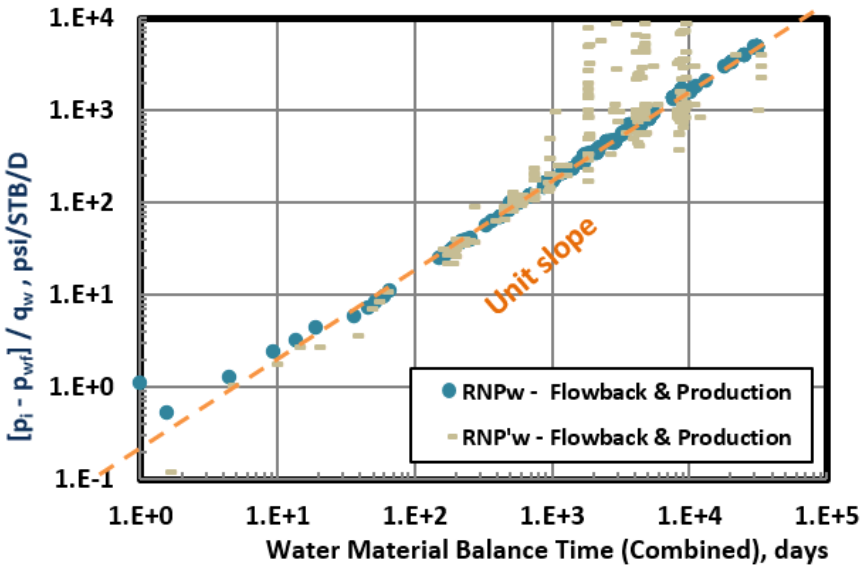

Fig. 61. Unit slope line is used to calculate slope of boundary dominated flow period to estimate effective fracture volume of water.

Table 11 - Effective water volume calculations from Well FF-1

Slope of BDF period, m_{pss}	0.157	Water FVF, B_w (res bbl/STB)	1
Gas compressibility, c_g (psi^{-1})	6.15 x 10^{-4}	Cumulative produced water, (STB)	10,177
Calculated Water Volume, V_w (STB)	10,400		

6.3 B-151

This well is in Barnett formation and was analyzed by several authors. This well was chosen to show how to include the flowback period even if the data is not available. As in Fig. 62, the well has bilinear flow for 150 days followed by linear flow. The completion data shows there is a period of 15 days between the fracing of the well and the time of production. If this delay period is included in the production data, the gas rate will

be as in Fig. 63 which is a longer linear flow. The disappearance of bilinear flow make a big difference in constructing a representative model of the well.

If water decline in both plots (with and without shift) is compared, it is noticed that water slope is 1 or less (without shift) and in the shifted data, water slope follows the normal decline of slopes higher than 1. Even if the flowback data is not available, the delay time should be included to avoid stretching the data and giving the wrong reservoir signature. Material balance time plot should be used carefully since data from the flowback period is not used and can give misleading results and smaller effective fracture volume value.

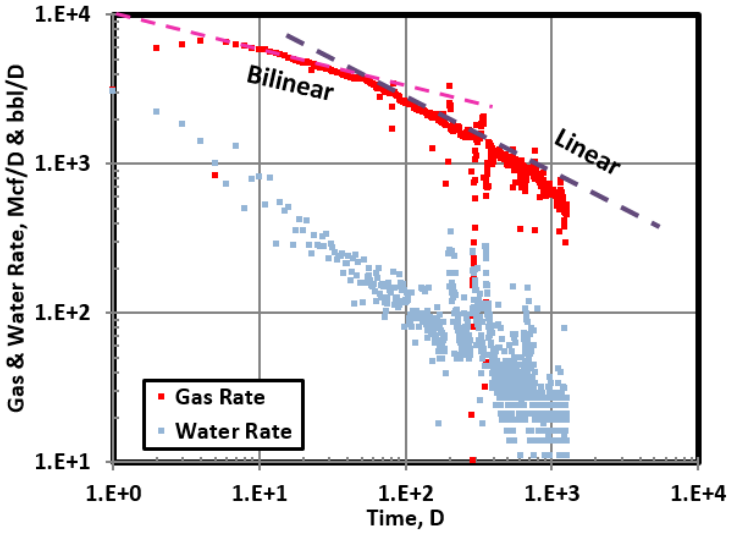

Fig. 62. Bilinear flow for 150 days followed by linear flow in gas rate and water has a low slope of around 1.

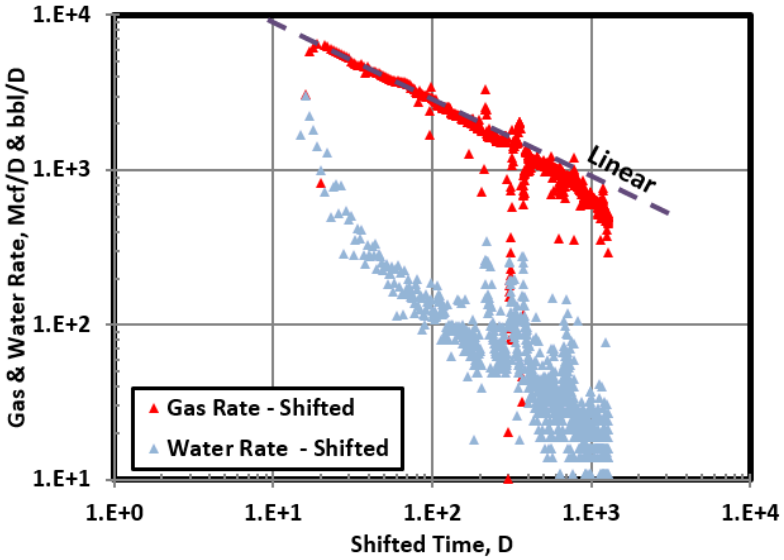

Fig. 63. Shifting the data 15 days due to delay caused the bilinear flow to disappear, a long linear flower to be created instead and water flow have the normal high slope of higher than 1.

6.4 Summary

Including flowback data has an effect on both time and material balance time diagnostic plots. In time plots, it will shift the data giving possibly a different signature than the original. In material balance time, the data is shifted due to adding extra high rates in the flowback period which will give the correct BDF in water data. If the production data was analyzed without flowback data and compared with combined data, the difference might be big. In some wells, including or excluding flowback data would make a difference in flow regime identification. To avoid misinterpretation, flowback data should be included in the analysis. In the next section, multi well data were analyzed.

CHAPTER VII

MULTI WELL EXAMPLES

7.1 Introduction

After applying the analysis to single wells, the presented method is applied to multi well examples to show broader benefits in evaluating and comparing between frac jobs. A four wells pad example illustrated the use of effective fracture volume as a monitoring and tracking method for the effect of nearby frac jobs. Finally, a five wells pad configuration showed how the frac sequence and placement of the well can affect the effective fracture volume and its relationship with gas production.

7.2 Four Wells Pad

A four wells pad is located in Fayetteville formation with the map shown in Fig. 64. The oldest well in the pad is FF-18 and the three wells were drilled next to it. The flow sequence of this well is studied over three periods with each period marking the fracing of a new well. Period 1 marks the time of FF-18 flowing only, period 2 marks the fracing of FF-13 and period 3 is after fracing wells FF-19 and FF-20. This period separation will help in understanding the effect of fracing new wells on estimated effective fracture volume.

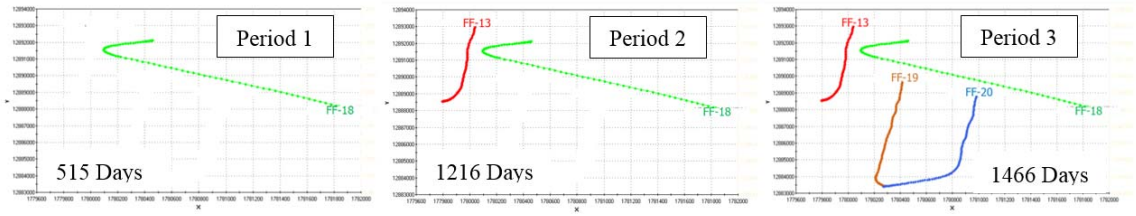

Fig. 64. A map of all wells in the four wells pad. The production of the well FF-18 is divided into 3 periods where period 1 is before well FF-13 is fraced, period 2 is before wells FF-19 and FF-20 are fraced and period 3 is to the end of the data.

Well FF-18 was fraced by injecting water volume of 132,586 STB as shown in Table 12. After 515 days of production, the cumulative water produced is 6% of the injected volume and water production is around 5 STB/D as in Fig. 65. Using Fig. 66, FF-18 water effective volume for period 1 can be calculated, which is reported in Table 12 as 8% of the injected volume and 77% of this effective water volume is already produced.

Well FF-13 was fraced which increased water production but the effective water volume did not change significantly as in the red line of period 2 in Fig. 66. This can be observed where period 1 and 2 are almost on the same unit slope line. This is not the case in period 3 where the slope is shifted to the right indicating an increase in effective water volume due to fracing wells FF-19 and FF-20. This increase in water volume affected gas rates which increased in FF-18. The new effective volume is 10% of the injected volume and 95% of this volume was produced water as in Table 12. This method can be a mean of tracking the interference effect of newly drilled wells on effective fracture volume.

Table 12 - Water data for Well FF-18

Water Volume, STB	Period 1	Period 3
Injected (Frac Job)	132,586	132,586
Cumulative Produced	8,799	12,992
Calculated	11,351	13,695

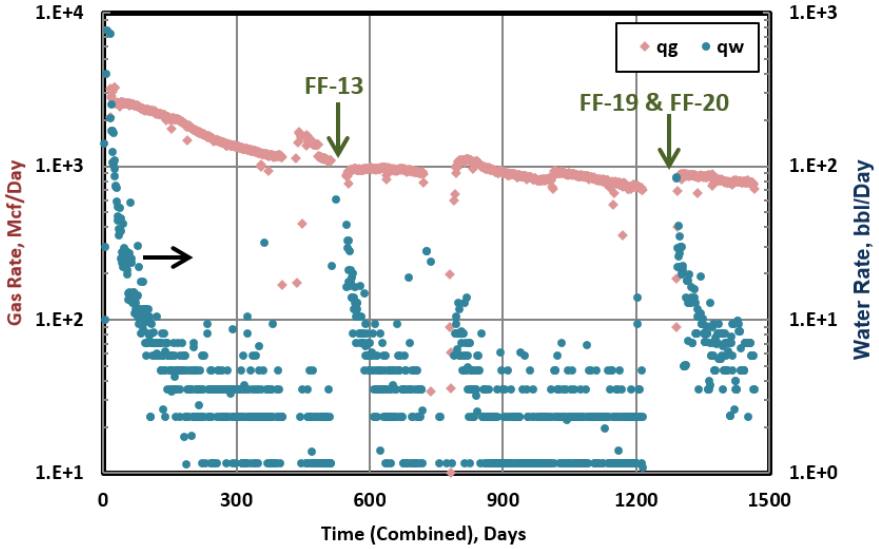

Fig. 65. Water and gas production of the combined period (flowback and production) for well FF-18 with the other wells effective as in FF-19 and FF-20 which increased gas and water production.

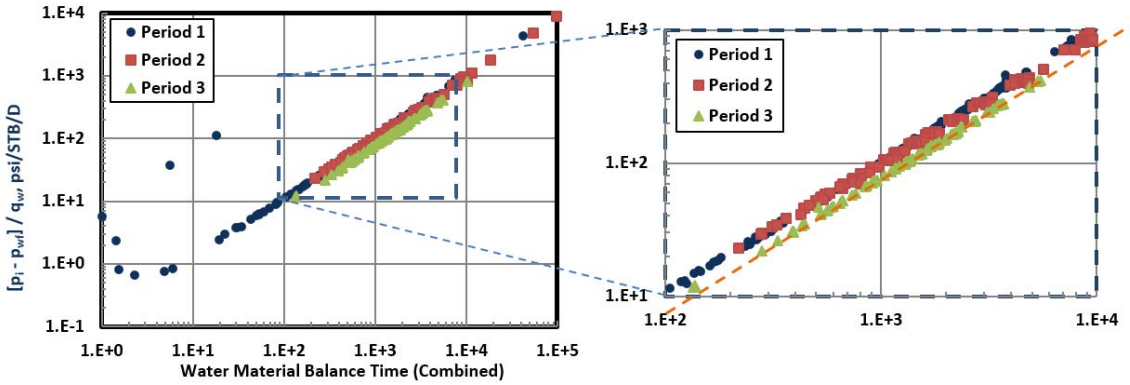

Fig. 66. Water RNP showing the three periods with a unit slope indicating boundary dominated flow and in period 3 the increase in water effective volume (unit slope moves to the right) related to fracing of wells FF-19 and FF-20.

7.3 Five Wells Pad

The pad in Fig. 67 were analyzed by Harpel et al. (2012) in order to find the optimum frac job. Three wells have the same well's properties and frac job treatment (FF-21, FF-22 and FF-24). Well FF-23 had the same well's properties but the frac job injected volume was decreased to 60%. Well FF-25 had a longer well length and the same frac job as the first three wells. This pad offered a great opportunity to test the presented methodology since the properties are the same and only the frac job injected volume is different.

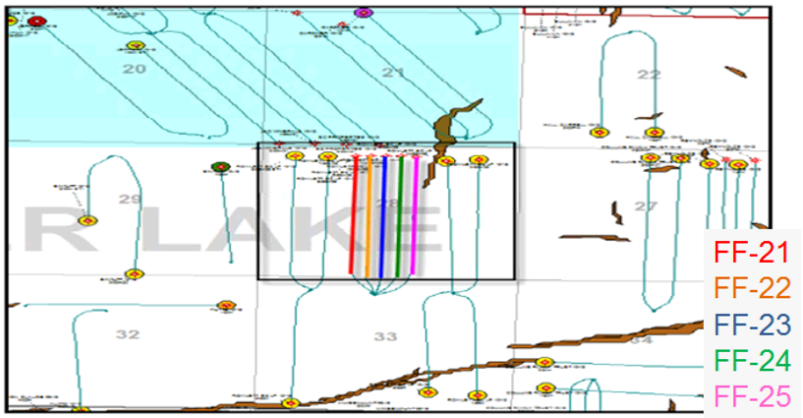

Fig. 67. Map of the five wells pad with well FF-23 in the middle with the frac volume reduced to 60% of the originally injected volume in the other wells.

Table 13 shows the well's data and it is important to notice the sequence of fracing which might have an effect over the created water volume. Since FF-25 had a longer well length, it was removed from the comparison analysis. The cumulative water produced and calculated water volumes as shown in Table 14. Fig. 68shows that the water values vary between the wells which suggest that not all the injected volume contributed to the created volume.

The results shows that FF-21 has the highest cumulative water and calculated volume. Although FF-22 used the same frac fluid volume, it produced less water and the calculated water volume is less if compared to FF-21. The difference between FF-21 and FF-22 might be due to the sequence of fracturing since FF-21 was fraced before FF-22. The same trends is noticed between FF-24, FF-21 and FF-22 which might be due to sequence and the location of the well.

On the other hand, well FF-23 used 60% of the originally injected volume and produced 50% of the cumulative water if compared to an average of the other wells' cumulative. The calculated water volume using the proposed method gives almost the same percentage. Well FF-23 produced more than the calculated water volume which might be due to communication with the other wells. The total cumulative produced water is 91% of the total calculated water volume which might suggest that the wells are in communication.

Table 13 - Data for the five Wells pad

Well	Well Length	No. of Frac	Injected Fluid, bbl	Frac Sequence
FF-21	4,542	60	93,221	1
FF-22	4,722	60	91,085	2
FF-23	4,722	60	62,052	5
FF-24	4,722	60	91,215	3
FF-25	5,137	66	97,659	4

Table 14 - Water data for five Wells pad

Well	Cum. Water, bbl	% Rec. Injected	Water Volume Calc., bbl	% Rec. Calc. Water Vol.
FF-21	11,000	12	12,900	85
FF-22	9,300	10	10,500	88
FF-23	4,500	7	4,200	107
FF-24	6,400	7	6,700	95
FF-25	7,300	7	7,600	80
Total	38,500		41,900	91

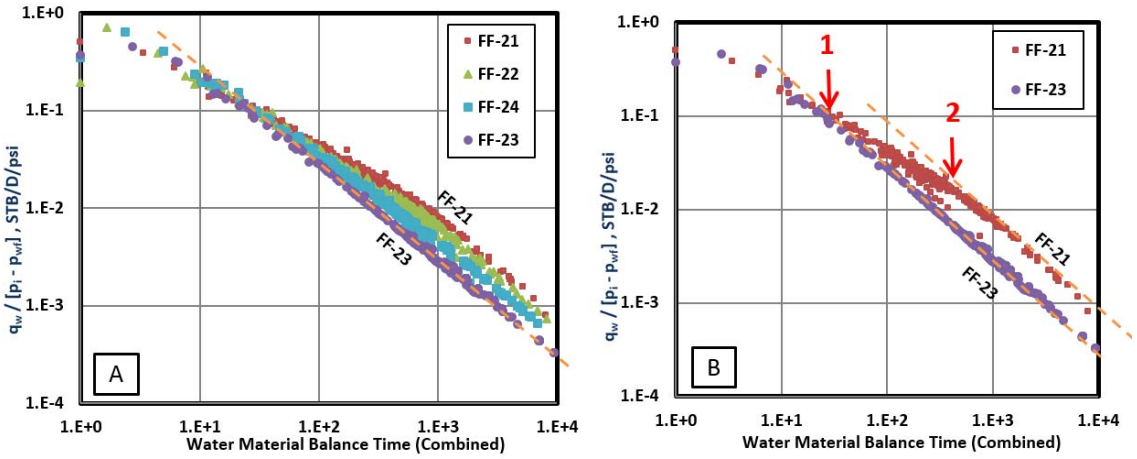

Fig. 68. A: Water RNP showing a unit slope indicating BDF in all wells with the smallest volume in FF-23 and the largest in FF-21; B: the start of BDF is fast in FF-23 compared to FF-21 which is delayed and with the bigger water volume, the start is delayed as seen in arrow 1 and 2.

Gas production data for the pad is presented in Fig. 69. Well FF-23 was the best producer in terms of gas rates (also cumulative) and in terms of the product $\sqrt{k_{eff}}A_{cm}$. The product is calculated from the slope of Fig. 69-B. Although the frac job volume was reduced to 60%, the well had the best performance which might be due to the placement in the middle of the 5 wells with the last one to be fraced. It is worth mentioning that this well produced the highest gas cumulative and the lowest water cumulative which is in agreement with previous reported results.

On the other hand, well FF-21 was the lowest gas producer (also cumulative) with the highest water cumulative. This might be due to the fact that it was fraced first with the left side of the well not stimulated since there is no well on this side. The results of this pad suggest that the wells in the middle of the pad if fraced last, will produced more gas

and less water if compared to the rest of the wells in the pad. This concept needs further investigation.

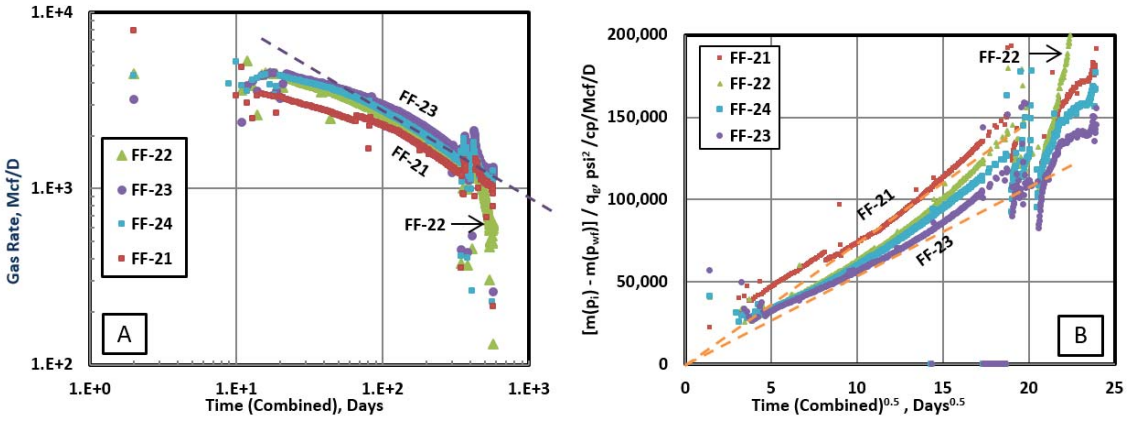

Fig. 69. A: Gas rate showing linear flow in all wells with well FF-23 having the highest gas rates although it was fraced with 60% injected volume compared to other wells; B: Straight line indicating linear flow in all wells with well FF-23 having the highest $\sqrt{k_{eff}}A_{cm}$ and well FF-21 having the lowest $\sqrt{k_{eff}}A_{cm}$ although it was fraced with the highest volume.

7.4 Summary

In multi well examples, the proposed method for estimating effective fracture volume help in comparing and evaluating frac jobs between wells in the same pad. Also, this method helped in monitoring and tracking changes in effective fracture volume due to nearby frac job.

CHAPTER VIII

CONCLUSIONS AND RECOMMENDATIONS

8.1 Conclusions

The main conclusions can be summarized as follows.

- Rules have been presented here for cases where low conductivity, large spacing natural fractures have no effect on production rates. For these cases, analytical solutions can be used.
- Rules have also been presented here for other cases where high conductivity, small spacing natural fractures have a great effect on production rates. For those cases, analytical solution can be used.
- For cases in between, simulation should be used instead of analytical solutions.
- The analytical solution and simulator will correctly produce bilinear flow only if $R_{sp} < 0.1$ and a low value of R_k.
- Effective permeability equation from analytical solution with the assumption of homogenous model can help the engineer avoid extra simulation work to match the model and avoid errors in calculating A_{cm}.
- No effect of tip refinement if the fracture is fully penetrating the reservoir as assumed in the analytical solution.
- Hydraulic fracture with a large width (0.1 ft) increases water saturation in the fracture and caused liquid loading effect. Liquid loading is not observed in natural fracture due to small width and low permeability.

- Unless the natural fracture is isolated, no fracture can be fully saturated with water due to its contribution to flow; the maximum water saturation that can be held in the natural fracture is 60% after 30 years of production.
- Relative permeability jail curves do not mimic field data after shut-ins.
- Hybrid relative permeability jail curves are developed which shows trapped water represents the signature that is observed in the field data. Hybrid relative permeability jail curve can match field data in periods of flowback, shut-in and production. Also, serves the purpose of trapping around 60% of the water in the natural fracture.
- Low natural fracture spacing could be one of the reasons for low water recovery. The existence of more natural fracture trapping water could be a possible explanation for the low water recovery in some wells. Natural fracture (spacing = 0.1 ft, width = 0.0001 ft) would justify a large percentage of the trapped injected water.
- Gas dominates the diffusivity equation in the water/gas system if the mobility and compressibility conditions are met which is usually around $S_w < 0.7$ in the fracture.
- A new method was developed to calculate effective fracture volume (water volume) by modifying the total compressibility calculation to include gas compressibility. Also, this method can be a means of tracking the interference effect of newly drilled wells on effective water volume of the existing wells.
- In production data analysis, ignoring flowback data can lead to misinterpretation in flow regime identification and any early gas/water data should be included in

the analysis even if it is separated by a shut-in period. Including flowback data has an effect on both time and material balance time diagnostic plots. Ignoring flowback period with high water rates might indicate a smaller effective water volume.

- Even if the flowback data is not available, the delay time should be included to avoid the stretching of data and giving the wrong reservoir signature.
- Water rate normalized pressure plot can be used as a tool to evaluate frac jobs based on effective fracture volume.

8.2 Recommendations

The followings are recommended for future work.

- The proposed methodology of estimating effective fracture volume can be applied to oil wells.
- Apply the proposed methodology to different fields.
- Simulate three phase (oil/gas/water) to investigate water distribution and the application of permeability jail curve.

REFERENCES

Abbasi, M., Dehghanpour, H., and Hawkes, R.V. 2012. Flowback Analysis for Fracture Characterization. Paper presented at the SPE Canadian Unconventional Resources Conference, Calgary, Alberta, Canada. Society of Petroleum Engineers SPE-162661-MS. DOI: 10.2118/162661-ms.

Arevalo-Villagran, J.A., Wattenbarger, R.A., Samaniego-Verduzco, F. et al. 2001. Production Analysis of Long-Term Linear Flow in Tight Gas Reservoirs: Case Histories. Paper presented at the SPE Annual Technical Conference and Exhibition, New Orleans, Louisiana. 2 Society of Petroleum Engineers 00071516. DOI: 10.2118/71516-ms.

Arogundade, O. and Sohrabi, M. 2012. A Review of Recent Developments and Challenges in Shale Gas Recovery. Paper presented at the SPE Saudi Arabia Section Technical Symposium and Exhibition, Al-Khobar, Saudi Arabia. Society of Petroleum Engineers SPE-160869-MS. DOI: 10.2118/160869-ms.

Bello and Wattenbarger, R.A. 2010. Multi-Stage Hydraulically Fractured Horizontal Shale Gas Well Rate Transient Analysis. Paper presented at the North Africa Technical Conference and Exhibition, Cairo, Egypt. Society of Petroleum Engineers SPE-126754-MS. DOI: 10.2118/126754-ms.

Blasingame, T.A. 2008. The Characteristic Flow Behavior of Low-Permeability Reservoir Systems. Paper presented at the SPE Unconventional Reservoirs Conference,

Keystone, Colorado, USA. Society of Petroleum Engineers SPE-114168-MS. DOI: 10.2118/114168-ms.

Chekani, M., Bagherpour, M.H., Alavi, M.F. et al. 2010. Novel Approach to Mitigate Gas Production in a High Gor Carbonate Reservoir with Drilled Wells—Case Study. Paper presented at the SPE Production and Operations Conference and Exhibition, Tunis, Tunisia. Society of Petroleum Engineers SPE-135875-MS. DOI: 10.2118/135875-ms.

Cheng, Y. 2010. Impact of Water Dynamics in Fractures on the Performance of Hydraulically Fractured Wells in Gas Shale Reservoirs. Paper presented at the SPE International Symposium and Exhibiton on Formation Damage Control, Lafayette, Louisiana, USA. Society of Petroleum Engineers SPE-127863-MS. DOI: 10.2118/127863-ms.

Clarkson, C.R. 2012. Modeling 2-Phase Flowback of Multi-Fractured Horizontal Wells Completed in Shale. Paper presented at the SPE Canadian Unconventional Resources Conference, Calgary, Alberta, Canada. Society of Petroleum Engineers SPE-162593-MS. DOI: 10.2118/162593-ms.

Crafton, J.W. 2008. Modeling Flowback Behavior or Flowback Equals "Slowback". Paper presented at the SPE Shale Gas Production Conference, Fort Worth, Texas, USA. Society of Petroleum Engineers SPE-119894-MS. DOI: 10.2118/119894-ms.

Crafton, J.W. 2010. Flowback Performance in Intensely Naturally Fractured Shale Gas Reservoirs. Paper presented at the SPE Unconventional Gas Conference,

Pittsburgh, Pennsylvania, USA. Society of Petroleum Engineers SPE-131785-MS. DOI: 10.2118/131785-ms.

De Swaan O., A. 1976. Analytic Solutions for Determining Naturally Fractured Reservoir Properties by Well Testing. *Society of Petroleum Engineers Journal* **16** (3): 117-122. DOI: 10.2118/5346-pa

Ehlig-Economides, C.A. and Economides, M.J. 2011. Water as Proppant. Paper presented at the SPE Annual Technical Conference and Exhibition, Denver, Colorado, USA. Society of Petroleum Engineers SPE-147603-MS. DOI: 10.2118/147603-ms.

El-Banbi, A., H. and Wattenbarger, R.A. 1998. Analysis of Linear Flow in Gas Well Production. Paper presented at the SPE Gas Technology Symposium, Calgary, Alberta, Canada. 1998 Copyright 1998, Society of Petroleum Engineers Inc. 00039972. DOI: 10.2118/39972-ms.

Everdingen, A.F.V. and Hurst, W. 1949. The Application of the Laplace Transformation to Flow Problems in Reservoirs. Paper presented at the AIME Annual Meeting in San Francisco, USA. DOI: 10.2118/949305-G.

Fan, L., Thompson, J.W., and Robinson, J.R. 2010. Understanding Gas Production Mechanism and Effectiveness of Well Stimulation in the Haynesville Shale through Reservoir Simulation. Paper presented at the Canadian Unconventional Resources and International Petroleum Conference, Calgary, Alberta, Canada. Society of Petroleum Engineers SPE-136696-MS. DOI: 10.2118/136696-ms.

Gdanski, R.D. and Walters, H.G. 2010. Impact of Fracture Conductivity and Matrix Relative Permeability on Load Recovery. Paper presented at the SPE Annual

Technical Conference and Exhibition, Florence, Italy. Society of Petroleum Engineers SPE-133057-MS. DOI: 10.2118/133057-ms.

Harpel, J.M., Barker, L.B., Fontenot, J.M. et al. 2012. Case History of the Fayetteville Shale Completions. Paper presented at the SPE Hydraulic Fracturing Technology Conference, The Woodlands, Texas, USA. Society of Petroleum Engineers SPE-152621-MS. DOI: 10.2118/152621-ms.

Ibrahim, M. and Wattenbarger, R.A. 2005. Analysis of Rate Dependence in Transient Linear Flow in Tight Gas Wells. Paper presented at the Canadian International Petroleum Conference, Calgary, Alberta. Petroleum Society of Canada PETSOC-2005-057. DOI: 10.2118/2005-057.

Jargon, J.R. and Van Poollen, H.K. 1965. Unit Response Function from Varying-Rate Data. Paper presented at the SPE Annual Fall Meeting, Houston, USA. DOI: 10.2118/981-PA.

Kazemi, H. 1969. Pressure Transient Analysis of Naturally Fractured Reservoirs with Uniform Fracture Distribution. Paper presented at the 43rd Annual Fall Meeting, Houston, USA. DOI:10.2118/2156-A.

King, G.E. 2010. Thirty Years of Gas Shale Fracturing: What Have We Learned? Paper presented at the SPE Annual Technical Conference and Exhibition, Florence, Italy. Society of Petroleum Engineers SPE-133456-MS. DOI: 10.2118/133456-ms.

Noe, S. and Crafton, J. 2013. Impact of Delays and Shut-Ins on Well Productivity. Paper presented at the 2013 SPE Eastern Regional Meeting, Pittsburgh, Pennsylvania,

USA. 2013, Society of Petroleum Engineers SPE-165705-MS. DOI: 10.2118/165705-ms.

Novlesky, A., Kumar, A., and Merkle, S. 2011. Shale Gas Modeling Workflow: From Microseismic to Simulation -- a Horn River Case Study. Paper presented at the Canadian Unconventional Resources Conference, Alberta, Canada. Society of Petroleum Engineers SPE-148710-MS. DOI: 10.2118/148710-ms.

Odusina, E.O., Sondergeld, C.H., and Rai, C.S. 2011. An Nmr Study of Shale Wettability. Paper presented at the Canadian Unconventional Resources Conference, Alberta, Canada. Society of Petroleum Engineers SPE-147371-MS. DOI: 10.2118/147371-ms.

Pagels, M., Hinkel, J.J., and Willberg, D.M. 2012. Measuring Capillary Pressure Tells More Than Pretty Pictures. Paper presented at the SPE International Symposium and Exhibition on Formation Damage Control, Lafayette, Louisiana, USA. Society of Petroleum Engineers SPE-151729-MS. DOI: 10.2118/151729-ms.

Palacio, J.C. and Blasingame, T.A. 1993. Unavailable - Decline-Curve Analysis with Type Curves – Analysis of Gas Well Production Data. Paper presented at the SPE Low Permebility Reservoir Symposium, Denver, Colorado, USA. DOI: 10.2118/25909-MS.

Penny, G.S., Dobkins, T.A., and Pursley, J.T. 2006. Field Study of Completion Fluids to Enhance Gas Production in the Barnett Shale. Paper presented at the SPE Gas Technology Symposium, Calgary, Alberta, Canada. Society of Petroleum Engineers SPE-100434-MS. DOI: 10.2118/100434-ms.

Roychaudhuri, B., Tsotsis, T.T., and Jessen, K. 2011. An Experimental and Numerical Investigation of Spontaneous Imbibition in Gas Shales. Paper presented at the SPE Annual Technical Conference and Exhibition, Denver, Colorado, USA. Society of Petroleum Engineers SPE-147652-MS. DOI: 10.2118/147652-ms.

Rubin, B. 2010. Accurate Simulation of Non Darcy Flow in Stimulated Fractured Shale Reservoirs. Paper presented at the SPE Western Regional Meeting, Anaheim, California, USA. Society of Petroleum Engineers SPE-132093-MS. DOI: 10.2118/132093-ms.

Serra, K., Reynolds, A.C., and Raghavan, R. 1983. New Pressure Transient Analysis Methods for Naturally Fractured Reservoirs(Includes Associated Papers 12940 and 13014). *Journal of Petroleum Technology* **35** (12): 2271-2283. DOI: 10.2118/10780-pa

Shaoul, J.R., Zelm, L.F.V., and Pater, H.J.D. 2011. Damage Mechanisms in Unconventional Gas Well Stimulation - a New Look at an Old Problem. Paper presented at the SPE Middle East Unconventional Gas Conference and Exhibition, Muscat, Oman. Society of Petroleum Engineers SPE-142479-MS. DOI: 10.2118/142479-ms.

Sharma, M. and Agrawal, S. 2013. Impact of Liquid Loading in Hydraulic Fractures on Well Productivity. Paper presented at the 2013 SPE Hydraulic Fracturing Technology Conference, The Woodlands, TX, USA. Society of Petroleum Engineers SPE-163837-MS. DOI: 10.2118/163837-ms.

Thompson, J.W., Fan, L., Grant, D. et al. 2010. An Overview of Horizontal Well Completions in the Haynesville Shale. Paper presented at the Canadian Unconventional Resources and International Petroleum Conference, Calgary, Alberta, Canada. Society of Petroleum Engineers SPE-136875-MS. DOI: 10.2118/136875-ms.

Tivayanonda, V., Apiwathanasorn, S., Economides, C. et al. 2012. Alternative Interpretations of Shale Gas/Oil Rate Behavior Using a Triple Porosity Model. Paper presented at the SPE Annual Technical Conference and Exhibition, San Antonio, Texas, USA. Society of Petroleum Engineers SPE-159703-MS. DOI: 10.2118/159703-ms.

Tran, T., Sinurat, P.D., and Wattenbarger, B.A. 2011. Production Characteristics of the Bakken Shale Oil. Paper presented at the SPE Annual Technical Conference and Exhibition, Denver, Colorado, USA. Society of Petroleum Engineers SPE-145684-MS. DOI: 10.2118/145684-ms.

Wang, D., Butler, R., Liu, H. et al. 2010. Flow Rate Behavior and Imbibition in Shale. Paper presented at the SPE Eastern Regional Meeting, Morgantown, West Virginia, USA. Society of Petroleum Engineers SPE-138521-MS. DOI: 10.2118/138521-ms.

Warren, J.E. and Root, P.J. 1963. The Behavior of Naturally Fractured Reservoirs. Paper presented at the SPE Fall Meeting, Los Angeles, USA. Society of Petroleum Engineers SPE-426. DOI:10.2118/426-PA.

Winestock, A.G. and Colpitts, G.P. 1965. Advances in Estimating Gas Well Deliverability. Paper presented at the 16th Annual Technical Meeting, Calgary, Canada. Petroleum Society of C.I.M. JCPT-65-03-01. DOI:10.2119/65-03-01.

APPENDIX A

SHALE WELL ANALYSIS

Linear flow characterized by half slope is to be identified in the log-log plot of q_g vs. t for gas wells. Then, plot $[m(p_i) - m(p_{wf})]/q_g$ vs. $t^{0.5}$ to calculate t_{esr} which is the end of straight line passing through the origin if the well did not have "skin effect". If the line did not pass through the origin, it is a sign of skin effect which was addressed in Bello & Wattenbarger (2010). From the same plot, calculate the slope $\tilde{m}_4$ matching the linear flow data and passing through the origin. Using Eq. 3.1, an effective permeability can be calculated based on t_{esr}. The equation below can be used to calculate total surface area draining into hydraulic fracture A_{cm}

$$A_{cm} = f_{cp} \frac{1262T}{\sqrt{k_{eff}}\sqrt{\phi\mu c_t}} \frac{1}{\tilde{m}_4} \qquad \text{..... (A1)}$$

Where f_{cp} is a correction factor to account for the level of pressure drawdown in gas wells only, Ibrahim & Wattenbarger (2005), which is defined as

$$f_{CP} = 1 - 0.0852\ D_D - 0.0857\ D_D^2 \qquad \text{..... (A2)}$$

And D_D is the dimensionless drawdown

$$D_D = \frac{m(p_i) - m(p_{wf})}{m(p_i)} \qquad \text{..... (A3)}$$

Fracture half length, x_f can be calculated using the equation below

$$x_f = \frac{A_{cm}}{4hn_F} \qquad \text{..... (A4)}$$

Total matrix bulk volume, V_{bm} is defined as

$$V_{bm} = 2L_F x_f hn_F = \frac{L_F}{2} A_{cm} \quad \text{..... (A5)}$$

OGIP can be calculated as shown below

$$OGIP = f_{CP} \frac{200.8 T S_{gi}}{\left(\mu c_t B_g\right)_i} \left(\frac{\sqrt{t_{esr}}}{\tilde{m}_4} \right) \quad \text{..... (A6)}$$

Conditions for Bilinear Flow

Bilinear flow of the matrix and natural fracture has a relationship indicating the start for the transient flow dominated by natural fracture as stated by Tivayanonda *et al*. (2012) shown below.

$$\frac{L_f}{L_F} < \sqrt{\frac{k_m}{k_f}} \quad \text{..... (A7)}$$

k_f in the equation is *effective* fracture permeability which is defined as in the equation.

$$k_{f,eff} = \frac{k_m L_f + k_{f,in} w_f}{L_f} \quad \text{..... (A8)}$$

Substituting, Eq. A8 into Eq. A7 we will have an equation defined by the inputs in the simulator only.

$$\frac{L_f}{L_F} < \sqrt{\frac{k_m L_f}{k_m L_f + k_{f,in} w_f}} \quad \text{..... (A9)}$$

Final form of the inequality is shown below.

$$k_{f,\text{int}} w_f < k_m \left(\frac{L_F^2 - L_f^2}{L_f} \right) \quad \text{..... (A10)}$$

The equation above will not work for the case if $L_F = L_f$.

APPENDIX B

SIMULATION CODE

```
INUNIT FIELD

WSRF WELL 1

WSRF GRID TIME

WSRF SECTOR TIME

OUTSRF WELL LAYER NONE

OUTSRF RES ALL

OUTSRF GRID BPP OILPOT PCOW PRES SG SO SSPRES SW WINFLUX

WPRN GRID 0

OUTPRN GRID NONE

OUTPRN RES NONE

RESULTS XOFFSET          0.0000

RESULTS YOFFSET          0.0000

RESULTS ROTATION          0.0000  **$  (DEGREES)

RESULTS AXES-DIRECTIONS 1.0 -1.0 1.0

GRID VARI 31 16 15

KDIR DOWN

DI IVAR

 9.6 6.708567 3.862209 2.223524 1.280111 0.7369767 0.4232 0.2433 0.1399

 0.0804 0.046 0.026 0.015 0.008 0.005 0.0001 0.005 0.008 0.015 0.026
```

0.046 0.0804 0.1399 0.2433 0.4232 0.7369767 1.280111 2.223524 3.862209

6.708567 9.6

DJ JVAR

43 20.95835 13.35417 8.508963 5.421712 3.454588 2.201183 1.402542

0.8936669 0.5694236 0.2847118 0.1423559 0.07117795 0.035588975 0.017794488 0.01

DK ALL

7440*10

DTOP

496*10000

NULL CON 1

POR CON 0.06

*MOD

16:16 1:16 1:15 = 0.95 ** NF

1:31 16:16 1:15 = 0.95 ** HF

PERMI CON 0.0001

MOD

16:16 1:16 1:15 = .1 ** NF

1:31 16:16 1:15 = 1000 ** HF

PERMJ CON 0.0001

MOD

16:16 1:16 1:15 = .1 ** NF

```
1:31  16:16 1:15 = 1000          ** HF
PERMK CON     0.00001
MOD
16:16 1:16 1:15  = .01         ** NF
1:31  16:16 1:15 = 100          ** HF
PINCHOUTARRAY CON           1
PRPOR 3000
CPOR 1E-6
MODEL GASWATER
TRES 160
**$        p        Eg       visg
**$        p        Eg       visg
**$        p          Bg       visg
**$        p          Bg       visg
PVTG ZG 1
**  All the PVT Data below is from Gasprops Program


**$        p         z         visg
        14.7  0.998999  0.012540001
       100.0  0.991001  0.012599698
       200.0  0.981997  0.012695659
```

300.0 0.973 0.01281005

400.0 0.964998 0.012939686

500.0 0.957001 0.013083086

600.0 0.949003 0.013239448

700.0 0.940997 0.013408301

800.0 0.933999 0.013589356

900.0 0.927 0.013782421

1000.0 0.919998 0.013987352

1100.0 0.914 0.01420402

1200.0 0.908001 0.014432289

1300.0 0.902 0.014671995

1400.0 0.897001 0.014922937

1500.0 0.893 0.015184864

1600.0 0.889002 0.015457471

1700.0 0.885 0.015740398

1800.0 0.882002 0.016033225

1900.0 0.88 0.01633548

2000.0 0.877999 0.01664664

2100.0 0.876001 0.01696614

2200.0 0.875001 0.017293404

2300.0 0.875004 0.017627781

2400.0 0.875002 0.017968643

2500.0 0.874997 0.018315347

2600.0 0.875999 0.018667251

2700.0 0.877004 0.019023722

2800.0 0.878999 0.019384144

2900.0 0.881999 0.019747923

3000.0 0.884002 0.02011449

3100.0 0.887001 0.020483306

3200.0 0.891001 0.020853863

3300.0 0.893996 0.021225684

3400.0 0.897996 0.021598328

3500.0 0.903001 0.021971383

3600.0 0.906999 0.022344473

3700.0 0.912001 0.022717252

3800.0 0.918002 0.023089403

3900.0 0.923003 0.023460638

4000.0 0.928997 0.023830699

4100.0 0.934998 0.024199349

4200.0 0.940997 0.024566379

4300.0 0.946998 0.024931601

4400.0 0.952997 0.025295412

4500.0 0.959998 0.025656293

4600.0 0.967 0.026014888

4700.0 0.974003 0.026371128

4800.0 0.981004 0.02672498

4900.0 0.988001 0.027076449

5000.0 0.994999 0.02742558

5100.0 1.002 0.027772459

5200.0 1.01 0.028117219

5300.0 1.018 0.02845685

5400.0 1.025 0.028795161

5500.0 1.033 0.029130824

5600.0 1.041 0.029463878

5700.0 1.049 0.029794379

5800.0 1.057 0.030119355

5900.0 1.065 0.030443615

6000.0 1.073 0.030765159

BWI 1.01412

CVW 0.0

CW 2.93601e-006

DENSITY WATER 61.9615

REFPW 3000

VWI 0.432871

GRAVITY GAS .65

ROCKFLUID

RPT 1

**$ Sw krw

**$ Sw krw Pcgw

SWT

0.25 0 400

0.3 3.00729E-24 304.2903097

0.4 1.04858E-14 197.6423538

0.5 2.86797E-10 141.4213562

0.6 2.39958E-07 107.5828707

0.7 3.65616E-05 85.3734721

0.75 0.000300729 76.98003589

0.8 0.002023152 69.8771243

0.9 0.057153373 58.56069741

1 1 50

**$ Sl krg

**$ Sg krg

SGT

0.1 0

0.2 1.97845E-18

0.25 2.59319E-13

0.3 2.55497E-10

0.4 1.50944E-06

0.5 0.000460247

0.6 0.032994915

0.75 1

RPT 2

**$ Sw krw

**$ Sw krw

SWT

0 0

0.0625 0.00390625

0.125 0.015625

0.1875 0.0351563

0.25 0.0625

0.3125 0.0976563

0.375 0.140625

0.4375 0.191406

0.5 0.25

0.5625 0.316406

0.625 0.390625

0.6875 0.472656

0.75 0.5625

0.8125 0.660156

0.875 0.765625

0.9375 0.878906

1 1

**$ Sg krg

**$ Sg krg

SGT

0 0

0.0625 0.00390625

0.125 0.015625

0.1875 0.0351563

0.25 0.0625

0.3125 0.0976563

0.375 0.140625

0.4375 0.191406

0.5 0.25

0.5625 0.316406

0.625 0.390625

0.6875 0.472656

0.75 0.5625

0.8125 0.660156

0.875 0.765625

0.9375 0.878906

1 1

```
RTYPE CON      1          **First assign everywhere 1
MOD
16:16 1:16 1:15  = 1       ** NF
1:31  16:16 1:15 = 2        ** HF
NDARCYCOR CON           0
INITIAL
USER_INPUT
GOC_PC 0
WOC_PC 0
PRES CON        3000
SW CON          .25
MOD
16:16 1:16 1:15  = 1       ** NF
1:31  16:16 1:15 = 1        ** HF
 NUMERICAL
DTMIN 1e-9
NORTH 40
ITERMAX 100
RUN
DATE 2000 1 1
DTWELL 1e-009
**$
```

```
WELL  'Well-1'
PRODUCER 'Well-1'
OPERATE  MIN  BHP  500.  CONT REPEAT
OPERATE  MAX  STG  5e+012  CONT REPEAT
**$ UBA             ff  Status  Connection
**$ UBA            ff  Status  Connection
**$ UBA      ff  Status  Connection
**$          rad  geofac  wfrac  skin
GEOMETRY  K  0.25  0.37  1.  0.
**$ UBA             ff  Status  Connection
**$ UBA            ff  Status  Connection
**$ UBA      ff  Status  Connection
**$          rad  geofac  wfrac  skin
**$ UBA       ff  Status  Connection
**$ UBA       wi       Status  Connection
PERF  WI  'Well-1'
**$ UBA      wi       Status  Connection
   16 16 8  1000.  OPEN    FLOW-TO  'SURFACE'

DATE 2000 1  1.04167
DATE 2000 1  1.08333
DATE 2000 1  1.12500
```

APPENDIX C

DIFFUSIVITY EQUATION

Darcy "Volumetric": $q = \frac{-A\,k}{\mu}\left(\frac{\Delta p}{L}\right)$

To obtain differential equation replace $\left(\frac{\Delta p}{L}\right)$ by $\frac{\partial p}{\partial x}$ so,

$$q = \frac{-A\,k}{\mu}\frac{\partial p}{\partial x}$$

For different fluids:

Gas : $q_g = \frac{-A\,k\,k_{rg}}{\mu_g}\frac{\partial p_g}{\partial x}$ Water : $q_w = \frac{-A\,k\,k_{rw}}{\mu_w}\frac{\partial p_w}{\partial x}$

Combine the above equation with continuity to obtain differential equation for the flow in porous media.

We carry a mass balance:

Pore Volume: $v_p = A\,\Delta x\,\emptyset$ Mass of Gas $= A\,\Delta x\,\emptyset\,\frac{S_g}{B_g}$

Sg and *Bg* are a function of time; change in volume with time:

$$\left(\frac{q_g}{B_g}\right)_x - \left(\frac{q_g}{B_g}\right)_{x+\Delta x} = A\ \Delta x\ \frac{\partial}{\partial t}\left(\frac{\emptyset\,S_g}{B_g}\right)$$

Divide by Δx and get limit to 0

Gas: $-\frac{\partial}{\partial x}\left(\frac{q_g}{B_g}\right) = A\ \frac{\partial}{\partial t}\left(\frac{\emptyset\,S_g}{B_g}\right)$ Water: $-\frac{\partial}{\partial x}\left(\frac{q_w}{B_w}\right) = A\ \frac{\partial}{\partial t}\left(\frac{\emptyset\,S_w}{B_w}\right)$

Now, Substitute Darcy in the above equation:

$$\frac{\partial}{\partial x}\left(\frac{A\,k\,k_{rg}}{B_g\,\mu_g}\frac{\partial p_g}{\partial x}\right) = A\ \frac{\partial}{\partial t}\left(\frac{\emptyset\,S_g}{B_g}\right)$$

If we assume capillary pressure ($p_c = 0$) and use $k_g = k\, k_{rg}$ and consider A constant and can be canceled we get

$$\frac{\partial}{\partial x}\left(\frac{k_g}{B_g\,\mu_g}\frac{\partial p}{\partial x}\right) = \frac{\partial}{\partial t}\left(\frac{\emptyset\, S_g}{B_g}\right)$$

Expand LHS using chain rule

$$\left(\frac{k_g}{B_g\,\mu_g}\right)\frac{\partial}{\partial x}\left(\frac{\partial p}{\partial x}\right) + \frac{\partial p}{\partial x}\,\frac{\partial}{\partial x}\left(\frac{k_g}{B_g\,\mu_g}\right) = \frac{\partial}{\partial t}\left(\frac{\emptyset\, S_g}{B_g}\right)$$

Assume k , φ are constants; k=f(S_w,S_g) ; u_g & B_g = f(p) not S_w & S_g

So we expand second term

$$\left(\frac{k_g}{B_g\,\mu_g}\right)\frac{\partial}{\partial x}\left(\frac{\partial p}{\partial x}\right) + \left[\frac{\partial p}{\partial x}\left(\frac{1}{B_g\mu_g}\right)\frac{\partial k_g}{\partial S_g}\frac{\partial S_g}{\partial x}\right] + \left[\frac{\partial p}{\partial x}\left(\frac{1}{B_g\mu_g}\right)\frac{\partial k_g}{\partial S_w}\frac{\partial S_w}{\partial x}\right]$$

$$+ \left[\frac{\partial p}{\partial x}\;k_g\,\frac{\partial}{\partial p}\left(\frac{1}{B_g\,\mu_g}\right)\frac{\partial p}{\partial x}\right] = \emptyset\,\frac{\partial}{\partial t}\left(\frac{S_g}{B_g}\right)$$

If we assumed $\left(\frac{\partial p}{\partial x}\right)^2$ and $\left[\frac{\partial p}{\partial x}\frac{\partial S_g}{\partial x}\right]$ and $\left[\frac{\partial p}{\partial x}\;\frac{\partial S_w}{\partial x}\right]$ are negligible, we get:

$$\frac{\partial}{\partial x}\left(\frac{\partial p}{\partial x}\right) = \emptyset\left(\frac{B_g\,\mu_g}{k_g}\right)\frac{\partial}{\partial t}\left(\frac{S_g}{B_g}\right)$$

Similarly for water we can write:

$$\frac{\partial}{\partial x}\left(\frac{\partial p}{\partial x}\right) = \emptyset\left(\frac{B_W\,\mu_w}{k_w}\right)\frac{\partial}{\partial t}\left(\frac{S_w}{B_w}\right)$$

We expand partial derivative with respect to time. B_g, S_g = f(p)

$$\frac{\partial}{\partial x}\left(\frac{\partial p}{\partial x}\right) = \emptyset\left(\frac{B_g\,\mu_g}{k_g}\right)\left[\frac{1}{B_g}\frac{\partial S_g}{\partial p}\frac{\partial p}{\partial t} + S_g\frac{\partial}{\partial p}\frac{1}{B_g}\frac{\partial p}{\partial t}\right]$$

For convenience we let all partial derivative with respect to pressure be denoted by B_g' and S_g' and we use:

$$\frac{\partial}{\partial p}\left(\frac{1}{B_g}\right) = \frac{\partial}{\partial p}\left(B_g^{-1}\right) = \frac{-1}{B_g^2}\frac{\partial B_g}{\partial p}$$

So,

$$\frac{\partial}{\partial x}\left(\frac{\partial p}{\partial x}\right) = \left(\frac{\emptyset\, B_g\, \mu_g}{k_g}\right)\left[\frac{S_g{}'}{B_g} - \frac{S_g\, B_g{}'}{B_g^2}\right]\frac{\partial p}{\partial t}$$

Simplify,

$$\frac{\partial}{\partial x}\left(\frac{\partial p}{\partial x}\right) = \left(\frac{\emptyset\, \mu_g}{k_g}\right)\left[S_g{}' - \frac{S_g\, B_g{}'}{B_g}\right]\frac{\partial p}{\partial t}$$

For water,

$$\frac{\partial}{\partial x}\left(\frac{\partial p}{\partial x}\right) = \left(\frac{\emptyset\, \mu_w}{k_w}\right)\left[S_w{}' - \frac{S_w\, B_w{}'}{B_w}\right]\frac{\partial p}{\partial t}$$

We derive a single equation for gas & water. We realizing that left side of both equations are equivalent. With the definition below we can rewrite the equation

$\lambda_g = \frac{k_g}{\mu_g}$ and $\lambda_w = \frac{k_w}{\mu_w}$

$$\left(\frac{\emptyset}{\lambda_g}\right)\left[S_g{}' - \frac{S_g\, B_g{}'}{B_g}\right]\frac{\partial p}{\partial t} = \left(\frac{\emptyset}{\lambda_w}\right)\left[S_w{}' - \frac{S_w\, B_w{}'}{B_w}\right]\frac{\partial p}{\partial t}$$

Simplifying,

$$\left(\frac{\lambda_w}{\lambda_g}\right)\left[S_g{}' - \frac{S_g\, B_g{}'}{B_g}\right] = \left[S_w{}' - \frac{S_w\, B_w{}'}{B_w}\right]$$

We know that S_w+S_g=1. If we differentiate with respect to pressure. S_w'+S_g'=0 so S_w'=S_g'

Also, $\lambda_g + \lambda_w = \lambda_t$

$$\left(\frac{\lambda_t - \lambda_g}{\lambda_g}\right)\left[S_g{}' - \frac{S_g\, B_g{}'}{B_g}\right] = \left[-S_g{}' - \frac{S_w\, B_w{}'}{B_w}\right]$$

Add $\frac{S_g\, B_g{}'}{B_g}$ and $\frac{S_w\, B_w{}'}{B_w}$ to both sides of the equation

$$\left(\frac{\lambda_t - \lambda_g}{\lambda_g}\right)\left[S_g{}' - \frac{S_g\, B_g{}'}{B_g}\right] + \frac{S_g\, B_g{}'}{B_g} + \frac{S_w\, B_w{}'}{B_w} = \left[-S_g{}' - \frac{S_w\, B_w{}'}{B_w}\right] + \frac{S_g\, B_g{}'}{B_g} + \frac{S_w\, B_w{}'}{B_w}$$

$$\left(\frac{\lambda_t - \lambda_g}{\lambda_g}\right)\left[S_g{}' - \frac{S_g\, B_g{}'}{B_g}\right] = -\frac{S_g\, B_g{}'}{B_g} - \frac{S_w\, B_w{}'}{B_w} - \left[S_g' - \frac{S_g\, B_g{}'}{B_g}\right]$$

$$\left(\frac{\lambda_t - \lambda_g}{\lambda_g} + 1\right)\left[S_g{}' - \frac{S_g\, B_g{}'}{B_g}\right] = -\frac{S_g\, B_g{}'}{B_g} - \frac{S_w\, B_w{}'}{B_w}$$

Where,

$c_g = -\frac{1}{B_g}(B_g{}')$ and $c_w = -\frac{1}{B_w}(B_w{}')$

$c_t = S_g c_g + S_w c_w$

$$c_t = S_g \frac{B_g{}'}{B_g} + S_w \frac{B_w{}'}{B_w}$$

$$\left(\frac{\lambda_t}{\lambda_g}\right)\left[S_g{}' - \frac{S_g\, B_g{}'}{B_g}\right] = c_t$$

$$\left(\frac{1}{\lambda_g}\right)\left[S_g{}' - \frac{S_g\, B_g{}'}{B_g}\right] = \frac{c_t}{\lambda_t}$$

So instead of

$$\frac{\partial}{\partial x}\left(\frac{\partial p}{\partial x}\right) = \left(\frac{\emptyset}{\lambda_g}\right)\left[S_g{}' - \frac{S_g\, B_g{}'}{B_g}\right]\frac{\partial p}{\partial t}$$

For multiphase flow, the diffusivity will be

$$\frac{\partial}{\partial x}\left(\frac{\partial p}{\partial x}\right) = \left(\frac{\emptyset\, c_t}{\lambda_t}\right)\frac{\partial p}{\partial t}$$

$$c_t = S_g c_g + S_w c_w$$

$$\lambda_t = \frac{k_g}{\mu_g} + \frac{k_w}{\mu_w} = k\left(\frac{k_{rg}}{\mu_g} + \frac{k_{rw}}{\mu_w}\right)$$

Substitute the above into the diffusivity equation

$$\frac{\partial}{\partial x}\left(\frac{\partial p}{\partial x}\right) = \left(\frac{\emptyset\,(\,S_g c_g + S_w c_w\,)}{k\left(\frac{k_{rg}}{\mu_g} + \frac{k_{rw}}{\mu_w}\right)}\right)\frac{\partial p}{\partial t}$$

If we assume gas is the dominant phase then

$$c_t = S_g c_g$$

$$\lambda_t = \frac{k_g}{\mu_g}$$

The diffusivity for multiphase flow is

$$\frac{\partial}{\partial x}\left(\frac{\partial p}{\partial x}\right) = \left(\frac{\emptyset\,(S_g\,c_g)\mu_g}{k_g}\right)\frac{\partial p}{\partial t}$$

APPENDIX D

DERIVATION OF FRACTURE VOLUME EQUATION

Assuming the fracture is full with water and it is in Pseudosteady state, $t > t_{pss}$

Material balance time equation will be.

$$p_i - \bar{p} = \frac{W_p B_w}{W B_{wi} c_t} \quad \text{..... (D1)}$$

Pseuodsteady state equation is

$$\bar{p} - p_{wf} = J q_w \quad \text{..... (D2)}$$

The difference between the bottomhole pressure and flowing bottomhole pressure can be written as.

$$p_i - p_{wf} = (p_i - \bar{p}) + (\bar{p} - p_{wf}) \quad \text{..... (D3)}$$

Substitution the material balance equation.

$$p_i - p_{wf} = \frac{W_p B_w}{W B_{wi} c_t} + J q_w \quad \text{..... (D4)}$$

Water material balance time is

$$t_{mBw} = \frac{W_p}{q_w} \quad \text{..... (D5)}$$

Substitution Eq. D5 into Eq. D4

$$\frac{q_w}{p_i - p_{wf}} = \frac{1}{\frac{B_w}{W B_{wi} c_t} t_{mBw} + J} \quad \text{..... (D6)}$$

At larger times.

$$\frac{q_w}{p_i - p_{wf}} = \frac{W B_{wi} c_t}{B_w} t_{mBw}^{-1} \quad \text{..... (D7)}$$

On a log-log graph of $\frac{q_w(t)}{p_i - p_{wf}(t)}$ vs. t_{mBW} will have a slope of -1 and the fracture volume will be

$$V_p = \frac{B_w}{c_t\, m_{pss}} \quad \text{..... (D8)}$$

Where $1/m_{pss}$ is the slope of $\frac{q_w(t)}{p_i - p_{wf}(t)}$ vs. t_{mBW} in Cartesian plot.